Modelling the Effect of Creep on the Behaviour of RC Deep Beams

Auteur : Heuse, Arthur
Promoteur(s) : Mihaylov, Boyan
Faculté : Faculté des Sciences appliquées
Diplôme : Master en ingénieur civil des constructions, à finalité spécialisée en "civil engineering"
Année académique : 2024-2025
URI/URL : http://hdl.handle.net/2268.2/23341

UNIVERSITE DE LIEGE
FACULTE DES SCIENCES APPLIQUEES

Modelling the Effect of Creep on the Behaviour of RC Deep Beams

Heuse Arthur

Thesis presented to obtain the degree of :
Master of Science in Civil Engineering

Thesis supervisor :
Mihaylov Boyan

Academic year: **2024 - 2025**

Abstract

This thesis investigates the long-term behaviour of reinforced concrete deep beams under sustained shear loading, with a particular focus on the influence of concrete creep. Deep beams, commonly found in bridge structures, are critical members subjected to high shear forces. As many bridges are approaching the end of their intended service life, understanding the time-dependent degradation of shear mechanisms has become essential.

The study relies on the 2PKT model [1], a kinematic-based analytical framework capable of reproducing the full shear response of RC deep beams up to failure, and on the fib Model Code for the implementation of creep [2]. Creep is first introduced independently into two primary shear transfer mechanisms: the Concrete Loading Zone (CLZ) and aggregate interlock. These mechanisms are then assembled within the full 2PKT framework to simulate the behaviour of deep beams under sustained loading conditions.

A relationship between sustained shear load level and time to failure is established, in order to assess the reduction in shear capacity over time. In terms of serviceability, the time evolution of crack-width and total mid-span deflection is studied to evaluate the impact of creep at service load levels. A parametric study is also conducted to assess the influence of key geometric and mechanical parameters, such as shear reinforcement ratio, span-to-depth ratio, and the size of the support and loading plates.

This work shows a decrease of approximately 20 % in shear capacity over 50 years except for deep beams with very short span-to-depth ratio (a/d=1) where the reduction in shear capacity is negligible over the same period.
Under service load levels, the crack-width increases by approximately 100%-150% over 50 years, depending on the parameters, except for deep beams with large span-to-depth ratio (a/d=2.28) where it is more moderate. The total mid-span deflection by approximately 30-40% over 50 years, with smaller increases observed for beams with a higher span-to-depth ratio.

Acknowledgments

I would like to express my gratitude to all those who contributed to this master's thesis and to everyone who supported, guided and encouraged me throughout these five wonderful years of study.

First, I want to thank my supervisor, Prof. Mihaylov, for always being available to organize meetings or promptly respond to my questions, wheter by email or phone. He ensured consistent follow-up of this work and I truly appreciated the interest he showed in the topic I developed. His experience and expertise in the field were invaluable to the success of this thesis.

I would like also to warmly thank my proofreaders Nathalie and my friend Martin for the time they devoted to review my work and for their valuable suggestions regarding language, presentation and content.

I am grateful to all my friends and especially Thibault, Noah and Valentin, without whom these years of study would not have been the same. Thank you for supporting me during moments of doubt, for your advices and for always being there when I needed help.

My heartfelt thanks go to my little sister, who has always been there to lift my spirits with humor and perspective, and to my parents, who have done everything possible to provide me the best working environment and who have encouraged me every step of the way.

Finally, I would like to thank my grandparents, who have always taken care for me since I was a child. They have supported me with love and dedication throughout my academic journey and I will be forever grateful to them.

Contents

Introduction **1**
0.1 Context and motivation . . . 1
0.2 Objectives . . . 2
0.3 Outline . . . 2

1 Background **3**
1.1 2PKT for deep beams . . . 3
1.1.1 Overview of the model . . . 3
1.1.2 Modeling of the CLZ . . . 7
1.1.3 Modelling of aggregate interlock . . . 8
1.2 Creep of concrete . . . 10
1.2.1 Creep coefficient in compression . . . 10
1.2.2 Effect of creep on compressive strength . . . 19

2 Modelling of Concrete Loading Zone (CLZ) **22**
2.1 Formulation . . . 22
2.1.1 Global approach . . . 22
2.1.2 Local approach . . . 25
2.2 Results . . . 27
2.2.1 Global approach . . . 27
2.2.2 Local approach . . . 30

3 Modelling of Aggregate Interlock **36**
3.1 Formulation . . . 36
3.2 Results . . . 39
3.2.1 w = slip . . . 39
3.2.2 w = 0.5 slip . . . 41
3.2.3 w = 1.25 slip . . . 43

4 Effect of creep on the behaviour of deep beams **46**
4.1 Problem statement . . . 46
4.2 Reference case: S1M . . . 48
4.2.1 Run to failure at prescribed load levels . . . 48
4.2.2 Constant-load service life assessment . . . 54
4.2.3 Conclusion . . . 59
4.3 Parametric and Comparative studies . . . 60
4.3.1 Shear reinforcement . . . 60
4.3.2 Support and loading plate width . . . 68
4.3.3 Size of the member (a/d) . . . 77
4.3.4 Conclusion of the parametric analysis . . . 90

5 Conclusion **92**

Bibliography **96**

List of Figures

1 Deep beam in the substructure of a bridge [3] 1

1.1 Details of the kinematic model (adapted from [1]) 4
1.2 Superposition of the two kinematic modes (adapted from [1]) 4
1.3 Shear-resisting mechanisms in the 2PKT (adapted from [4]) 6
1.4 Total shear resistance and four shear mechanisms computed by the 2PKT model . 7
1.5 Modeling of the CLZ (adapted from [1]) 8
1.6 Aggregate interlock (adapted from [5]) 9
1.7 Three phases of the creep strain (adapted from [6]) 14
1.8 Response of concrete under uniaxial compressive stresses (adapted from [6]) . . . 15
1.9 Time evolution of the creep coefficient for C30/35, RH=50%, $h_0 = 100mm$ 16
1.10 Time evolution of the creep coefficient according for C80/95, RH=50%, $h_0 = 100mm$ 16
1.11 Time evolution of the creep coefficient for C30/35, RH=80%, $h_0 = 100mm$ 16
1.12 Time evolution of the creep coefficient with time for C80/95, RH=80%, $h_0 = 100mm$ 16
1.13 Evolution of the creep coefficient with the characteristic strength for C30/35, RH=80%, $h_0 = 100mm$ 17
1.14 Evolution of the creep coefficient with the characteristic strength for C80/95, RH=80%, $h_0 = 100mm$ 17
1.15 Evolution of the creep coefficient at 50 years with the loading age t_0 17
1.16 Evolution of the creep coefficient at 50 years with the Relative Humidity (RH) . . 17
1.17 Evolution of the creep coefficient at 50 years with the notional size h_0 for $RH = 50\%$ 18
1.18 Evolution of the creep coefficient at 50 years with the notional size h_0 for $RH = 80\%$ 18
1.19 Time evolution of $\beta_{cc}(t)$ 20
1.20 For $t_0 = 7$ days 21
1.21 For $t_0 = 28$ days 21
1.22 Evolution of $\beta_{c,sus}(t, t_0)$ with $log(\Delta t)$ 21
1.23 For $t_0 = 7$ days 21
1.24 For $t_0 = 28$ days 21
1.25 Evolution of $f_{cm,sus}(t, t_0)$ with $log(\Delta t)$ 21

2.1 CLZ (adapted from [4]) 22
2.2 Loading with the time 23
2.3 Δ corresponding to a given $V/V_{u,0}$ 23
2.4 Interpolation of each single σ_i for N fibers 25
2.5 Discretization of the CLZ into N fibers for local creep analysis. 26
2.6 Beam S1M 27
2.7 Corresponding Δ for each load level considered 28
2.8 Stress-strain relationship in the CLZ without creep and with creep for the three different load levels 29
2.9 $V_{clz} - \Delta_c$ without creep and for the three different load levels 30
2.10 Stress-strain response after local creep analysis 32

2.11 V_{CLZ}-Δ_c response after local creep analysis . . . 33
2.12 V_{CLZ}-Δ_c response including high-stress strength reduction . . . 34

3.1 Elastic-perfectly plastic $\sigma_{con} - w_q$ relationship . . . 38
3.2 Δ corresponding to different load levels . . . 38
3.3 Evolution of V_{ci} with slip for w=slip . . . 39
3.4 Evolution of V_{ci} with slip for w=slip . . . 40
3.5 Evolution of V_{ci} with slip for w=0.5 slip . . . 42
3.6 Springs that reached f_{cy} for w=slip , slip = 1.5 mm and for $V/V_{u,0} = 0.9$ . . . 43
3.7 Springs that reached f_{cy} for w= 0.5 slip , slip = 1.5 mm and for $V/V_{u,0} = 0.9$ . . . 43
3.8 Evolution of V_{ci} with slip for w=1.25 slip . . . 44
3.9 Springs that reached f_{cy} for w= 1.25 slip , slip = 1.5 mm and for $V/V_{u,0} = 0.9$ . . . 45

4.1 Shear-resisting contributions versus Δ for $V/V_{u,0} = 0.60$ . . . 48
4.2 Shear-resisting contributions versus Δ for $V/V_{u,0} = 0.75$ . . . 49
4.3 Shear-resisting contributions versus Δ for $V/V_{u,0} = 0.90$ . . . 49
4.4 Time-dependent shear resistance components for $V/V_{u0} = 0.60$ . . . 51
4.5 Time-dependent shear resistance components for $V/V_{u0} = 0.75$. . . . 52
4.6 Time-dependent shear resistance components for $V/V_{u0} = 0.90$. . . . 52
4.7 Time-dependent shear resistance components over 100 years . . . 53
4.8 Time of failure . . . 54
4.9 Sustained load level $V/V_{u,0}$ vs time of failure (in log scale) . . . 55
4.10 Time evolution of the crack-width $w(t)$ over 50 years . . . 57
4.11 Time evolution of the total midspan deflection $\Delta(t)$ over 50 years . . . 58
4.12 Time evolution of the CLZ displacement $\Delta_c(t)$ over 50 years . . . 58
4.13 Beam S0M . . . 60
4.14 Shear-resisting contributions versus Δ at 50 years for the beam S0M . . . 61
4.15 Time-dependent shear resistance components for the beam S0M . . . 63
4.16 Sustained load level $V/V_{u,0}$ vs time of failure (in log scale) . . . 64
4.17 Time evolution of the crack-width $w(t)$ over 50 years . . . 65
4.18 Time evolution of the total mid-span deflection $\Delta(t)$ over 50 years . . . 66
4.19 Time evolution of the CLZ displacement $\Delta_c(t)$ over 50 years . . . 66
4.20 Geometric parameters of the *2PKT model* (adapted from [1]) . . . 68
4.21 V_{CLZ}-Δ_c response for $lb_1 = 450\,mm$ and $lb_2 = 225\,mm$ . . . 69
4.22 Shear-resisting contributions versus Δ for $lb_1 = 450\,mm$ and $lb_2 = 225\,mm$ . . . 70
4.23 Time-dependent shear resistance components for the beam S1M with $lb_1 = 450\,mm$ and $lb_2 = 225\,mm$ . . . 71
4.24 Sustained load level $V/V_{u,0}$ vs time of failure (in log scale) . . . 72
4.25 Time-dependent shear resistance components for the beam S1M with $lb_1 = 450\,mm$ and $lb_2 = 225\,mm$ . . . 73
4.26 Shear-resisting contributions versus Δ for $V/V_{u0} = 0.76$ at t= 29 797 days . . . 74
4.27 Shear-resisting contributions versus Δ for $V/V_{u0} = 0.77$ at t= 26 073 days . . . 74
4.28 Time evolution of the crack-width $w(t)$ over 50 years . . . 74
4.29 Time evolution of the total mid-span deflection $\Delta(t)$ over 50 years . . . 75
4.30 Time evolution of the CLZ displacement Δ_c over 50 years . . . 76
4.31 Size effect in deep beams (adapted from [1]) . . . 77
4.32 V_{CLZ}-Δ_c response for a/d=1 . . . 78
4.33 Shear-resisting contributions versus Δ after 50 years for a/d=1 . . . 79
4.34 Time-dependent shear resistance components for a/d=1 . . . 80
4.35 Time evolution of the crack-width $w(t)$ for a/d=1 . . . 81
4.36 Time evolution of the total deflection Δ for a/d=1 . . . 82

4.37 Time volution of the CLZ displacement Δ_c for a/d=1 82
4.38 V_{CLZ}-Δ_c response for a/d=2.28 84
4.39 Shear-resisting contributions versus Δ for a/d=2.28 85
4.40 Time-dependent shear resistance components for a/d=2.28 86
4.41 Sustained load level $V/V_{u,0}$ vs time of failure 87
4.42 Time evolution of the crack-width $w(t)$ for a/d=2.28 88
4.43 Time evolution of the total deflection Δ for a/d=2.28 89
4.44 Time evolution of the CLZ displacement Δ_c for a/d=2.28 89

List of Tables

2.1 Characteristic properties of beam S1M . . . 27
2.2 Average sustained stress and corresponding parameters for different load levels . . 28
2.3 Peak strain ε_{c1} for no-creep and three sustained-load levels . . . 29
2.4 Displacement capacity $\Delta_{cu}$for no-creep and three sustained-load levels . . . 30
2.5 Analysis of the stresses reported in Tab. 2.6 . . . 31
2.6 Local fiber stresses σ_i (MPa) for $N = 20$ fibers at sustained load levels . . . 31
2.7 Ultimate strain ε_{c1} and peak stress f_c for sustained-load conditions . . . 33
2.8 Displacement capacity Δ_{cu} and shear resistance $V_{CLZ,\max}$ after local creep analysis 34
2.9 Displacement capacity Δ_{cu} and shear resistance $V_{CLZ,\max}$ after high-stress strength reduction . . . 35

3.1 Slip capacity and shear resistance by aggregate interlock . . . 40
3.2 Slip capacity and shear resistance by aggregate interlock . . . 41
3.3 Shear resistance by aggregate interlock . . . 42
3.4 Comparison of the two cases . . . 42
3.5 Shear resistance by aggregate interlock . . . 44
3.6 Comparison of the two cases . . . 44

4.1 Failure displacement and shear capacities (short-term vs. 50-year creep) for beam S1M. . . . 50
4.2 Comparison of short-term, 50-year, and 100-year total shear capacities for S1M. . 54
4.3 Sustained Load Level vs. Time to Failure . . . 56
4.4 Critical crack-width w at $t = t_0$ and $t = 50$ years for different sustained load levels. 57
4.5 Total deflection Δ at $t = t_0$ and $t = 50$ years for different sustained load levels. . . 58
4.6 CLZ displacement Δ_c at $t = t_0$ and $t = 50$ years for different sustained load levels. 59
4.7 Characteristic properties of beam S1M . . . 60
4.8 Proportion of V_{CLZ} contributing to the total shear resistance V_{tot} . . . 62
4.9 Failure displacement and shear capacities (short-term vs. 50-year creep) for beam S0M. . . . 62
4.10 Sustained Load Level vs. Time to Failure for S0M . . . 64
4.11 Critical crack-width w at $t = t_0$ and $t = 50$ years for various sustained load levels. 65
4.12 Total deflection Δ at $t = t_0$ and $t = 50$ years for different sustained load levels. . . 66
4.13 CLZ displacement Δ_c at $t = t_0$ and $t = 50$ years for different sustained load levels. 67
4.14 Displacement capacity Δ_{cu} and shear resistance $V_{CLZ,\max}$ . . . 69
4.15 Failure displacement and shear capacities (short-term vs. 50-year creep) for $lb_1 = 450\,mm$ and $lb_2 = 225\,mm$ . . . 70
4.16 Load levels and corresponding time to failure for beam S1M with $lb_1 = 450\,mm$ and $lb_2 = 225\,mm$. . . . 72
4.17 Critical crack-width w at $t = t_0$ and $t = 50$ years for various sustained load levels. 75
4.18 Total deflection Δ at $t = t_0$ and $t = 50$ years for different sustained load levels. . . 75

4.19 CLZ displacement Δ_c at $t = t_0$ and $t = 50$ years for different sustained load levels. 76
4.20 Displacement capacity Δ_{cu} and shear resistance $V_{CLZ,\max}$ for a/d=1 78
4.21 Failure displacement and shear capacities (short-term vs. 50-year creep) for $a/d = 1$ 79
4.22 Critical crack-width w at $t = t_0$ and $t = 50$ years for various sustained load levels. 81
4.23 Total deflection Δ at $t = t_0$ and $t = 50$ years for different sustained load levels. . . 82
4.24 CLZ displacement Δ_c at $t = t_0$ and $t = 50$ years for different sustained load levels. 83
4.25 Displacement capacity Δ_{cu} and shear resistance $V_{CLZ,\max}$ 84
4.26 Failure displacement and shear capacities (short-term vs. 50-year creep) for $a/d =$ 2.28 85
4.27 Load levels and corresponding time to failure for beam S1M with a/d=2.28 87
4.28 Critical crack-width w at $t = t_0$ and $t = 50$ years for various sustained load levels. 88
4.29 Total deflection Δ at $t = t_0$ and $t = 50$ years for different sustained load levels. . . 89
4.30 CLZ displacement Δ_c at $t = t_0$ and $t = 50$ years for different sustained load levels. 90

5.1 Loss of shear capacity over 50 years 93
5.2 Loss of shear capacity over 50 years 93
5.3 Loss of shear capacity over 50 years 93
5.4 Increase in % between t_0 and t=50 years for $V/V_{u,0} = 0.6$ 94
5.5 Increase in % between t_0 and t=50 years for $V/V_{u,0} = 0.65$ 94

Introduction

0.1 Context and motivation

Reinforced concrete (RC) deep beams are structural elements with a small span-to-depth ratio (a/d) for which classical beam theory is not applicable. Such members are frequently used in bridge construction as deep piles or pier caps to transmit large shear forces as shown on Fig.1.

In Wallonia, the average age of bridges is nearly 60 years, with many having been built between 1960 and 1990. These older structures were detailed using now obsolete design rules, resulting in relatively light reinforcement, deficient shear detailing, and progressive deterioration under increased service loads.

Given the extensive stock of aging deep-beam bridges, it is imperative to deepen the understanding of long-term effects such as creep in RC deep beams. Accurate creep modeling will enable more reliable prediction of shear capacity reduction over decades, inform targeted inspection and maintenance plans, and ultimately extend the safe service life of these critical infrastructures.

The nominal short-term shear capacity and deformation behavior of RC deep beams have been extensively investigated for example, *by Mihaylov et al.* [1] using a kinematic model. However, the influence of long-term sustained loading on shear resistance remains largely unexplored. The present work integrates creep into the 2PKT framework to quantify its effect on shear strength and deformation patterns over service-life horizons of 50 to 100 years.

Figure 1: Deep beam in the substructure of a bridge [3]

0.2 Objectives

This thesis consists in the implementation of various linear and nonlinear models for creep, detailed understanding of advanced kinematics-based models for deep beams and their implementation in Matlab codes, and further development of these models and codes to incorporate the effects of creep.
The main objective is to see if these models can reveal important effects, such as a significant long-term reduction in the shear resistance of deep beams.

0.3 Outline

This thesis consists of 5 chapters :

In Chapter 1, an overview of the *Two-Parameter kinematic theory (2PKT)* [1] is presented, explaining how it captures the full shear response of a reinforced concrete deep beam up to failure. This chapter also reviews the state of the art on concrete creep in compression, detailing the computation of the compressive creep coefficient according to the *fib Model Code* [2] and the reduction of concrete strength under high sustained stresses using the *fib Model Code* strength-reduction formula.

In Chapter 2, creep is incorporated into the Concrete Loading Zone (CLZ) modelling through both a global (uniform) and a local (stress-dependent) approach. The Concrete Loading Zone (CLZ) governs short-term shear failure in deep beams and the impact of each methodology on the CLZ shear resistance and ultimate displacement is assessed.

In Chapter 3, creep is incorporated into the aggregate-interlock component V_{ci}, another key contributor to the total shear resistance. Two modelling approaches (a global approach and a local approach) are employed to investigate how creep affects the relationship $V_{ci} - slip$, considering different slip-crack-width correlations, which are the two primary parameters governing aggregate-interlock shear resistance.

In Chapter 4, the creep-modified mechanisms (V_{CLZ} and V_{ci}) are incorporated into the full 2PKT framework. First, a reference case is analyzed to generate a sustained load level versus time of failure curve, which predicts the service lifetime before shear failure for any sustained load level. The time-dependent evolution of crack-width and total mid-span deflection under these sustained loads is also examined. Then, a parametric study explores how key deep-beam parameters such as span-to-depth ratio (a/d), the shear reinforcement and the size of the loading plate influence both the failure time and long-term deformations.

In Chapter 5, conclusions are drawn and suggestions are proposed for further studies.

Chapter 1

Background

1.1 2PKT for deep beams

1.1.1 Overview of the model

The *Two-Point Kinematic Theory (2PKT)* [1] models the entire shear response of a deep beam up to failure by describing how its shear span deforms using two distinct, interacting mechanisms. By assigning just two kinematics degrees of freedom, *2PKT* can accurately track the opening and sliding of the shear critical crack [4].

Specifically, these two degrees of freedom are :

- $\epsilon_{t,avg}$: the average strain in the bottom flexural reinforcement
- Δ_c: the vertical displacement that develops within the Concrete Loading Zone of the beam (CLZ) at the top of the crack

As described by *B.Myhalov and al.* [1] :

The model assumes that a critical crack runs from the interior face of the support up to the edge of the loading-plate's tributary region which transmits the applied shear force V .
Above this crack, the concrete of the beam acts as a single rigid block; below it, the concrete behaves as a series of rigid radial struts or flexural-shear cracks (all with $\varepsilon_r = 0$). These struts span from the load application point to the bottom flexural reinforcement. The CLZ at the top, the bottom flexural bars, and any transverse reinforcement (stirrups) tie the two blocks together transferring shear across the crack [1].

- For DOF ε_{avg} : when the bottom reinforcement elongates, the rigid block and struts rotate about the loading point and the crack opens. This DOF is associated with flexural deformations.
- For DOF Δ_c : in the CLZ, the rigid block translates vertically and is associated with shear deformations.

Fig. 1.2 shows these deformation patterns with the associated DOFs.

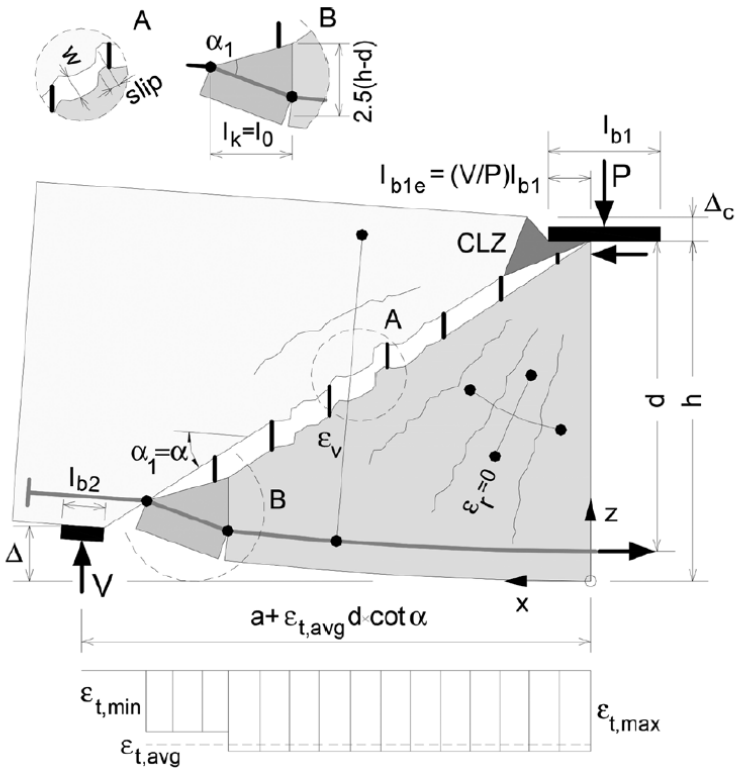

Figure 1.1: Details of the kinematic model (adapted from [1])

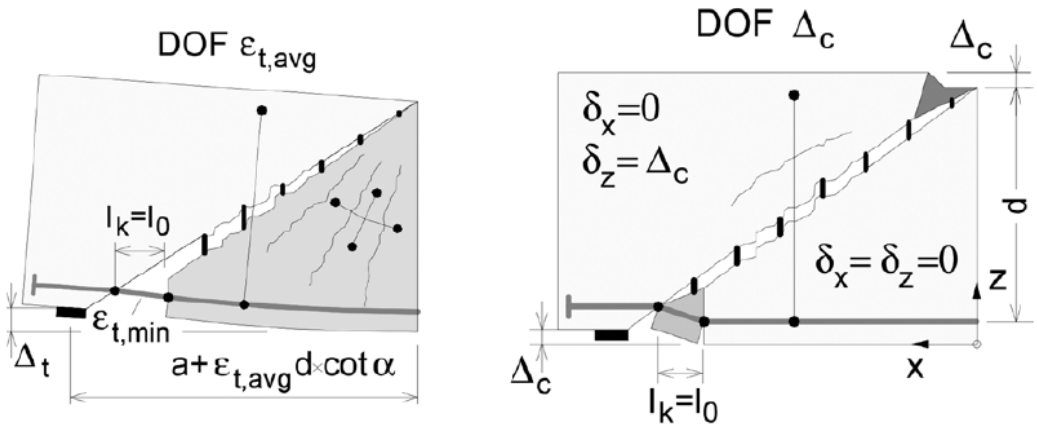

Figure 1.2: Superposition of the two kinematic modes (adapted from [1])

First, it is important to define the geometry of the kinematic model :

- The effective width of loading plate :

$$l_{b1e} = \frac{V}{P} l_{b1} \tag{1.1}$$

It refers to the portion of the plate responsible for the shear force V and determines the size of the CLZ [1].

- Angle α_1 :

$$\alpha_1 = \alpha \geq \theta \tag{1.2}$$

where :

α = angle of line connecting inner end of l_{b2} to outer end of l_{b1e},
θ = angle of the shear cracks obtained from sectional models for slender beams .

It refers to the angle between the critical crack and the axis of the beam [1] .

- Length of the crack along bottom reinforcement l_t :

$$l_t = d\ \cot\alpha_1\ +\ l_k\ -\ l_0 \tag{1.3}$$

- Distance between kinks in bottom reinforcement :

$$l_k = l_0 + d\big(\cot\alpha - \cot\alpha_1\big)\ \leq\ 2\,l_0 \tag{1.4}$$

$$l_0 = 1.5\,(h-d)\ \cot\alpha_1\ \geq\ s_{\text{cr}} \tag{1.5}$$

$$s_{\text{cr}} = \frac{0.28\,d_b\,2.5\,(h-d)}{\rho_l\,d} \tag{1.6}$$

Then, it is necessary to define the deformations :

- Stirrup strain :

$$\varepsilon_v = 2\,\frac{\Delta_c\ +\ 0.25\,\varepsilon_{t,\text{avg}}\ d\ \cot^2\alpha_1}{0.9\,d} \tag{1.7}$$

- Crack width and slip

$$w = \varepsilon_{t,\text{avg}}\,\frac{l_k}{2\sin\alpha_1}\ +\ \Delta_c\cos\alpha_1 \tag{1.8}$$

$$s = \Delta_c\sin\alpha_1 \tag{1.9}$$

- Deflection of the shear span of the beam :

It is expressed as a function of the the two DOFs :

$$\Delta = \frac{\varepsilon_{t,\text{avg}}\,l_t}{d}\,a\ +\ \Delta_c = \Delta_t\ +\ \Delta_c \tag{1.10}$$

It exists four shear-resisting mechanisms across the critical crack. (see Fig.1.3):

1. Shear carried by the CLZ, V_{CLZ},
2. Aggregate interlock, V_{ci},
3. Tension in the transverse web reinforcement, V_s,
4. Dowel action of the flexural reinforcement, V_d.

These mechanisms are computed with the two DOFs ($\varepsilon_{t,avg}$ and Δ_c) :

$$V_{\text{CLZ}} = f(\varepsilon_{\text{max}}), \quad V_{\text{ci}} = f(w,\, s), \quad V_s = f(\varepsilon_v), \quad V_d = f(\Delta_c,\, \varepsilon_{t,\text{avg}})$$

Additionally, the flexural reinforcement tension T is obtained from its average strain $\varepsilon_{t,\text{avg}}$.

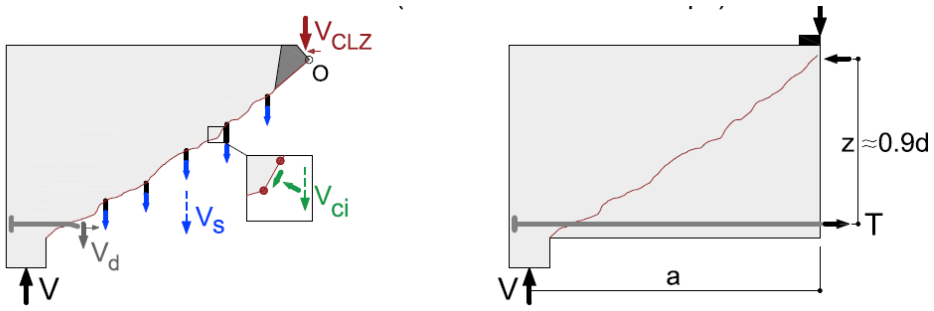

Figure 1.3: Shear-resisting mechanisms in the 2PKT (adapted from [4])

Finally, the model enforces two equilibrium conditions: the vertical equilibrium of the concrete block above the crack and the moment equilibrium of the shear span. Because each term in these equations depends on the two DOFs ($\varepsilon_{t,avg}$ and Δ_c), they form a nonlinear system that must be solved iteratively for a prescribed shear V.

By incrementally increasing V, the response until the shear capacity V_u is reached [4].

By summing the contributions of all shear-resisting mechanisms, the total shear capacity is expressed as :

$$V_{\text{total}} \;=\; V_{\text{CLZ}} \;+\; V_{\text{ci}} \;+\; V_s \;+\; V_d, \tag{1.11}$$

while the applied shear relates to the internal shear force T by :

$$V \;=\; \frac{T\,z}{a}. \tag{1.12}$$

with :

$$T \;=\; E_s\,A_s\,\varepsilon_{t,\text{avg}} \;+\; \frac{0.33\,\sqrt{f_c}}{\sqrt{1 \;+\; 200\,\varepsilon_{t,\text{avg}}}}\,A_{c,\text{eff}} \;\leq\; A_s\,f_y$$

The intersection of these two equations is computed with the method of the bisection and so for each Δ c the corresponding shear force V is found as explained by *B.Mihaylov* in [7]. Step by step the deflection is increased to compute all the $\Delta - V$ relationship and one example of the results provided by the *2PKT model* [1] is shown on Fig. 1.4.

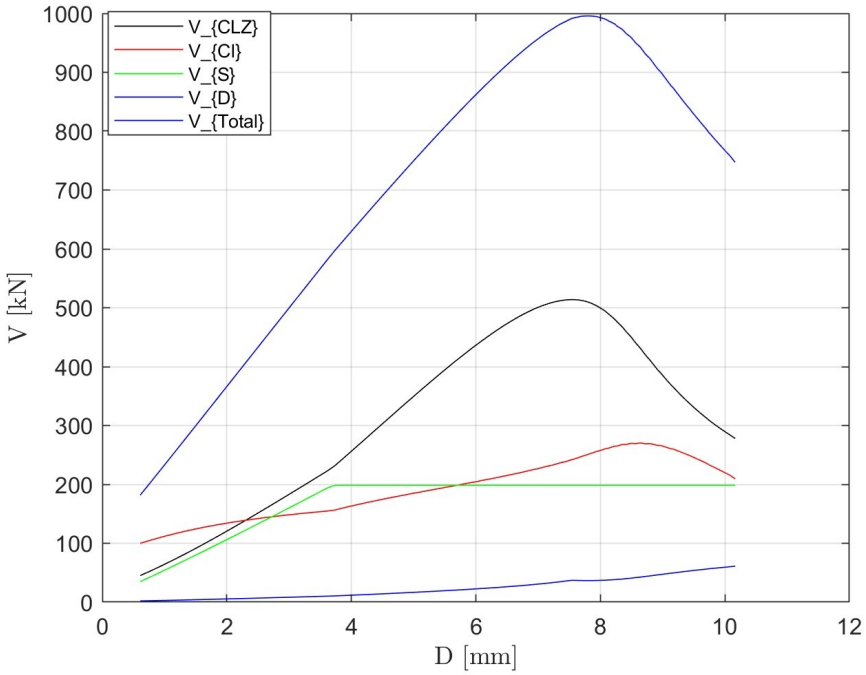

Figure 1.4: Total shear resistance and four shear mechanisms computed by the 2PKT model

1.1.2 Modeling of the CLZ

As deep beams fail by crushing of the CLZ, its behavior is examined more closely.

A compatibility relation

$$\varepsilon_{max} = f(\Delta_c) \tag{1.13}$$

and a constitutive law

$$V_{CLZ} = f(\varepsilon_{max}) \tag{1.14}$$

In the *2PKT framework* [1], the CLZ is represented by a symmetric triangular region (see Fig. 1.5), defined by its inclination angle α_{CLZ} and its base length l_{b1e} along the loading plate. Both α_{CLZ} and l_{b1e} are determined from the geometry of the beam and its material properties.

The compressive strain varies linearly from zero at the top face to ε_{max} at the bottom face, leading to :

$$\varepsilon_{max} = \frac{\Delta_c \, \tan\alpha_{CLZ}}{3\, b\, l_{b1e}}. \tag{1.15}$$

The corresponding average compressive stress is :

$$\sigma_{avg} = \frac{\int_0^{\varepsilon_{max}} \sigma_c(\varepsilon_c)\, d\varepsilon}{\varepsilon_{max}}, \tag{1.16}$$

and the shear strength of the CLZ becomes

$$V_{CLZ} = \sigma_{avg}\, b\, l_{b1e}\, \sin^2\alpha_{CLZ}. \tag{1.17}$$

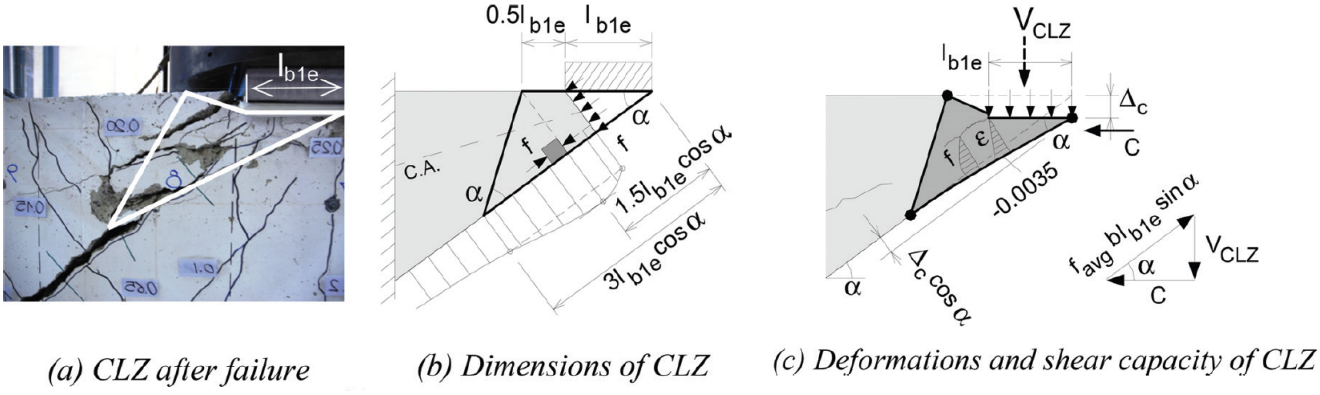

(a) CLZ after failure *(b) Dimensions of CLZ* *(c) Deformations and shear capacity of CLZ*

Figure 1.5: Modeling of the CLZ (adapted from [1])

1.1.3 Modelling of aggregate interlock

"Aggregate interlock is one of the shear resisting mechanisms of structural concrete. Because the strength of the hardened cement paste in most concretes is lower than the strength of the aggregate particles, cracks intersect the cement paste along the edges of the aggregate particles. So the aggregate particles, extending from one of the crack faces, "interlock" with the opposite face and resist shear displacements [8]. The aggregate interlock shears depend on the surface roughness of the cracks, the aggregate type and the displacements across the cracks (Taylor 1974)" as defined by this study from *Delft University* [9].

Fig. 1.6 represents what the aggregate interlock is.

Walraven's aggregate-interlock model [8] treats cracked concrete as a two-phase composite-rigid aggregate particles embedded in an ideally plastic mortar matrix and is based on beam tests demonstrating that cracks open and slip simultaneously rather than opening fully before shearing. As a result, the interlock shear resistance depends on both the normal stress σ across the crack surfaces and the shear stress τ along them.

In the 2PKT model, these two stresses are computed thanks to the Contact Density Model (CDM) introduced by *Li et Al.* [10]

This routine discretizes the crack face into a set of planes at various inclinations.

The steps of this routine are :

1. To discretize crack-face orientations. To divide the crack surface into N micro-elements at inclinations θ_i.
2. To compute material parameters.

$$w_{\text{lim}} = 0.04 \text{ mm}, \quad A_t = 1.27, \quad f_{cy} = k_{fcy}\, 13.7\, f_c^{1/3}. \tag{1.18}$$

Here f_{cy} is the peak tensile strength of the cracked concrete face.

3. Aggregate-size penalty factor.

$$K = \max\Big(1 - \exp\big(1 - 0.5\,G_{\max}/w\big),\, 0\Big), \tag{1.19}$$

so that for $w \gg G_{\max}$ the interlock vanishes ($K \to 0$).

4. Local micro-opening for each plane .
For each θ_i, the relative opening of that element is

$$w_i = \text{slip}\,\sin\theta_i \;-\; w\,\cos\theta_i. \tag{1.20}$$

5. Local stress.
If the planes are in contact, the springs are active and so a stress is computed and if not the stress is zero.

$$\sigma_{\text{con}}^{(i)} = \min\Big(\frac{f_{cy}}{w_{\text{lim}}}\,w_i,\; f_{cy}\Big), \sigma_{\text{con}}^{(i)} \geq 0. \tag{1.21}$$

6. To integrate normal and shear components. The normal closure force σ_n and shear transfer τ are

$$\sigma_n = \sum_{i=1}^{N}\Big[\sigma_{\text{con}}^{(i)}\,K\,A_t\,\Omega_i\,\cos\theta_i\Big]\,\frac{\pi}{N}, \tag{1.22}$$

$$\tau = \sum_{i=1}^{N}\Big[\sigma_{\text{con}}^{(i)}\,K\,A_t\,\Omega_i\,\sin\theta_i\Big]\,\frac{\pi}{N}, \tag{1.23}$$

with $\Omega_i = \frac{1}{2}\cos\theta_i$. In the 2PKT model, the normal stress is neglected.

7. Shear force V_{ci}.

$$V_{ci} = 0.18\,v_{ci}\,b\,d,$$

with $v_{ci} = \tau$.

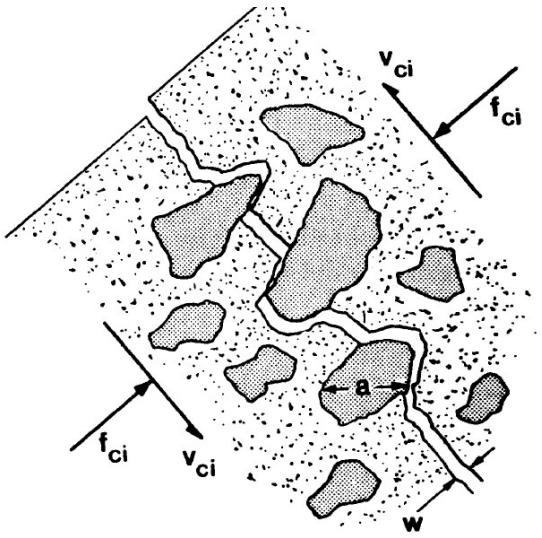

Figure 1.6: Aggregate interlock (adapted from [5])

1.2 Creep of concrete

1.2.1 Creep coefficient in compression

Fib Model Code 2010 and 2020

For the modeling of creep, *fib Model Code 2010* and *fib Model Code 2020* include both the same equations except for the compressive strength which will be discussed later in section 1.2.2.

In the *fib Model Code* [2], the phenomenon of creep under sustained loading is characterized using the creep coefficient, which quantifies the extent of delayed strain relative to the immediate elastic response.

All the following equations are taken from *fib Model Code* [2].

This coefficient is defined as the ratio between the creep strain $\varepsilon_{\text{cr}}(t, t_0)$ and the initial elastic strain $\varepsilon_{\text{el}}(t_0)$, both corresponding to a constant stress σ_0 applied at a reference age t_0, typically taken as 28 days.

When a sustained uniaxial stress σ_0 is imposed from age t_0 onward, the creep coefficient is expressed as

$$\varphi(t, t_0) = \frac{\varepsilon_{\text{cr}}(t, t_0)}{\varepsilon_{\text{el}}(t_0)} \tag{1.24}$$

where

$$\varepsilon_{\text{el}}(t_0) = \frac{\sigma_0}{E_{\text{c}}(t_0)} \quad \text{and} \quad E_{\text{c}}(t_0) = \text{modulus of elasticity at age } t_0.$$

The stress-dependent strain $\varepsilon_\infty(t, t_0)$ at time t may be expressed as:

$$\varepsilon_\infty(t, t_0) = \sigma_\varepsilon(t_0) \left[\frac{1}{E_{c,\varepsilon}(t_0)} + \frac{\varphi(t, t_0)}{E_{c,\varepsilon}} \right] = \sigma_\varepsilon(t_0) J(t, t_0) \tag{1.25}$$

where:

- $J(t, t_0)$ is the creep function or creep compliance, representing the total stress-dependent strain per unit stress.
- $E_{c,\varepsilon}(t_0)$ is the modulus of elasticity at the time of loading t_0 ; hence $1/E_{c,\varepsilon}(t_0)$ represents the initial elastic strain per unit stress at loading.

For engineering purposes, concrete can be idealized as an ageing linear viscoelastic material. Under this assumption, the superposition principle is considered applicable when dealing with varying stresses and strains. Based on these premises and the definitions previously introduced, the constitutive law for concrete can be expressed as:

$$\varepsilon_\varepsilon(t) = \sigma_\varepsilon(t_0) J(t, t_0) + \int_{t_0}^{t} \frac{\partial \sigma_\varepsilon(\tau)}{\partial \tau} J(t, \tau) \, \mathrm{d}\tau + \varepsilon_\infty(t) \tag{1.26}$$

Equation 1.26 provides a general formulation of the constitutive behavior of concrete. It enables the analysis of arbitrary creep and relaxation problems, provided that either the time-dependent

stress $\sigma_\varepsilon(t, t_0)$ or strain $\varepsilon(t, t_0)$ history is known, along with the material property described by the creep compliance function $J(t, t_0)$.

The expressions used to evaluate the creep coefficient are empirical and have been derived from experimental data, primarily obtained through compression tests on structural concrete specimens. In this framework, total creep is considered as the sum of two distinct components: basic creep and drying creep, each associated with different physical processes.

The creep coefficient $\varphi(t, t_0)$ may be calculated from:

$$\varphi(t, t_0) = \xi_{bc1} \cdot \varphi_{bc}(t, t_0) + \xi_{dc1} \cdot \varphi_{dc}(t, t_0) \tag{1.27}$$

where:

- $\varphi_{bc}(t, t_0)$ is the basic creep coefficient according to Eq.1.28.
- $\varphi_{dc}(t, t_0)$ is the drying creep coefficient according to Eq. 1.31
- ξ_{bc1}, ξ_{dc1} are equal to 1.0 when no specific tests have been carried out on the concrete in question. Otherwise, they are determined by least-squares fitting to experimental data.
- t is the age of the concrete in days at the time of interest.
- t_0 is the age of the concrete at loading, in days, adjusted according to Eq.1.40 and Eq.1.41

The basic (non-drying) creep coefficient is

$$\varphi_{bc}(t, t_0) = \beta_{bc}(f_{\text{cm}})\,\beta_{bc}(t, t_0), \tag{1.28}$$

with

$$\beta_{bc}(f_{\text{cm}}) = 1.8\, f_{\text{cm}}^{-0.07}, \tag{1.29}$$

$$\beta_{bc}(t, t_0) = \left(\frac{t - t_0}{30 + 0.035\,(t - t_0)}\right)^{0.3}. \tag{1.30}$$

Here f_{cm} is the mean compressive strength at 28 days (MPa), t_0 is the age at loading, t is the current age.

The drying creep coefficient is

$$\varphi_{dc}(t, t_0) = \beta_{dc}(f_{\text{cm}})\,\beta(RH)\,\beta_{dc}(t_0)\,\beta_{dc}(t, t_0), \tag{1.31}$$

with

$$\beta_{dc}(f_{cm}) = \frac{412}{(f_{cm})^{1.4}} \tag{1.32}$$

$$\beta(RH) = \left(\frac{1 - \frac{RH}{100}}{0.1 \cdot \frac{h}{100}} \right)^{1/3} \tag{1.33}$$

$$\beta_{dc}(t_0) = \frac{1}{0.1 + t_{0,\text{adj}}^{0.2}} \tag{1.34}$$

$$\beta_{dc}(t, t_0) = \left[\frac{t - t_0}{\beta_h \cdot \xi_{dc2} + (t - t_0)} \right]^{\eta(t_0)} \tag{1.35}$$

The development of drying creep with time is described by:

$$\beta_{dc}(t, t_0) = \left[\frac{t - t_0}{\beta_h \cdot \xi_{dc2} + (t - t_0)} \right]^{\eta(t_0)} \tag{1.36}$$

with:

$$\eta(t_0) = \frac{1}{2.3 + \frac{3.5}{\sqrt{t_{0,\text{adj}}}}} \tag{1.37}$$

$$\beta_h = 1.5h + 250\,\alpha_{f_{cm}} \quad \text{with} \quad \beta_h \leq 1500\,\alpha_{f_{cm}} \tag{1.38}$$

$$\alpha_{f_{cm}} = \left(\frac{35}{f_{cm}} \right)^{0.5} \tag{1.39}$$

where:

- f_{cm} is the mean compressive strength at an age of 28 days in MPa
- RH is the relative humidity of the ambient environment in %,
- $h = 2A_c/u$ is the notional size of the member in mm, where:
  - A_c is the cross-sectional area in mm^2,
  - u is the perimeter in contact with the atmosphere in mm,
- $t_{0,\text{adj}}$ is the adjusted age at loading (in days), as defined in Eq1.40.

The effect of the type of concrete on the creep coefficient of concrete may be taken into account by modifying the age at loading t_0 to $t_{0,\text{adj}}$:

$$t_{0,\text{adj}} = t_{0,\text{r}} \left[\frac{9}{2 + t_{0,\text{r}}^{1.2}} + 1 \right]^{\alpha} \geq 0.5 \text{ days} \tag{1.40}$$

where:

- $t_{0,r}$ is the age of concrete at loading in days adjusted according to Eq.1.41.
- α is a coefficient which depends on the strength development class of the concrete :
  - $\alpha = -1$ for class CS which includes 32.5 N
  - $\alpha = 0$ for class CN which includes 32.5 R and 42.5 N
  - $\alpha = 1$ for class CR which includes 42.5 R, 52.5 N and 52.5 R

The effect of elevated or reduced temperatures on the maturity of concrete may be taken into account by adjusting the concrete age:

$$t_T = \sum_{i=1}^{n} \Delta t_i \cdot \exp\left[13.65 - \frac{4000}{273 + T(\Delta t_i)}\right] \tag{1.41}$$

where:

- t_T is the temperature-adjusted concrete age which replaces t in the corresponding equations, in days.
- Δt_i is the number of days during which a temperature T prevails.
- $T(\Delta t_i)$ is the mean temperature in °C during the time period Δt_i.

Creep in concrete has historically been regarded as a serviceability issue and has mainly been investigated within the elastic domain, typically up to about 40% of the short-term compressive strength.

At these moderate stress levels ($\sigma_c/f_c \leq 0.4$), the creep response remains predominantly linear, characterized by gradual deformation in the absence of significant microcracking. However, once this stress threshold is exceeded, microcracks begin to initiate and propagate, leading to non-linear creep behavior and progressive internal damage. [6]

The *fib Model Code*, for example, provides empirical formulations to estimate both linear and non-linear creep effects for stress-to-strength ratios up to approximately 0.6, beyond which tertiary creep and failure under sustained loading tend to occur. [6]

Nevertheless, the simplified form given in Eq. 1.42 only reflects the overall time-dependent increase in creep strain and does not capture the reduction of non-linear effects with prolonged loading durations. Additionally, it assumes a uniform treatment of all creep components, thereby neglecting the specific non-linear characteristics that distinguish basic creep from drying creep. [2]

For stress levels within the range:

$$0.4\, f_{cm}(t_0) < |\sigma_c| \leq 0.6\, f_{cm}(t_0)$$

the influence of non-linearity in creep can be considered using the following expression:

$$\varphi_\sigma(t, t_0) = \varphi(t, t_0) \cdot \exp\left[1.5\,(k_\sigma - 0.4)\right] \quad \text{for } 0.4 < k_\sigma \leq 0.6 \tag{1.42}$$

where:

- $\varphi_\sigma(t, t_0)$ is the non-linear creep coefficient.
- $\varphi(t, t_0)$ is the linear creep coefficient as defined in Eq. 1.27.
- $k_\sigma = \dfrac{|\sigma_c|}{f_{cm}(t_0)}$ denotes the ratio of applied stress to mean compressive strength at age t_0.

Another formula called "affinity concept" was proposed by *Fernandez Ruiz et al.* [11] to take into account the non-linear behaviour for stress levels σ_c/f_c below 0.7 :

$$\varphi_{nl}\left(t, t_0, \frac{\sigma_c}{f_c}\right) = \eta\left(\frac{\sigma_c}{f_c}\right) \cdot \varphi_{lin}(t, t_0) \tag{1.43}$$

where :

$$\eta\left(\frac{\sigma_c}{f_c}\right) = 1 + 2\left(\frac{\sigma_c}{f_c}\right)^4 \tag{1.44}$$

It is exactly the same idea than in the *fib Model Code* [2], there is a factor which takes into account the stress/strength ratio (σ_c/f_c) multiplying the linear creep coefficient.

In this thesis, the choice was to work only with fib for modeling creep so the first Eq. 1.42 is chosen but Eq.1.44 is also completely valid and provides good results.

According to *Bockhold and Stangenberg 2004* [12], the development of inelastic strains due to material damage typically progresses through three distinct phases :

1. During the primary creep phase, which occurs immediately after the load is applied, the strain rate is initially high but gradually decreases and stabilizes over time. This first phase corresponds to the crack formation as described by *Ruiz and al.* [11].
2. This is followed by the secondary creep phase, where the strain rate remains approximately constant. This second phase corresponds to the range where crack grows in a stable way [11].
3. The third phase (at elevated stress levels) corresponds to an uncontrolled microcrack propagation up to concrete failure [11].

That is why the equations of the fib are limited to $\sigma_c/f_c = 0.6$ and the affinity concept until $\sigma_c/f_c = 0.7$ because, for higher ratios, the tertiary creep takes place.

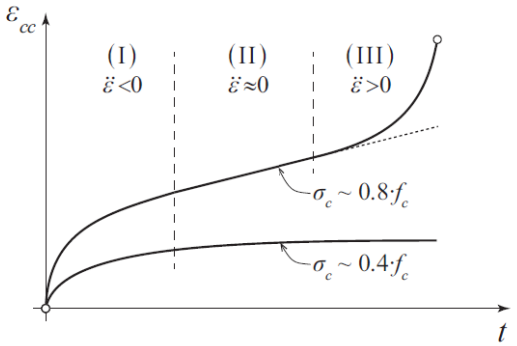

Figure 1.7: Three phases of the creep strain (adapted from [6])

As explained by *Darko Tasevski* in [6], these codes also account for the reduction of strength due to high sustained loads (ratios $\sigma_c/f_c > 0.75$ according to Fig 1.8).
This reduction of compressive strength will be discussed in Section 1.2.2.

Despite these indications, no guidelines are normally provided on how to calculate the strains at failure when tertiary creep develops (necessary to calculate potential stress redistribution and system strength) or on how to evaluate the response of concrete for variable stress levels implying nonlinear creep strains (potentially influencing the final material strength) [6]

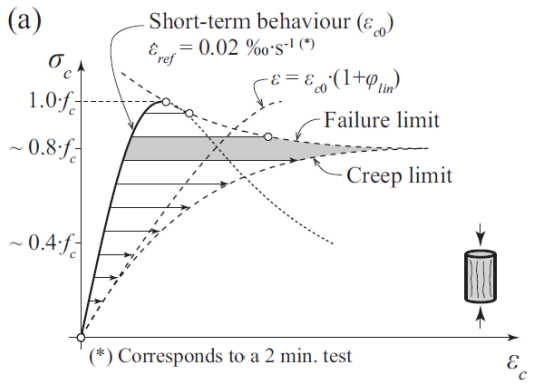

Figure 1.8: Response of concrete under uniaxial compressive stresses (adapted from [6])

Parametric study on linear creep

To better understand all these equations and how the creep coefficient works, a parametric study is done to see the influence of the different parameters of the model over the creep coefficient.

These formulas are valid for :

- Ordinary structural concrete with mean compressive strength f_{cm} = 20 to 120 MPa
- Climate conditions with a relative humidity RH = 40 to 100%
- A mean temperature in the range of T = 5°C to 30°C
- The age at loading t_0 should be at least 1 day

The formulas were implemented in a Matlab code.

Fig. 1.9 and 1.10 show the time development of the creep function for different initial times of loading t_0. Fig. 1.9 is performed for C30/35 while Fig. 1.10 for C80/95, the other inputs remain the same : RH=50%, the notional size $h_0 = 100mm$.

Fig. 1.11 is performed for C30/35 while Fig. 1.12 for C80/95 but RH=80%, the notional size remains $h_0 = 100mm$.

Fig. 1.9, 1.10, 1.11 and 1.12 show that early-age loading leads to higher creep coefficients than late-age loading, in other words, the creep coefficient decreases while the initial time of loading t_0 increases.
Then, for equal humidity conditions, the creep coefficient for low-strength concrete (C20/25) is

much more significant than high-strength concrete. In term of humidity, a higher relative humidity (RH=80%) leads to a lower creep coefficient.

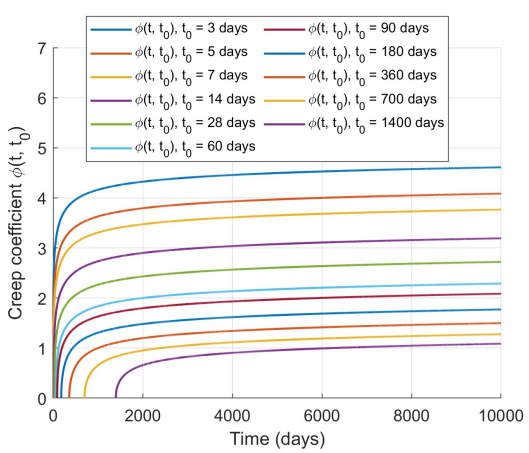

Figure 1.9: Time evolution of the creep coefficient for C30/35, RH=50%, $h_0 = 100mm$

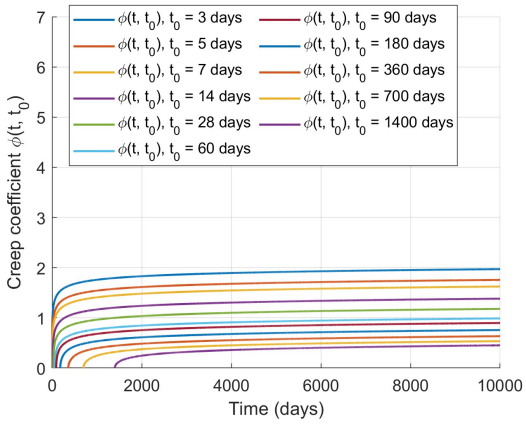

Figure 1.10: Time evolution of the creep coefficient according for C80/95, RH=50%, $h_0 = 100mm$

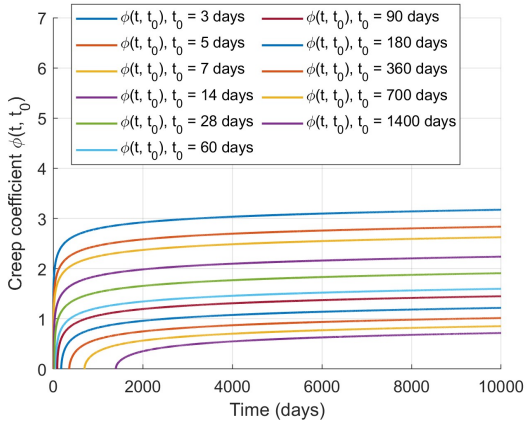

Figure 1.11: Time evolution of the creep coefficient for C30/35, RH=80%, $h_0 = 100mm$

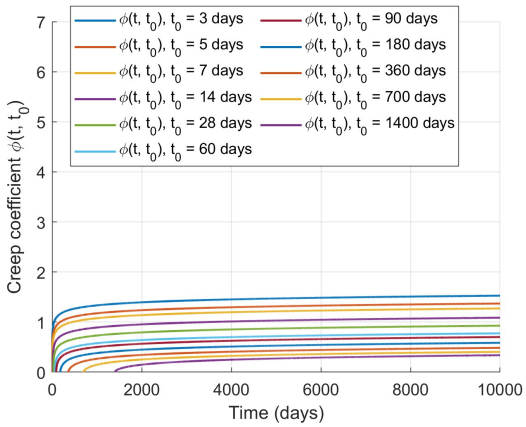

Figure 1.12: Time evolution of the creep coefficient with time for C80/95, RH=80%, $h_0 = 100mm$

Fig. 1.13 and 1.14 show the evolution of the creep coefficient calculated after 50 years with the characteristic strength f_{ck} for two different times of loading ($t_0 = 7$ days and $t_0 = 28$ days) .

The ultimate creep coefficients are typically evaluated at t=50 years after loading for ordinary buildings and at 100 years for critical structures (e.g majors bridges). These durations correspond to the design service life specified in *fib Model Code* [2]. According to the model, the provided expressions accurately predict creep development up to 50 years.

Fig. 1.13 and 1.14 confirm that creep is lower for high-strength concrete and for high relative humidity. It shows also that the difference between the two curves corresponding to different time of loading becomes smaller as the strength increases.

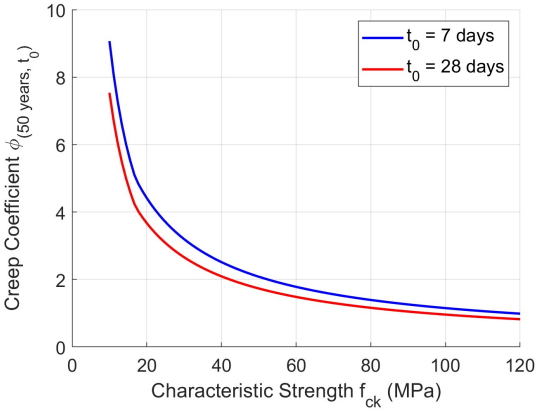

Figure 1.13: Evolution of the creep coefficient with the characteristic strength for C30/35, RH=80%, $h_0 = 100mm$

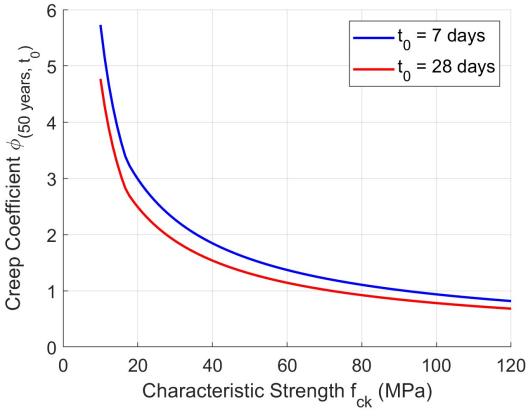

Figure 1.14: Evolution of the creep coefficient with the characteristic strength for C80/95, RH=80%, $h_0 = 100mm$

Fig. 1.15 shows the creep coefficient values after 50 years with different times of loading for two different relative humidity values and two different strength classes. Fig. 1.16 shows the creep coefficient values after 50 years with relative humidity values for two different loading times and two different strength classes.
The figures confirm again that higher concrete strength is associated with lower creep coefficient. Furthermore, the sensitivity of creep to the age of loading decreases as the strength increases. By analyzing the Fig. 1.16, the sensitivity of creep to the relative humidity decreases as strength increases.

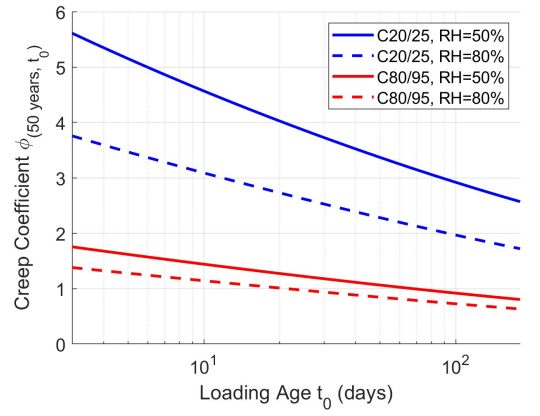

Figure 1.15: Evolution of the creep coefficient at 50 years with the loading age t_0

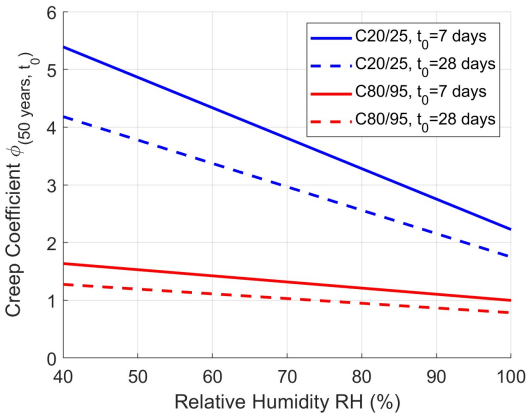

Figure 1.16: Evolution of the creep coefficient at 50 years with the Relative Humidity (RH)

Finally, Fig. 1.17 and 1.18 describe the evolution of the creep coefficient values after 50 years with the notional size for the two different strength classes and times of loading. The relative humidity is set at RH=50% for Fig. 1.17 and RH=80% for Fig. 1.18.
The sensitivity of creep to the age of loading decreases as the strength increases and creep coefficient is obviously higher with RH= 50 % than 80%.

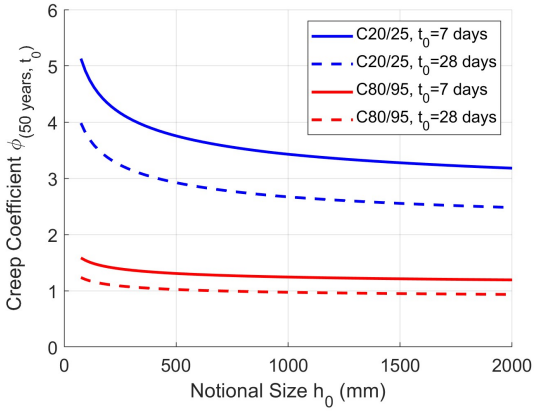

Figure 1.17: Evolution of the creep coefficient at 50 years with the notional size h_0 for $RH = 50\%$

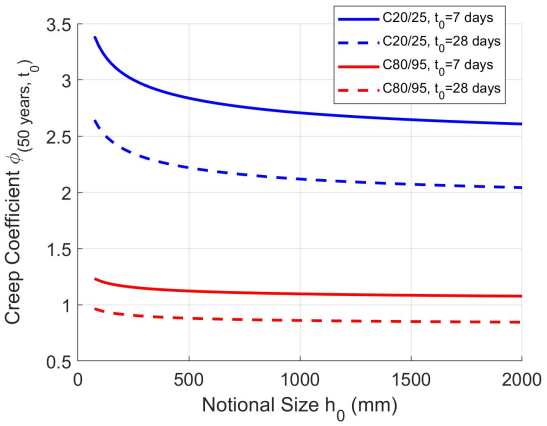

Figure 1.18: Evolution of the creep coefficient at 50 years with the notional size h_0 for $RH = 80\%$

1.2.2 Effect of creep on compressive strength

According to the *fib Model Code 2020* [2], under the effect of sustained high compressive stresses, the compressive strength of concrete tends to decrease over time due to the initiation and growth of micro-cracks. This degradation is partially offset by the strength gain resulting from ongoing cement hydration.

The combined influence of these two opposing mechanisms-damage due to long-term loading and strength development due to hydration is expressed as follows:

$$f_{cm,\text{sust}}(t, t_0) = f_{cm} \cdot \beta_{cc}(t) \cdot \beta_{c,\text{sust}}(t, t_0) \tag{1.45}$$

with:

$$\beta_{c,\text{sust}}(t, t_0) = \beta_0(t_0) + [1 - \beta_0(t_0)] \left[1 + 10^4 \left(\frac{t - t_0}{t_0}\right)\right]^{-0.1} \tag{1.46}$$

where:

- $f_{cm,\text{sust}}(t, t_0)$ is the mean compressive strength (in MPa) at time t when the concrete is subjected to a high sustained compressive stress starting from age t_0;
- $\beta_{cc}(t)$ is the time-dependent strength development factor as defined in Eq. 1.47;
- $\beta_{c,\text{sust}}(t, t_0)$ is a factor describing the strength reduction due to sustained compressive loading over time. It depends on both the duration under sustained load ($t - t_0$ in days) and the age at loading t_0 (also in days). This function is valid for $(t - t_0) > 0.015$ days (i.e., 20 minutes);
- $\beta_{t_0}(t_0)$ is a maturity-related parameter defined in Eq. 1.48;
- t_0 is the age at the beginning of loading, in days, Eq. 1.46 applies for $t_0 \geq 7$ days;
- $t - t_0$ is the duration of sustained loading, in days. For loading durations exceeding 10 years, a maximum value of $t - t_0 = 3650$ days should be adopted.

$$\beta_{cc}(t) = \exp\left[s\left(1 - \sqrt{\frac{28}{t}}\right)\right] \tag{1.47}$$

$$\beta_{t_0}(t_0) = 0.64 + 0.01 \cdot \ln(t_0), \quad \text{with } t_0 \text{ in days} \tag{1.48}$$

The graphs below illustrate how both the duration of sustained loading and the age at loading affect the evolution of concrete compressive strength. The formulation distinguishes between two main effects:

- $\beta_{\text{sust}}(t, t_0)$, which accounts for strength loss due to micro-cracking under sustained load;
- $\beta_{cc}(t)$, which represents strength gain due to continued hydration.

First, it is important to understand how these functions work separately to understand after how they work together to provide the curves on Fig. 1.23 and 1.24.

Fig. 1.19 shows the evolution of $\beta_{cc}(t)$ with the time (in log scale). A rapid increase is observed from an initial value of 0.82 and then for t= 28 days, $\beta_{cc}(28) = 1$ and finally there is an asymptotic approach towards approximately 1.22 for large t.

According to *fib Model Code* [2], s is a coefficient that depends on the cement type :

- s= 0.15 corresponds to very high early strength class concrete
- s= 0.25 corresponds to ordinary early strength class concrete
- s= 0.35 corresponds to low early strength class concrete

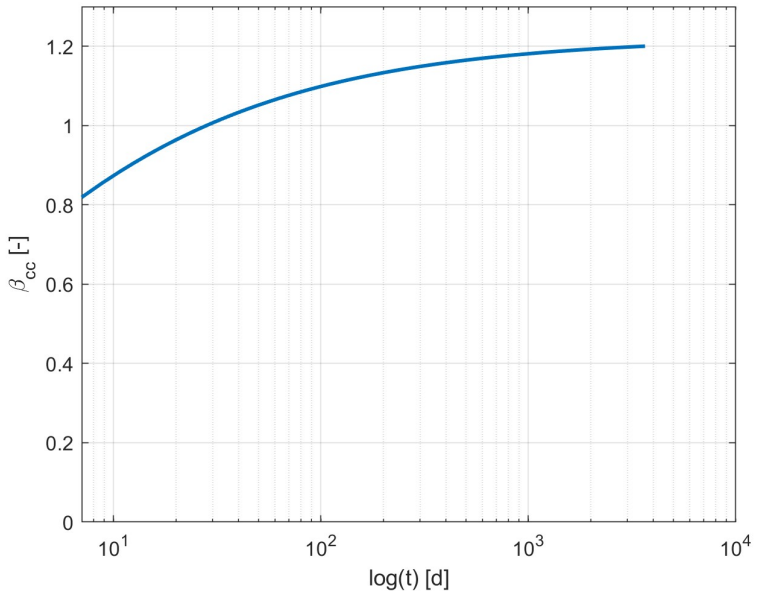

Figure 1.19: Time evolution of $\beta_{cc}(t)$

Fig. 1.20 and Fig. 1.21 show the evolution of $\beta_{c,sus}(t, t_0)$ with Δt (in log scale).

$\beta_{c,sus}(t, t_0)$ falls monotonically on a log-time scale, with the steepest decline in the first few days under load and a gradual leveling off as t grows large. Physically, that reflects rapid micro-crack growth immediately after loading, then slowing rate of additional damage.

- For $t_0 = 7$ days :
  the sustained-load factor $\beta_{c,\text{sus}}(t, t_0)$ decreases more sharply, reaching a minimum of about 0.73. This is because younger concrete is more susceptible to strength loss under long-term loading due to micro-cracking.
- For $t_0 = 28$ days:
  the minimum is higher (around 0.78), since the concrete has gained more initial strength by 28 days and thus withstands sustained stress with less damage and fewer micro-cracks.

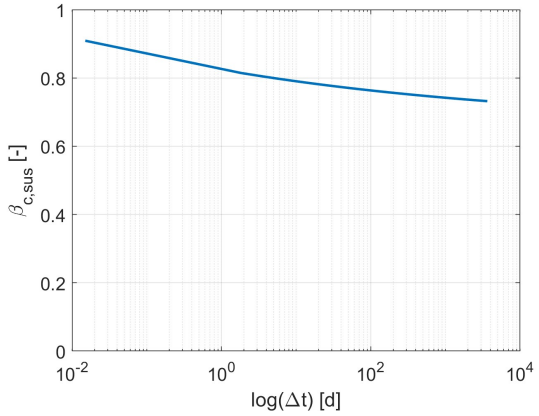

Figure 1.20: For $t_0 = 7$ days

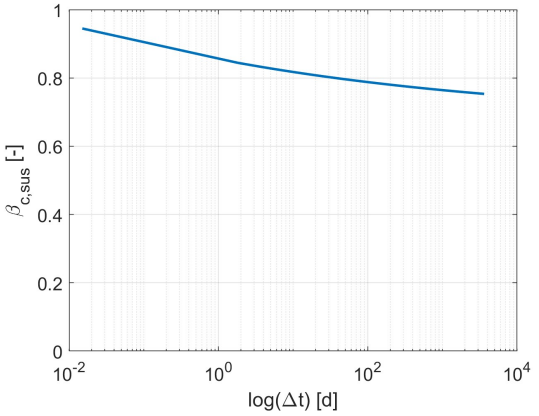

Figure 1.21: For $t_0 = 28$ days

Figure 1.22: Evolution of $\beta_{c,sus}(t, t_0)$ with $log(\Delta t)$

An analysis of the plot $f_{cm,sus} - log(\Delta t)$ based on Fig. 1.20 and Fig. 1.21 is performed :

Initially, micro-cracks caused by the applied stress dominate, leading to a reduction in strength from its starting value. It reaches a minimum when damage from prolonged loading is maximal (around $\Delta t \approx$ 10-20 days). Beyond this point, continued cement hydration gradually restores stiffness, so $f_{cm,\text{sust}}$ rises again and asymptotically approaches a plateau.

Comparison the two cases:

- For $t_0 = 7$ days the initial drop is deeper (to about $0.70\, f_{cm}$) and the recovery steeper, reflecting that younger concrete both suffers more creep damage and gains strength more rapidly through hydration.
- For $t_0 = 28$ days the minimum is shallower (around $0.83\, f_{cm}$) and the rebound more moderate, since the concrete is already more mature at loading and thus less sensitive to sustained-load degradation.

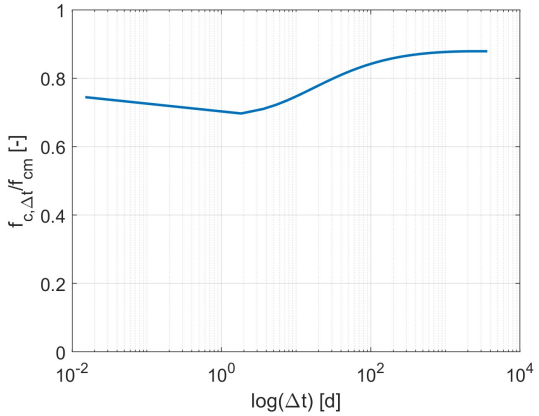

Figure 1.23: For $t_0 = 7$ days

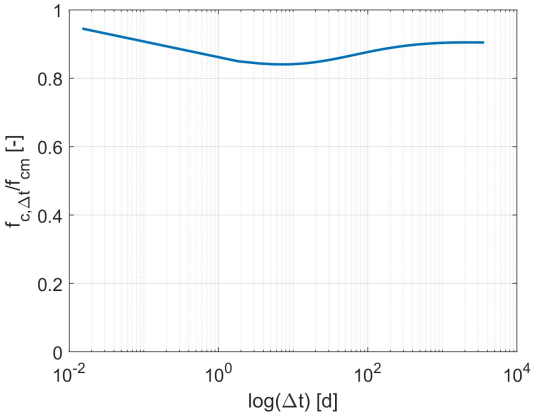

Figure 1.24: For $t_0 = 28$ days

Figure 1.25: Evolution of $f_{cm,sus}(t, t_0)$ with $log(\Delta t)$

Chapter 2

Modelling of Concrete Loading Zone (CLZ)

2.1 Formulation

2.1.1 Global approach

As shown on Fig. 2.1, the CLZ diagonal compressive stresses σ and stains ε. Within the CLZ, the axial strain is supposed to vary linearly from zero at the top face of the beam down to a maximum value ε_{max} along the bottom inclined face . The deformed geometry of the CLZ implies that ε_{max} is as a function of the CLZ displacement Δ_c as described by *B.Mihaylov* [7].

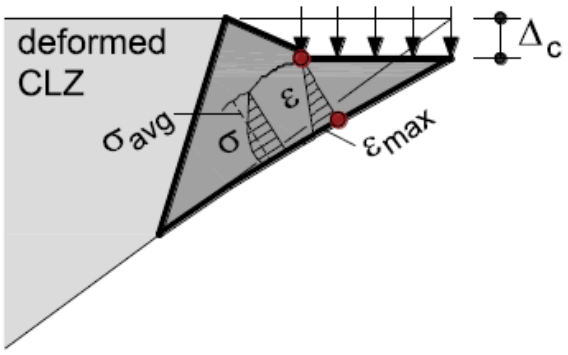

Figure 2.1: CLZ (adapted from [4])

Creep effects are then introduced by sustaining the load at the specified level $V/V_{u,0}$ over time (see Fig. 2.2) from time of loading t_0 to time t_1 which corresponds to the time when the beam is pushed up of failure, making $V/V_{u,0}$ the primary input parameter for creep assessment.

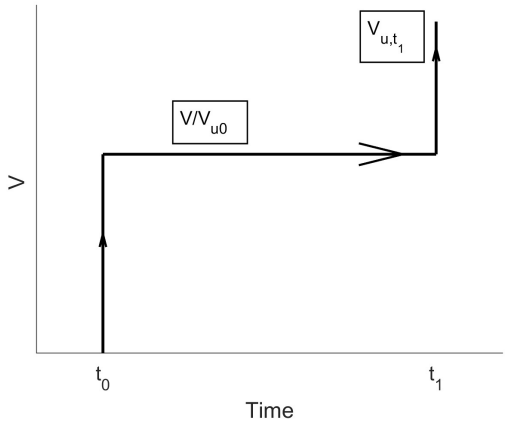

Figure 2.2: Loading with the time

It's important also to remember that the main input to compute the creep coefficient is the stress-strength ratio :

- For $\sigma_c/f_c \leq 0.4$: $\phi(t, t_0)$ is linear.
- For $0.4 < \sigma_c/f_c < 0.6$: $\phi(t, t_0, \sigma_c/f_c)$ is non-linear and depends on the ratio σ_c/f_c.

In the CLZ method, the average compressive stress σ_{avg} is evaluated according to Eq. 2.4 under short-term (no creep) conditions for each load level $V/V_{u,0}$.

Because each load level $V/V_{u,0}$ corresponds to a displacement Δ under short-term conditions as shown on Fig. 2.3, it is easy to get Δ_c because Δ is the superposition of the two kinematic modes ($\Delta = \Delta_c + \Delta_t$).
Finally, σ_{avg} for each level can be obtained by interpolation in the relationship $V_{clz} - \Delta_c$.

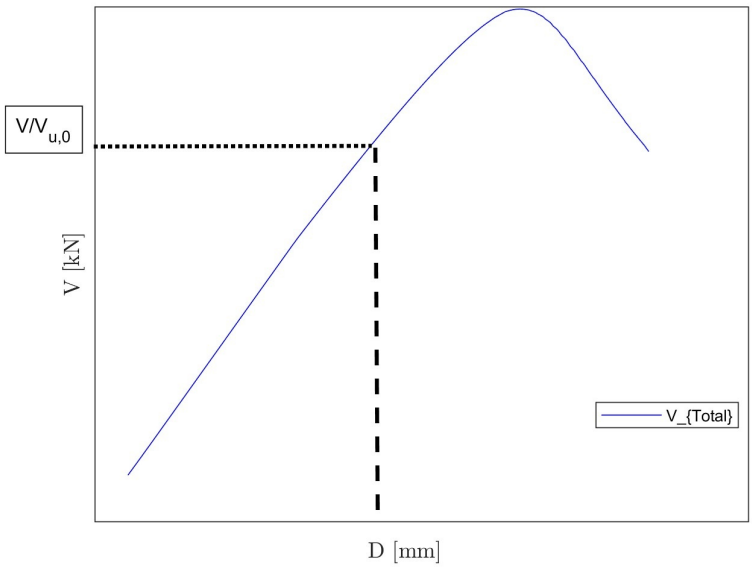

Figure 2.3: Δ corresponding to a given $V/V_{u,0}$

The resulting σ_{avg} is used to determine the creep coefficient ϕ, which depends on the stress ratio σ_{avg}/f_{cm} but when :

- $\sigma_{avg}/f_{cm} \leq 0.4$: ϕ varies linearly and is therefore independent of the value of σ_{avg} and just depends on the initial parameters to compute the creep coefficient.

Creep coefficient $\phi\big(\sigma_{avg}/f_{cm}\big)$ is obtained from *the fib Model Code* [2].

The effective secant modulus is then computed as

$$E_{c,\text{eff}} = \frac{E_c}{1 + \phi(\sigma_{avg}/f_{cm})} \tag{2.1}$$

where

$$E_c = 3320\,\sqrt{f_{cm}} + 6900$$

This reduction in stiffness modifies the CLZ stress-strain response by altering the ultimate compressive strain:

$$\varepsilon_{c,\text{creep}} = -\,\frac{f_{cm}}{E_{c,\text{eff}}}\,\frac{n}{n-1}, \tag{2.2}$$

and the constitutive law becomes

$$\sigma_{c,creep}(\varepsilon) = f_{cm}\,\frac{n\,\big(\varepsilon/\varepsilon_{c,\text{creep}}\big)}{n - 1 + \big(\varepsilon/\varepsilon_{c,\text{creep}}\big)^{\,n\,k_k}} \tag{2.3}$$

with

$$n = 0.8 + \frac{f_{cm}}{17}, \quad k_k = 0.67 + \frac{f_{cm}}{62}.$$

The resulting stress-strain curve is used to update σ_{avg} for each load level $V/V_{u,0}$.
It means that the integral is computed under the new stress-strain curve to get the new $\sigma_{avg,creep}$:

$$\sigma_{\text{avg,creep}} = \frac{\displaystyle\int_0^{\varepsilon_{\max}} \sigma_{c,creep}(\varepsilon_{c,creep})\,\mathrm{d}\varepsilon}{\varepsilon_{\max}}, \tag{2.4}$$

and the CLZ capacity V_{CLZ} is then recalculated using this σ_{avg} :

$$V_{\text{CLZ}} = \sigma_{\text{avg,creep}}\,b\,l_{b1e}\,\sin^2\!\alpha_{\text{CLZ}}. \tag{2.5}$$

2.1.2 Local approach

In this alternative formulation, the full stress distribution within the CLZ is resolved by discretizing the zone into N fibers, each characterized by its own stress σ_i and strain ε_i. As before, the global load level $V/V_{u,0}$ defines the CLZ displacement $\Delta_{c,V/V_{u,0}}$, from which the maximum fiber strain is computed:

$$\varepsilon_{\max,V/V_{u,0}} = -\frac{\Delta_{c,V/V_{u,0}} \tan(\alpha)}{3\, l_{b1e}}. \tag{2.6}$$

The strain interval $[0, \varepsilon_{\max}]$ is partitioned into N equidistant points ε_i, and the corresponding short-term stresses σ_i are obtained by interpolating the CLZ constitutive curve at each ε_i as shown on 2.4

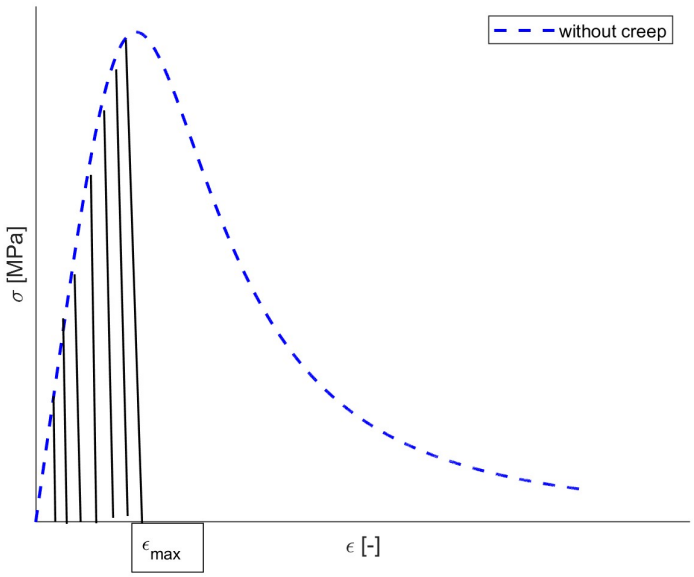

Figure 2.4: Interpolation of each single σ_i for N fibers

For each fiber, the local creep coefficient $\phi_i = \phi(\sigma_i/f_{cm})$ is evaluated for the stress σ_i found just before.

Fig 2.5 shows that numerous fibers sustain stresses exceeding the average stress σ_{avg} but also some stresses are lower than this mean value so this procedure allows to treat each stress σ_i as it has to be by computing the right creep coefficient ϕ_i.
Then, this procedure accurately captures the non-linear dependence of the creep coefficient on stress because for stresses with a ratio $0.4 < \sigma_i/f_{cm} < 0.6$, the creep coefficient is non-linear and so a higher stress σ_i will lead to a higher creep coefficient ϕ_i.

Therefore, the local effective secant modulus :

$$E_{c,\text{eff},i} = \frac{E_c}{1+\phi_i} \quad \text{with} \quad E_c = 3320\sqrt{f_{cm}} + 6900. \tag{2.7}$$

The ultimate compressive strain for each fiber becomes

$$\varepsilon_{c,\text{creep},i} = -\frac{f_{cm}}{E_{c,\text{eff},i}} \frac{n}{n-1}, \tag{2.8}$$

and the fiber constitutive law is

$$\sigma_{c,i}(\varepsilon) = f_{cm} \frac{n\,(\varepsilon/\varepsilon_{c,\text{creep},i})}{n-1+(\varepsilon/\varepsilon_{c,\text{creep},i})^{\,n\,k_k}}, \tag{2.9}$$

where

$$n = 0.8 + \frac{f_{cm}}{17}, \quad k_k = 0.67 + \frac{f_{cm}}{62}.$$

At this step, each fiber has its own stress-strain law based on its stiffness but the aim is to rebuild the global stress-strain response of the CLZ taking into account the law of each fiber.

The global CLZ stress-strain response is then reconstructed by averaging the fiber stresses at each common strain level $\varepsilon^{(j)}$:

$$\bar{\sigma}^{(j)} = \frac{1}{N} \sum_{i=1}^{N} \sigma_{c,i}\left(\varepsilon^{(j)}\right). \tag{2.10}$$

This new stress-strain curve is used to update σ_{avg} for each load level $V/V_{u,0}$:

$$\sigma_{\text{avg},creep} = \frac{\int_0^{\varepsilon_{\max}} \bar{\sigma}(\varepsilon)\,\mathrm{d}\varepsilon}{\varepsilon_{\max}} \tag{2.11}$$

and the CLZ capacity V_{CLZ} is then recalculated using Eq. 4.7 :

$$V_{\text{CLZ}} = \sigma_{\text{avg,creep}}\, b\, l_{b1e}\, \sin^2\alpha_{\text{CLZ}}. \tag{2.12}$$

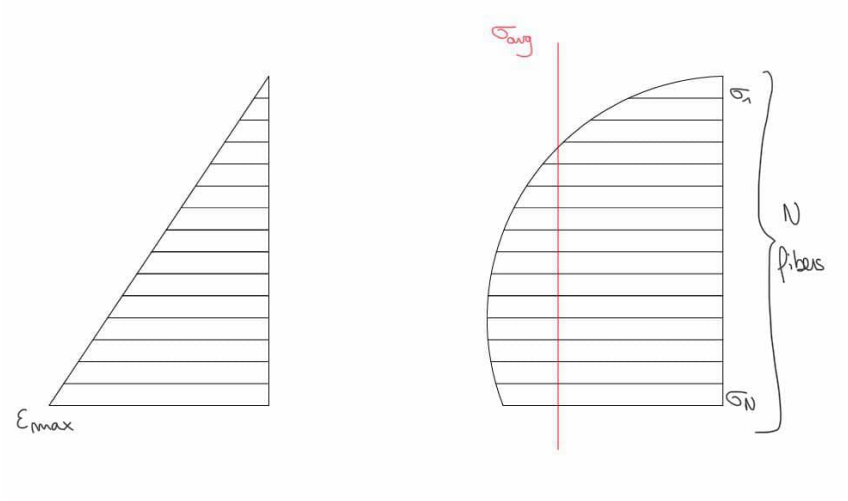

Figure 2.5: Discretization of the CLZ into N fibers for local creep analysis.

2.2 Results

2.2.1 Global approach

Results presented in this section correspond to the deep beam S1M (a/d = 1.55) tested by *Prof. Mihaylov* at the University of Toronto as part of his PhD research [13].

Its characteristic properties are listed in Table 2.1.

Parameter	Value (unit)
f_{cm}	33 MPa
h	1200 mm
d	1095 mm
a	1700 mm
b	400 mm
A_s	3060 mm^2
f_y	652 MPa
E_r	200,000 MPa
n_b	6
a_g	20 mm
ρ_v	0.1%
f_{yv}	490 MPa
E_v	200,000 MPa
l_{b1}	300 mm
l_{b2}	150 mm
V/P	0.50
l_f	0 mm
L	3400 mm
A_{st}	3060 mm^2

Table 2.1: Characteristic properties of beam S1M

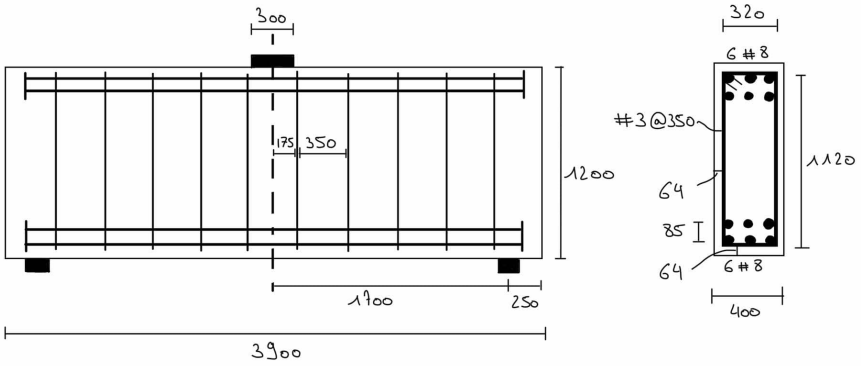

Figure 2.6: Beam S1M

Tab. 2.2 summarizes the average compressive stress σ_{avg} calculated with the process explained in Section 2.1.1 and it is illustrated on Fig. 2.7 for the three load levels we considered

Each σ_{avg} is normalized by f_{cm} and the ratio is used to compute the creep coefficient after 50 years ϕ_{50y} (if $\sigma_{avg}/f_{cm} > 0.4$).
From this creep coefficient the effective modulus $E_{c,eff}$ is calculated.

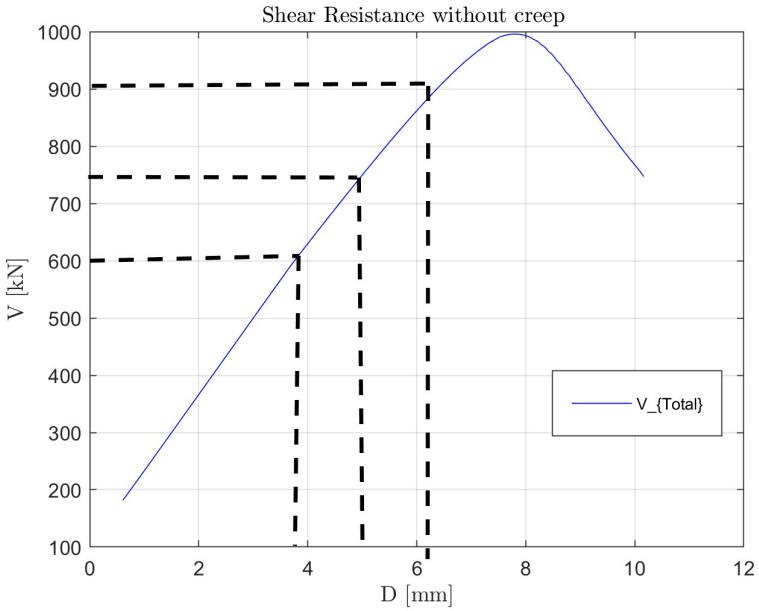

Figure 2.7: Corresponding Δ for each load level considered

The creep coefficient is computed with these inputs :

- $f_{cm} = 33$ Mpa (this is the value for S1M)
- Relative humidity (RH) = 50%
- The notional size $h = 2 \cdot A_c/u = 300\,mm$ with $A_c = 480000\,mm^2$ and $u = 3200\,mm$
- $t_{0,adj}$ (see 1.40) with a cement 32.5 R which corresponds to $\alpha = 0$

$V/V_{u,0}$	σ_{avg} [MPa]	$\sigma_{\text{avg}}/f_{cm}$	$\phi(50\,\text{yr})$	$E_{c,\text{eff}}$ [MPa]
0.6	10.9	0.33	3.7	5521
0.75	16.5	0.50	4.3	4890
0.9	21.7	0.65	5.4	4014

Table 2.2: Average sustained stress and corresponding parameters for different load levels

- For $V/V_{u,0} = 0.6$:
  $\sigma_{\text{avg}}/f_{cm} = 0.33 \leq 0.4$, indicating a linear creep regime independent of the average stress σ_{avg}.
- For $V/V_{u,0} = 0.75$:
  $\sigma_{\text{avg}}/f_{cm} = 0.50$ lies within the non-linear range (0.4-0.6), so ϕ depends on σ_{avg} and the creep coefficient is computed with Eq. 1.42.

- For $V/V_{u,0} = 0.9$:
  $\sigma_{avg}/f_{cm} = 0.65$ exceeds the valid range of Eq. 1.42; tertiary creep and uncontrolled micro-cracking occur for $\sigma/f_{cm} > 0.75$ as detailed in 1.2.1, so Eq. 1.42 is extrapolated to estimate ϕ.

As shown in Table 2.2, $E_{c,\text{eff}}$ decreases by increasing $V/V_{u,0}$ and resulting in progressive flattening of the stress-strain response (Fig. 2.8). The corresponding ultimate strains ε_c are listed in Table 2.3, which shifts the peak of the curve to the right on Fig. 2.8. In this analysis, f_{cm} remains at its initial value; therefore, the peak stress is unchanged whether creep is considered or not.

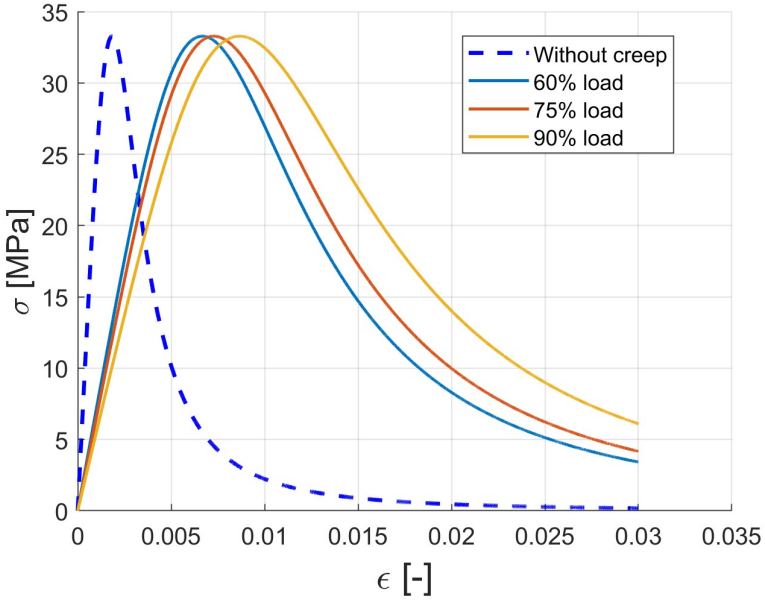

Figure 2.8: Stress-strain relationship in the CLZ without creep and with creep for the three different load levels

Load condition	ε_{c1}
No creep	0.002
$V/V_{u,0} = 0.60$	0.0073
$V/V_{u,0} = 0.75$	0.0081
$V/V_{u,0} = 0.90$	0.0097

Table 2.3: Peak strain ε_{c1} for no-creep and three sustained-load levels

Then, with this stress-strain relationship for each load level, the $V_{clz}-\Delta_c$ can be computed.

As expected, the displacement capacity of the CLZ, Δ_{cu}, increases under sustained loading, shift the $V_{clz}-\Delta_c$ curves to the right and the shear resistance of the CLZ remains the same for each curve as shown on Fig. 2.9.

Tab. 2.4 summarizes the computed values of Δ_{cu} for each load level. Notably, the peak displacement increases from 1.8 mm (no creep) to:

$$6.44 \text{ mm at } V/V_{u,0} = 0.6 \quad (\times 3.6),$$
$$7.37 \text{ mm at } V/V_{u,0} = 0.75 \quad (\times 4.1),$$
$$9.07 \text{ mm at } V/V_{u,0} = 0.9 \quad (\times 5.0).$$

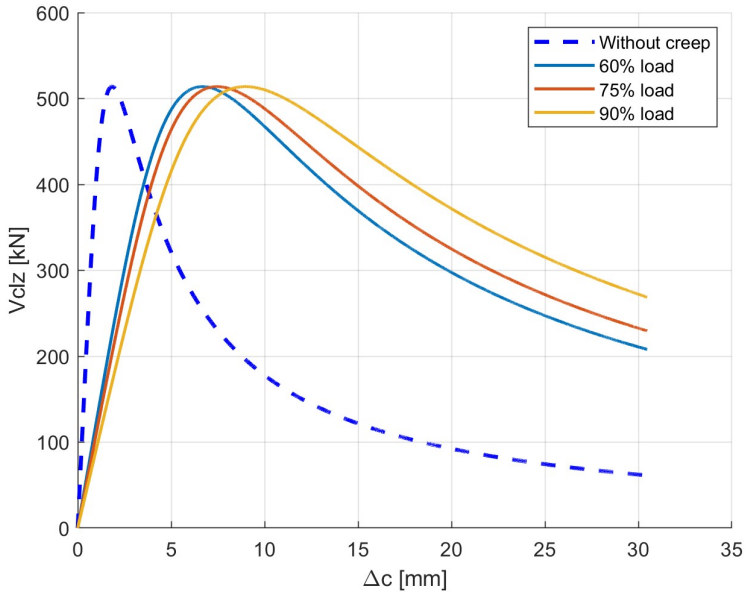

Figure 2.9: $V_{clz} - \Delta_c$ without creep and for the three different load levels

Load condition	Δ_{cu} [mm]
No creep	1.8
$V/V_{u,0} = 0.60$	6.44
$V/V_{u,0} = 0.75$	7.37
$V/V_{u,0} = 0.90$	9.07

Table 2.4: Displacement capacity $\Delta_{cu}$for no-creep and three sustained-load levels

2.2.2 Local approach

As explained in Section 2.1.2, the full stress distribution within the CLZ is resolved by discretizing the zone into N fibers, each characterized by its own stress σ_i and strain ε_i.

Local fiber stresses σ_i (MPa) for $N = 20$ fibers at sustained load levels $V/V_{u,0} = 0.60, 0.75, 0.90$ are reported in Tab. 2.6. In reality, minimum 50 fibers are used but here the aim is to show the values of the stesses an so it is easier for the reading to take less fibers.

- Stresses exceeding $0.4\, f_{cm}$ (non-linear creep regime) are highlighted in orange.

- Stresses exceeding 0.6 f_{cm} (beyond *fib Model Code* range) are highlighted in red.

The proportion of fibers for the different important ranges of stresses ar reported in Tab. 2.5. A substantial proportion of fibers lies outside the recommended range as shown in the last column of Tab. 2.5, necessitating extrapolation of Eq. 1.42 despite its underestimation of tertiary creep effects.

	% of fibers with 0.4< σ_i < 0.6	% of fibers with σ_i > 0.6
$V/V_{u,0} = 0.60$	30	10
$V/V_{u,0} = 0.75$	20	40
$V/V_{u,0} = 0.90$	15	60

Table 2.5: Analysis of the stresses reported in Tab. 2.6

$V/V_{u,0} = 0.60$	$V/V_{u,0} = 0.75$	$V/V_{u,0} = 0.90$
0.0	0.0	0.0
1.2	1.8	2.7
2.3	3.6	5.5
3.5	5.5	8.2
4.7	7.3	10.9
5.8	9.1	13.6
7.0	10.9	16.2
8.2	12.7	18.8
9.3	14.4	21.2
10.5	16.2	23.5
11.6	17.9	25.6
12.8	19.5	27.5
13.9	21.2	29.2
15.0	22.7	30.6
16.1	24.2	31.7
17.2	25.6	32.5
18.3	26.8	33.0
19.4	28.0	33.3
20.4	29.1	33.2
21.4	30.1	33.0

Table 2.6: Local fiber stresses σ_i (MPa) for $N = 20$ fibers at sustained load levels

The creep coefficient after 50 years, $\phi_{50,i}(t, t_0)$, was computed for each fiber.

The creep coefficient is computed with these inputs :

- $f_{cm} = 33$ Mpa (this is the value for S1M)
- Relative humidity (RH) = 50%
- The notional size $h = 2 \cdot A_c/u = 300\,mm$ with $A_c = 480000\,mm^2$ and $u = 3200\,mm$
- $t_{0,adj}$ (see 1.40) with a cement 32.5 R which corresponds to $\alpha = 0$

The stress-strain and V_{CLZ}-Δ_c responses were reconstructed following the procedure in Section 2.1.2.

Fig. 2.10 and 2.11 illustrate these responses.

At load levels of 75 % and 90 %, fiber-level creep analysis reveals a reduction in compressive strength within the CLZ, confirming that localized creep consideration induces strength loss.
The shear resistance decreases more markedly at 90 % loading, consistent with the presence of fibers approaching the concrete strength as reported in Tab. 2.6.

Tab. 2.7 summarizes the ultimate compressive strains ε_{c1} and corresponding peak stresses f_c for each loading condition.
Compared to the global approach (Tab. 2.3), the ultimate strain increases from 0.0073 to 0.0075 at 60 % loading, from 0.0081 to 0.0085 at 75 %, and from 0.0097 to 0.0089 at 90 %. So, there is an increase in the values of the ultimate strain ε_{c1} by using the local approach.

Compared to the short-term loading (without creep), the peak stress decreases by :

- 1 % at $V/V_{u,0} = 0.60$
- 5 % at $V/V_{u,0} = 0.75$
- 20 % $V/V_{u,0} = 0.90$

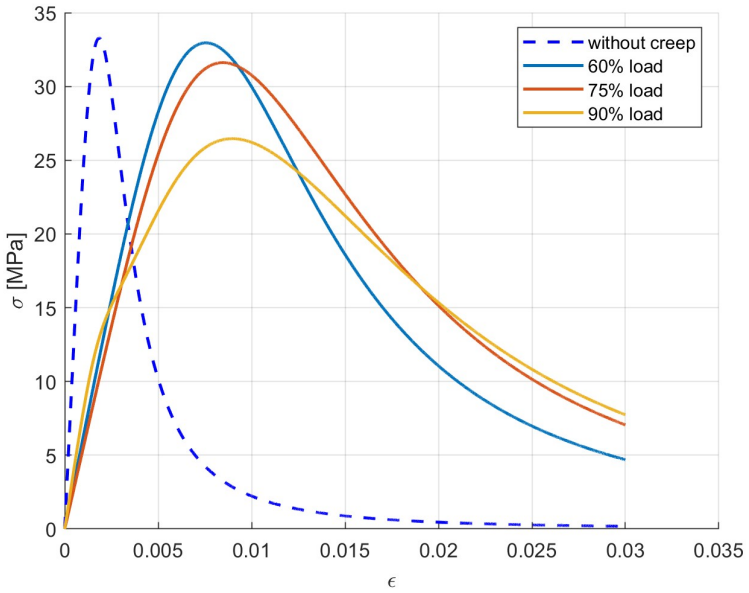

Figure 2.10: Stress-strain response after local creep analysis

Load condition	ε_{c1}	f_c [MPa]
Short-term (no creep)	0.0020	33.2
$V/V_{u,0} = 0.60$	0.0075	32.9
$V/V_{u,0} = 0.75$	0.0085	31.6
$V/V_{u,0} = 0.90$	0.0089	26.4

Table 2.7: Ultimate strain ε_{c1} and peak stress f_c for sustained-load conditions

Fig. 2.11 and Tab. 2.8 show the displacement capacity Δ_{cu} and maximum shear resistance $V_{CLZ,\max}$ obtained from the local creep model.

Compared to the short-term values, Δ_{cu} increases from 1.8 mm to :

- 7.6 mm at 60 % loading
- 8.9 mm at 75 % loading
- 9.2 mm at 90 % loading

The shear resistance decreases by :

- 1 % at $V/V_{u,0} = 0.60$
- 3 % at $V/V_{u,0} = 0.75$
- 14 % at $V/V_{u,0} = 0.90$.

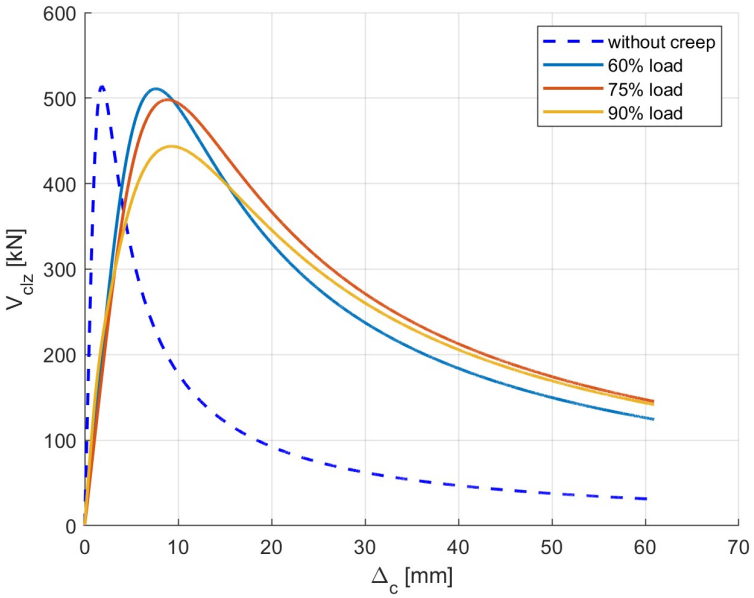

Figure 2.11: V_{CLZ}-Δ_c response after local creep analysis

Load condition	Δ_{cu} [mm]	$V_{CLZ,\max}$ [kN]
Short-term (no creep)	1.8	513
$V/V_{u,0} = 0.60$	7.6	510
$V/V_{u,0} = 0.75$	8.9	498
$V/V_{u,0} = 0.90$	9.2	443

Table 2.8: Displacement capacity Δ_{cu} and shear resistance $V_{CLZ,\max}$ after local creep analysis

To account for fibers with stresses exceeding $0.75\,f_{cm}$, Eq.1.45 from *the fib Model Code 2020* was applied to reduce the local compressive strength.
Fig. 2.12 and Tab. 4.25 show the resulting V_{CLZ}-Δ_c responses and numerical values.

The shear resistance decreases by :

- 5 % at at $V/V_{u,0} = 0.75$
- 17 % at $V/V_{u,0} = 0.90$

while remaining unchanged at $V/V_{u,0} = 0.60$, consistent with the absence of fibers beyond the threshold.
Such reductions in shear resistance at $V/V_{u,0} = 0.75$ and 0.90 are consistent with the presence of fibers whose stresses exceed the threshold :

$$0.75\,f_{cm} = 0.75 \times 33\,\text{MPa} = 24.75\,\text{MPa},$$

as shown in Tab. 2.6.

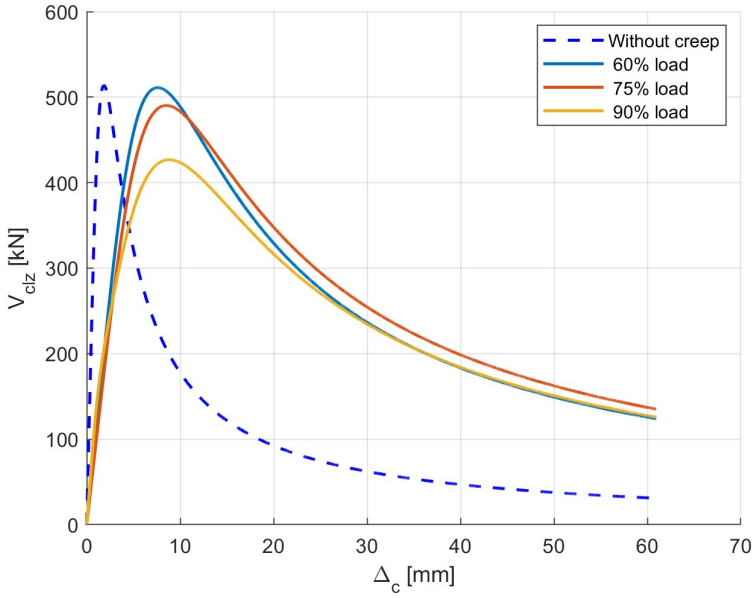

Figure 2.12: V_{CLZ}-Δ_c response including high-stress strength reduction

Load condition	Δ_{cu} [mm]	$V_{CLZ,\max}$ [kN]
Short-term (no creep)	1.8	513
$V/V_{u,0} = 0.60$	7.5	510
$V/V_{u,0} = 0.75$	8.6	490
$V/V_{u,0} = 0.90$	8.9	426

Table 2.9: Displacement capacity Δ_{cu} and shear resistance $V_{CLZ,\max}$ after high-stress strength reduction

Chapter 3

Modelling of Aggregate Interlock

3.1 Formulation

To compute the aggregate interlock component, there are 6 inputs :

1. Concrete strength : f_c
2. Maximum nominal size of the coarse aggregate : a_g
3. Crack slip : s
4. Crack width : w
5. The number of springs

The function follows the steps described in the section 1.1.3 and then gives at the end the shear component.

In this section, the aggregate interlock will be discussed out of the 2PKT model and the aim is to see the evolution of the shear resisted by aggregate interlock with the crack slip.
As it was done in the previous section for the CLZ, two different approaches will be studied :

1. Global approach
2. Local approach

Global Approach

As explained in the background, each spring has an inclination angle θ_i, carries a stress $\sigma_{\text{con},i}$, and undergoes a relative opening $w_{q,i}$. For a given slip and crack width, a constitutive relation $\sigma_{\text{con}} = f(w_q)$ is obtained (see Fig. 3.1).

In the first, simplified approach, the creep coefficient ϕ is taken to be the same for all springs because the linear creep coefficient is computed (i.e., independent of the local stress level $\sigma_{\text{con}}/f_{cy}$). Consequently, ϕ reduces the stiffness of every spring by the same factor. Concretely, the original (elastic) slope of each constitutive law is

$$\text{slope} \;=\; \frac{f_{cy}}{w_{\text{lim}}}\,, \tag{4.1}$$

where

- f_{cy} is the elastic limit stress of the concrete,

- w_{lim} is the crack width at which the behavior transitions from elastic to perfectly plastic.

Introducing creep reduces this slope to

$$\text{slope}_{\text{eff}} \;=\; \frac{\dfrac{f_{cy}}{w_{\text{lim}}}}{1+\phi}\,. \tag{4.2}$$

This is analogous to how, in the CLZ model, the creep coefficient is applied to the concrete modulus of elasticity E_c, which itself is the slope of the stress-strain curve.

Once $\text{slope}_{\text{eff}}$ is known, the local stress of each spring is computed as

$$\sigma_{\text{con},i} \;=\; \min\!\big(\text{slope}_{\text{eff}}\; w_i\,,\; f_{cy}\big)\,.$$

Because ϕ is uniform, all springs share the same reduced slope. Those springs, whose elastic response would exceed f_{cy}, instead remain capped at $\sigma_{\text{con},i} = f_{cy}$, so creep no longer affects them beyond that point.

Fig. 3.1 illustrates how the creep coefficient progressively reduces the slope over time. Some springs marked by red crosses have already reached the plateau at f_{cy}; for those, further creep-induced softening has no effect.

Local approach

Then, the idea is to account for the stress supported by each spring. It is the same approach as for the CLZ, in a first time to use a general approach to apply the creep coefficient and then to try to work more in detail in the model to find a local approach.

First, the analysis is performed without creep. Each level of loading that $V/V_{u,0}$ corresponds to a specific slip. As shown on Fig. 3.1, for each level considered (60%, 75 % and 90% of the total shear resistance $V_{u,0}$)), correspond a given displacement.

In the 2PKT model, the slip is related to the displacement Δ_c :

$$s = \Delta_c \sin\alpha_1 \tag{3.1}$$

In this section, the effect of creep is studied alone on aggregate interlock so a relation between the slip and the crack-width has to be set. The basic case is crack-width equals to slip.

With crack-width (w) = slip, the Contact Density Model introduced in Section 1.1.3, computes σ_{con} for this slip and so for this level of loading. This vector is used to compute a vector ϕ and so each $\sigma_{con,i}$ (from each spring) gives a different ϕ_i because in this case the creep coefficient ϕ_i depends on the ratio $\sigma_{con,i}/f_{cy}$.

For the same reasons as in the CLZ, this local approach allows to take into account the non-linear behaviour for high stresses of the creep coefficient. In this case, it depends on the ratio $\frac{\sigma_{con}}{f_{cy}}$ and not $\frac{\sigma}{f_{cm}}$ as in the CLZ.

Then, to get the V_{ci}-slip plot, it is necessary to use the Contact Density Model for each value of slip, in order to have at the end the shear component t (or v_{ci}) which allows to compute the V_{ci}

associated to this slip.

It is exactly the same process as in the linear way. The equation 3.2 remains the same but now slope_{eff} is a vector because it includes each single slope for each single spring computed with each single ϕ_i :

$$\text{slope}_{eff,i} = \frac{(\frac{f_{cy}}{w_{lim}})}{1+\phi_i} \tag{3.2}$$

And then :

$$\sigma_{con,i} = \min\Big(\text{slope}_{eff,i}\, w_i,\ f_{cy}\Big) \tag{3.3}$$

This vector is then used to compute the shear component t as described in **??** and then V_{ci} (**??**).

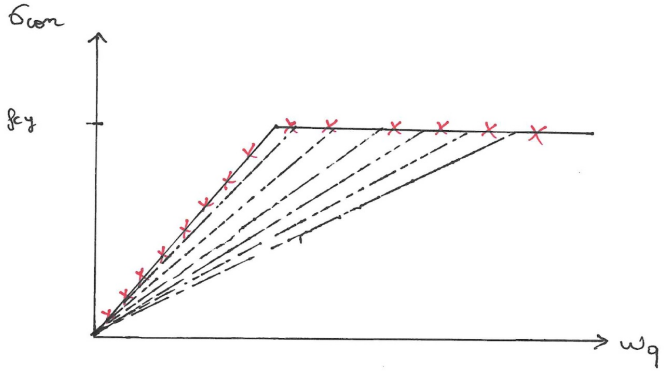

Figure 3.1: Elastic-perfectly plastic $\sigma_{con} - w_q$ relationship

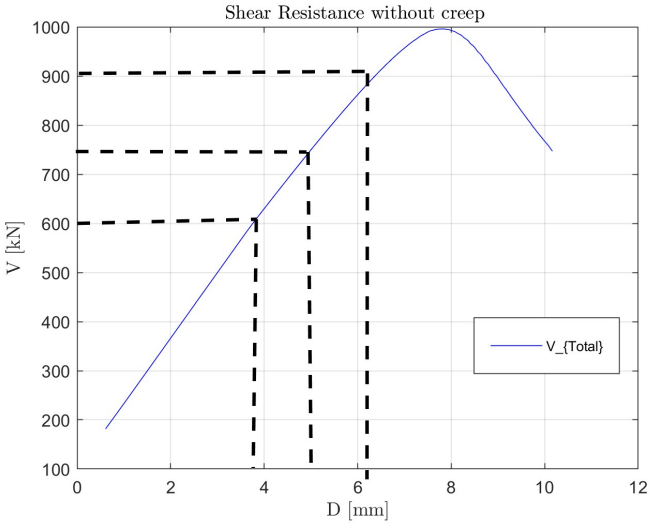

Figure 3.2: Δ corresponding to different load levels

3.2 Results

3.2.1 w = slip

Global approach

In this first case, the crack width is taken equal to the slip.

This analysis is made with the parameters of the beam "S1M" as for the CLZ. The parameters useful for this section are recalled just below.

1. Concrete strength : $f_{cm} = 33$ Mpa
2. Maximum nominal size of the coarse aggregate : $a_g = 20$ mm
3. The number of springs : $N = 400$

Fig. 3.3 shows the evolution of V_{ci} with the slip when a linear creep coefficient is applied and so it doesn't depend on the level of loading.
First, it is important to understand the global behaviour of these curves. In both cases, there is a first steep increase because the crack faces interlock tightly : even a tiny amount of slip mobilizes large shear traction.
Progressively, the crack opens more and so the increase of shear becomes smaller and V_{ci} reaches its peak when the interlock effect is maximal.
After that, the crack opens too much and so the edges slide more than lock to provide the shear component.

The initial stiffness is smaller for the case with creep. It makes sense because as described in Eq. 4.2 the slope is reduced with the creep coefficient and this slope is applied to all the springs so it decreases the global stiffness.

Therefore, it leads to a shift of the peak but also decreases the value of the resistance $V_{ci,max}$. In fact, as reported in Table 3.1, the shear resistance with creep is equal to 513 kN so it represents a decrease of $\approx 5\%$ compared to the shear resistance without creep. As mentionned, the peak also moves from 1.4 mm to 1.8 mm.

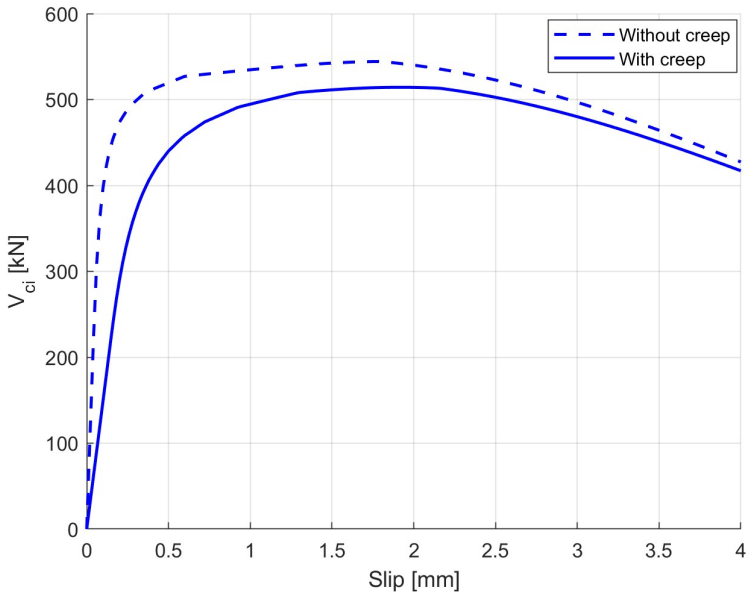

Figure 3.3: Evolution of V_{ci} with slip for w=slip

	$slip_u$ [mm]	$V_{ci,max}$ [kN]
No creep	1.4	538
Creep	1.8	513

Table 3.1: Slip capacity and shear resistance by aggregate interlock

Local approach

Fig. 3.4 shows the evolution of V_{ci} with the slip, without creep and with creep for three load levels (0.6 $V_{u,0}$,0.75 $V_{u,0}$, 0.9 $V_{u,0}$). Here as explained in 3.1, each load level corresponds to a given slip and a given σ_{con} vector where each single $\sigma_{con,i}$ is used to compute the creep coefficients ϕ_i and then these ϕ_i are applied to change locally the stiffness of each spring in the Contact Density Model.

The results reported in Tab. 3.2 are interesting because they show again (as for the CLZ) that by considering each stress separately and by applying the creep coefficient locally, the shear resistance by aggregate interlock decreases with creep effect.

In fact, the values of $V_{ci,max}$ are reported in Tab. 3.2 and for 0.6 $V_{u,0}$, there is a decrease of $\approx 6\%$, for 0.75 $V_{u,0}$ it is $\approx 9\%$ and finally for 0.9 $V_{u,0}$ it is $\approx 10\%$.

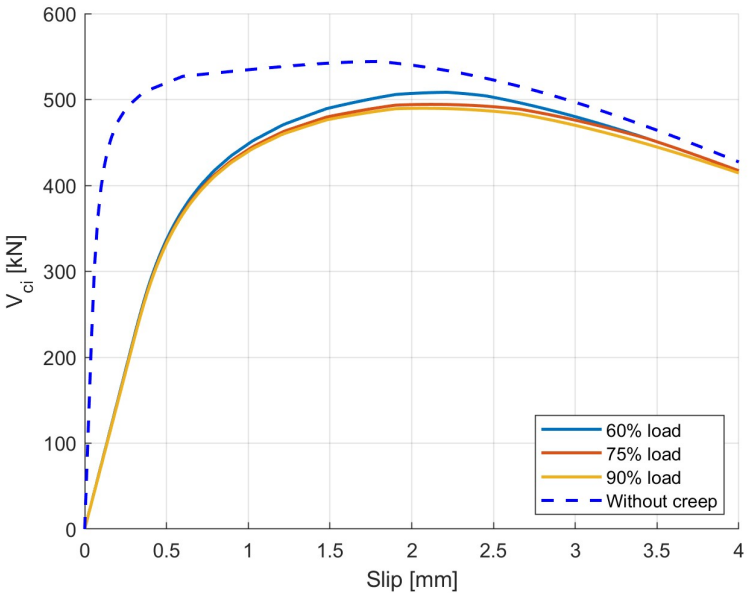

Figure 3.4: Evolution of V_{ci} with slip for w=slip

Load condition	slip$_u$ [mm]	$V_{ci,max}$[kN]
No creep	1,4	538
$V/V_{u,0} = 0.60$	2.2	507
$V/V_{u,0} = 0.75$	2.1	493
$V/V_{u,0} = 0.90$	2.1	488

Table 3.2: Slip capacity and shear resistance by aggregate interlock

3.2.2 w = 0.5 slip

First, by analyzing only the absolute shear capacity without creep,$V_{ci,max} = 538$ kN for w=slip and $V_{ci,max} = 872$ kN for w=0.5 slip.

Assuming a smaller crack-width for the same slip significantly increases the interlock capacity because narrower gaps bring aggregate "teeth" into contact and more micro-contacts mobilize more shear resistance. In fact, the local pressure is higher and therefore it increases the contact stress and friction on each asperity.

When the crack is wide, a few big contact spots between the aggregates hit their maximum stress f_{cy} almost immediately and once they can't hold any more, the rest of the crack just slips freely.

If the crack is narrower, those same spots don't max out right away. Instead, many small contacts share the load and only gradually reach their grip limit. So extra resistance out of the crack surface is squeezed longer and the crack as a whole carries more shear before everything finally gives way.

The values of $V_{ci,max}$ accounting creep for the three load levels are reported in Tab. 3.3. From Fig. 3.5 and from Tab.3.3, it is easy to see that the creep effect is much less important in this case than for w=slip.
In fact, compared to the value without creep, there there is a decrease of $\approx 2\%$ for $V/V_{u,0} = 0,60$, $\approx 2\%$ for $V/V_{u,0} = 0,75$ and $\approx 3\%$ for $V/V_{u,0} = 0,90$.

The comparison in term of loss of resistance between the two cases is made in Tab. 3.4. It is clear that creep has clearly a bigger impact on shear resistance for the case w=slip.

It can be explained by the fact that with lower crack-width, many of the local stresses are pushed right up against their limit f_{cy} and as explained before with Eq. 3.2 and Eq. 3.3, the creep acts on the springs which are still in the elastic/linear portion of the curve. In contrast, for w=slip, more micro-elements are operating in this linear part (below f_{cy}) so a reduction of stiffness directly scales down every local stress $\sigma_{con,i}$.

To illustrate this explanation, it can be very interesting for one fixed value of the slip (slip=1.5 mm) to see how many springs reached the plateau/the limit f_{cy} for each case and compare these numbers.
On Fig. 3.6 and Fig.3.7, the red dots represent the springs that reached the upper bound f_{cy}. It is clear by looking at these figures that the case "w=0.5 slip" possesses more springs at the limit

f_{cy}. It is also important to precise that these plots correspond to the load level $V/V_{u,0} = 0.9$. By doing that the code is run with N = 100 springs to see easily the dots on the plot.
Exactly 21 springs reached the limit for w=slip and 30 for w=0.5 slip.

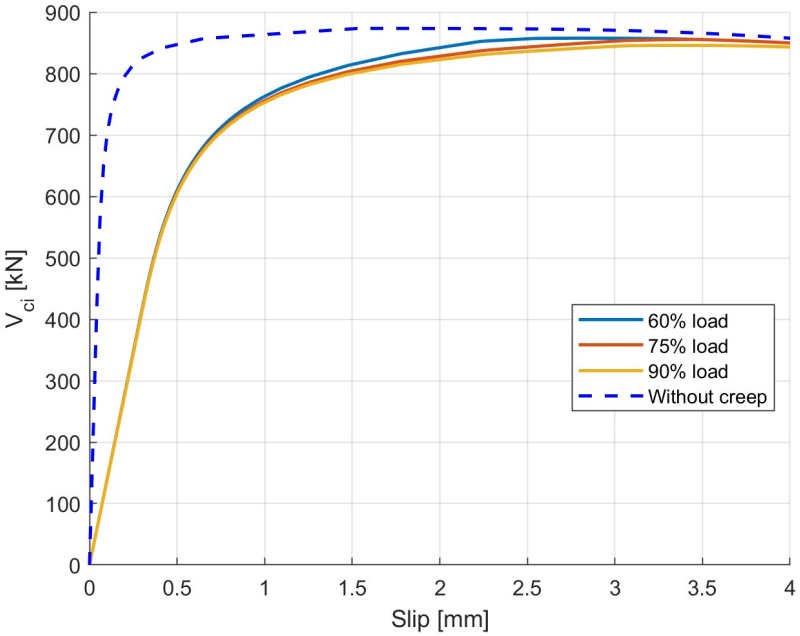

Figure 3.5: Evolution of V_{ci} with slip for w=0.5 slip

Load condition	$V_{ci,max}$ [kN]
No creep	871
$V/V_{u,0} = 0.60$	856
$V/V_{u,0} = 0.75$	855
$V/V_{u,0} = 0.90$	845

Table 3.3: Shear resistance by aggregate interlock

	w = slip	**w = 0.5 slip**
$V/V_{u,0} = 0.60$	-6%	-2%
$V/V_{u,0} = 0.75$	-9%	-2%
$V/V_{u,0} = 0.90$	-10%	-2%

Table 3.4: Comparison of the two cases

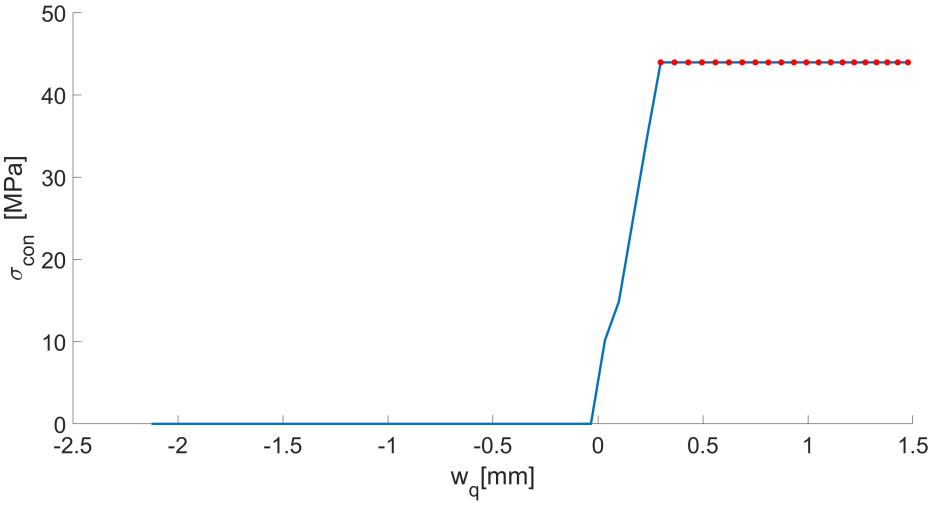

Figure 3.6: Springs that reached f_{cy} for w=slip , slip = 1.5 mm and for $V/V_{u,0} = 0.9$

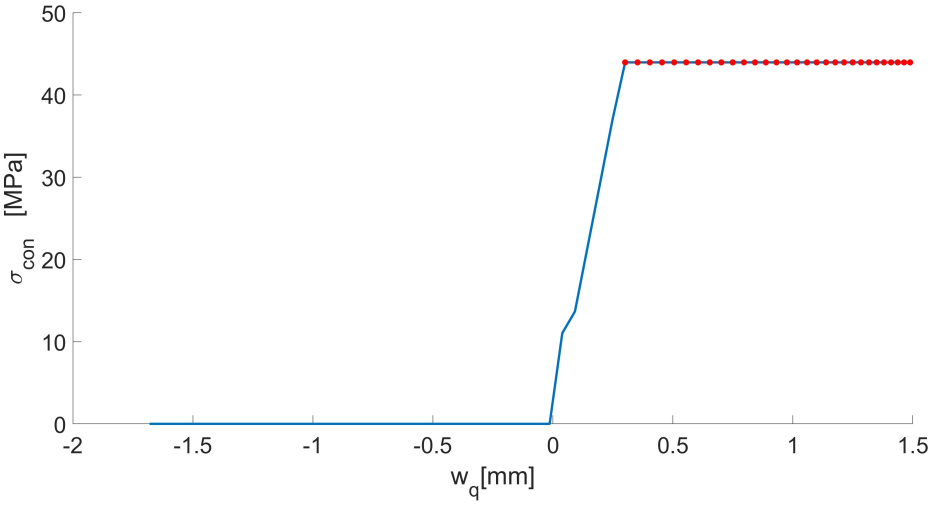

Figure 3.7: Springs that reached f_{cy} for w= 0.5 slip , slip = 1.5 mm and for $V/V_{u,0} = 0.9$

3.2.3 w = 1.25 slip

A last case to confirm what was said just before but here with the crack-width greater than the slip.
First, by analyzing only the absolute shear capacity without creep : $V_{ci,max} = 538$ kN for w=slip and $V_{ci,max} = 413$ kN for w=1.25 slip.

The values of $V_{ci,max}$ accounting creep for the three load levels are reported in Tab. 3.3. From Fig. 3.8 and from Tab.3.5, it is easy to see that the creep effect is more important in this case than for w=slip.
In fact, compared to the value without creep, there is a decrease of $\approx 8\%$ for $V/V_{u,0} = 0,60$, $\approx 11\%$ for $V/V_{u,0} = 0,75$ and $\approx 12\%$ for $V/V_{u,0} = 0,90$.

The comparison in term of loss of resistance between the two cases is made in Tab.3.4. It is clear that creep has clearly a bigger impact on shear resistance for the case w= 1.25 slip.

To be complete, it can be also interesting for one fixed value of the slip (slip=1.5 mm) to see how

many springs reached the plateau/the limit f_{cy} for w=1.25 slip, in order to confirm what was said in the previous section.

On Fig. 3.9, the red dots represent the springs that reached the upper bound f_{cy}. It is clear by looking at these figures that the case w=1.25 slip possesses less springs at the limit f_{cy} than the case w=slip illustrated on Fig. 3.6. It is also important to precise that these plots correspond to the load level $V/V_{u,0} = 0.9$. By doing that, the code is run with N = 100 springs to see clearly the dots on the plot.

Exactly 21 springs reached the limit for w=slip and 30 for w=0.5 slip.

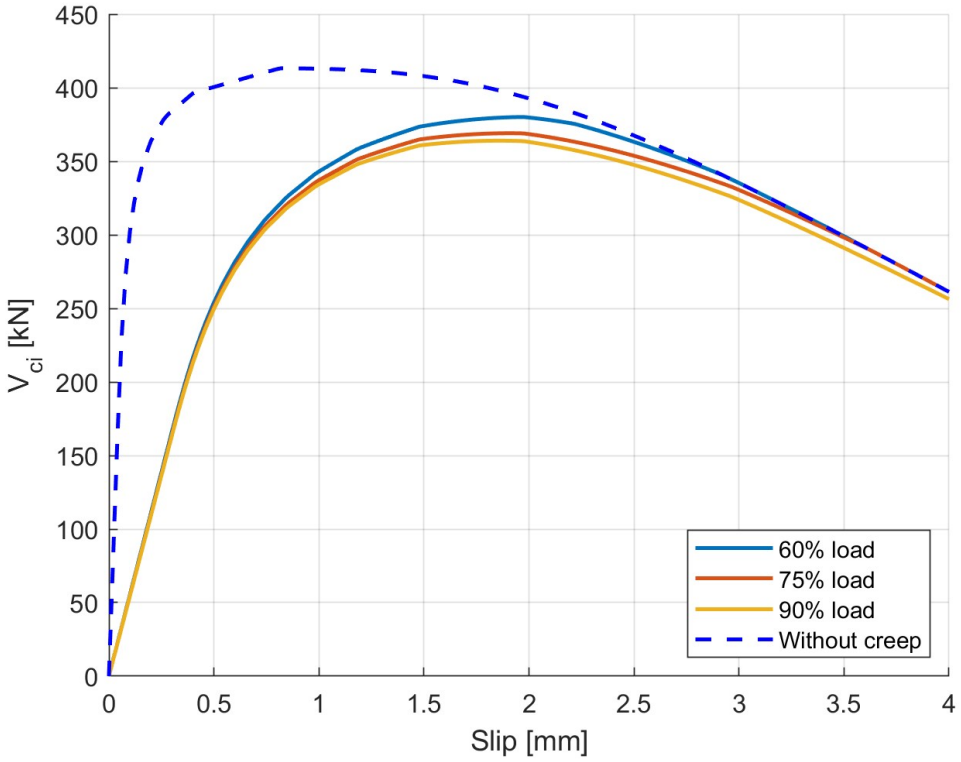

Figure 3.8: Evolution of V_{ci} with slip for w=1.25 slip

Load condition	$V_{ci,max}$ [kN]
No creep	413
$V/V_{u,0} = 0.60$	380
$V/V_{u,0} = 0.75$	369
$V/V_{u,0} = 0.90$	364

Table 3.5: Shear resistance by aggregate interlock

	w = slip	**w = 1.25 slip**
$V/V_{u,0} = 0.60$	-6%	-8%
$V/V_{u,0} = 0.75$	-9%	-11%
$V/V_{u,0} = 0.90$	-10%	-12%

Table 3.6: Comparison of the two cases

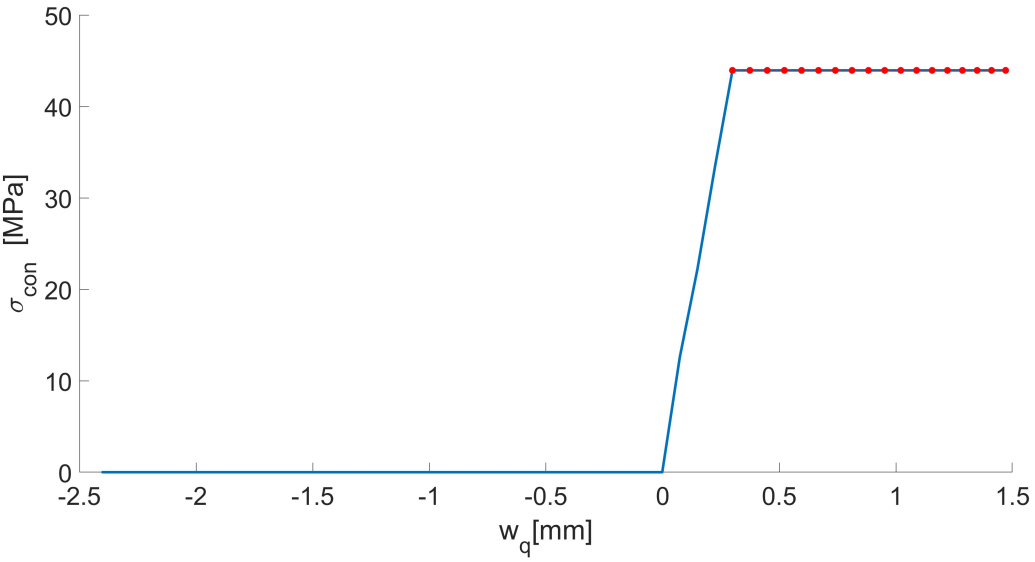

Figure 3.9: Springs that reached f_{cy} for w= 1.25 slip , slip = 1.5 mm and for $V/V_{u,0} = 0.9$

Chapter 4

Effect of creep on the behaviour of deep beams

4.1 Problem statement

In Chapters 2 and 3, the effect of creep on two principal mechanisms of the 2PKT model was examined to elucidate how the concrete strut mechanism V_{clz} and the aggregate-interlock mechanism V_{ci} behave in deep beams under sustained loading.

In this chapter, the objective is to integrate the modelling of these components and assess their combined influence over the total shear resistance. Ultimately, the goal is to determine whether sustained loading significantly alters the shear capacity of deep beams.

This chapter is organized as follows:

1. *Reference case : S1M* (all the properties of the beam are reported in Tab. 2.1)

    - Run to failure at prescribed load levels

      Each sustained load level ($0.60\,V/V_{u,0}$, $0.75\,V/V_{u,0}$, and $0.90\,V/V_{u,0}$) are maintained for a 50-year duration and each case is pushed to failure. For each load level, the reduction in total shear resistance is computed after 50 years and the individual contributions of V_{clz}, V_{ci}, and the remaining mechanisms are examined.
      Then, for each time increment within a 50 year horizon, the corresponding ultimate shear resistance is determined for the beam "S1M".

    - Constant-load service life assessment

      The difference here is that the beam is not pushed to failure immediately after sustaining the load level, but rather the load is maintained constant until failure occurs.

      One of the main goals is to plot the resulting relationship between sustained load level and time-to-failure. This curve indicates, for any given sustained load level, the expected service lifetime before shear failure. All simulations in this section will focus initially on the "S1M" specimen studied throughout this thesis. In addition to shear-capacity degradation, the time-dependent evolution of crack-width w under each load level will be examined. Even when no ultimate shear failure occurs, it is instructive to

track how w grows over time. Furthermore, other displacements such as the total mid-span deflection Δ and the displacement of the CLZ Δ_c are monitored over the same time frame in order to provide a comprehensive picture of the long-term deformation behaviour of the beam.

2. *Parametric Analysis and comparative studies*

- Shear reinforcement
  - $\rho_v = 0\%$ (S0M)
- Size of loading plate and support
  - $lb_1 = 450\,mm, lb_2 = 225\,mm$
- Size of the member (a/d)
  - a/d = 1
  - a/d = 2.28

Including creep in all the 2PKT shear model will allow to see what are the changes.

The component V_{clz} is calculated exactly as in Chapter 2 but for V_{ci} it is different because in the 2PKT, the crack-width (w) and the slip (s) depend on the two DOFs of the model : $\varepsilon_{t,avg}$ and Δ_c.

The equations 1.8 and 1.9 are restated just below because it changes compared to Chapter 3 where the crack-width was related to the slip.

$$w = \varepsilon_{t,\text{avg}} \frac{l_k}{2\sin\alpha_1} + \Delta_c \cos\alpha_1 \tag{4.1}$$

$$s = \Delta_c \sin\alpha_1 \tag{4.2}$$

The total shear resistance accounting creep is driven by V_{clz} and V_{ci} because the two other shear mechanisms V_d (shear resisted by dowel action) and V_s (shear carried by the stirrups) are not directly impacted by creep in their expressions :

$$V_d = min(K_d\,\Delta_c, \frac{n_b\,f_{ye}\,d_b^3}{3\,l_k}) \tag{4.3}$$

with : $K_d = = \frac{n_b\,12\,E_r\,\pi\,d_b^4}{64\,l_k^3}$

$$V_s = A_v\,f_v \tag{4.4}$$

with : $f_v = min(E_s\,\varepsilon_s, f_{yv})$

4.2 Reference case: S1M

4.2.1 Run to failure at prescribed load levels

First, the long-term and short-term shear responses of beam S1M are compared. The geometry and material properties remain as specified in Tab. 2.1.

For calculations of the creep coefficient, the following parameters are used:

- $f_{cm} = 33$ MPa.
- Relative humidity RH $= 50\%$.
- Notional size $h = 2A_c/u = 300$ mm, with $A_c = 480\,000\,\text{mm}^2$ and $u = 3\,200$ mm.
- Adjusted loading age $t_{0,\text{adj}}$ corresponding to cement class 42.5N (for which $\alpha = 0$).

Fig.4.1, 4.2, and 4.3 show, for each sustained load level (60%, 75%, and 90% of $V_{u,0}$), the individual contributions of the four shear-resisting mechanisms : V_{clz} (concrete-strut action), V_{ci} (aggregate-interlock), V_d (dowel action), and V_s (stirrup action) plotted against the combined displacement $\Delta = \Delta_c + \Delta_t$.

In each plot, dashed lines represent the short-term (no creep) response, while solid lines correspond to the long-term behavior after 50 years of sustained loading.

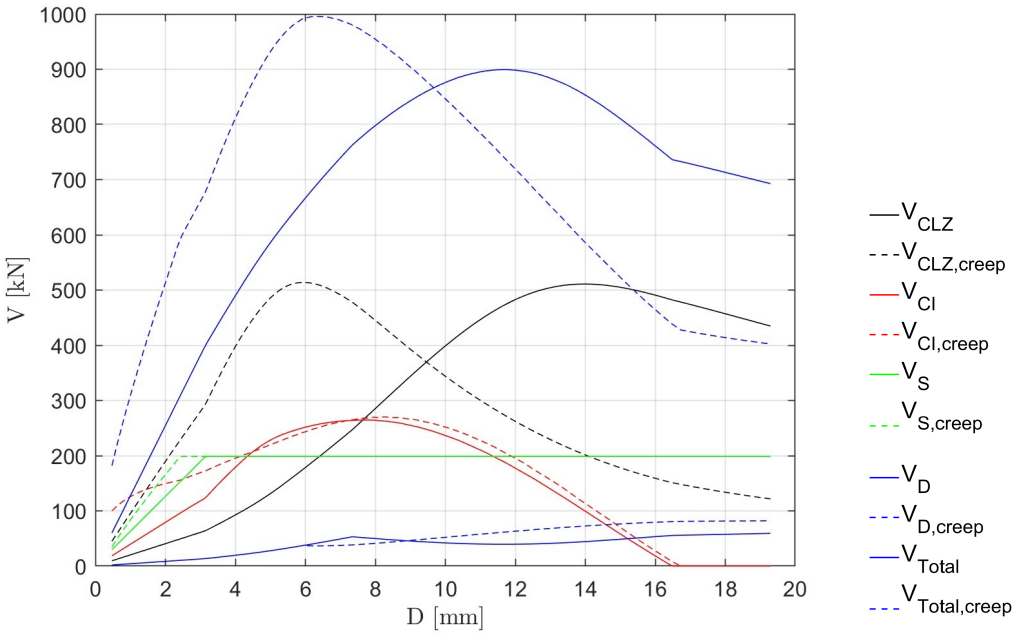

Figure 4.1: Shear-resisting contributions versus Δ for $V/V_{u,0} = 0.60$

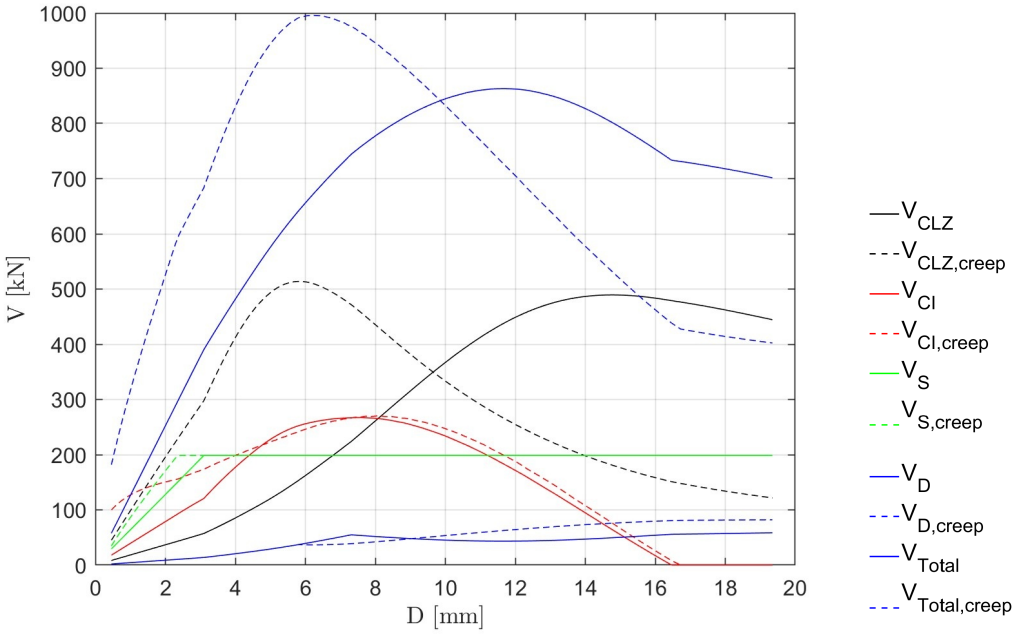

Figure 4.2: Shear-resisting contributions versus Δ for $V/V_{u,0} = 0.75$

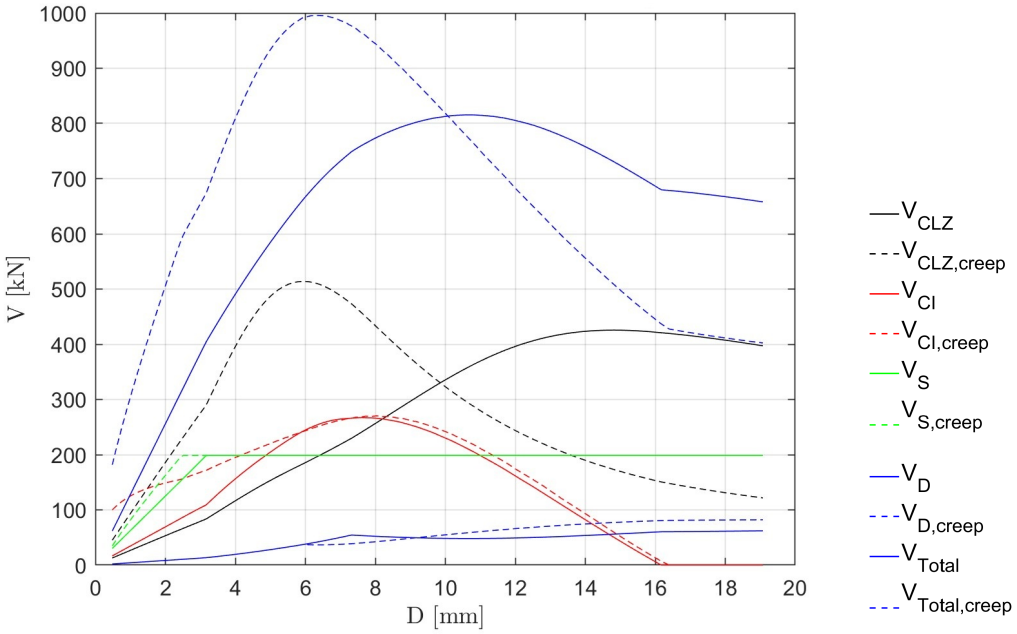

Figure 4.3: Shear-resisting contributions versus Δ for $V/V_{u,0} = 0.90$

Discussion of Mechanism-by-Mechanism Behavior

- Concrete Loading Zone (V_{clz})

  Without creep (dashed black), the beam fails when V_{clz} reaches its peak, coinciding with the peak of V_{tot}.
  With 50 years of creep (solid black), the peak of V_{clz} shifts to larger Δ, causing the failure of the beam before the failure of the CLZ.

For $V/V_{u,0} = 0.60$, the peak of the CLZ occurs only slightly after the short-term peak while for higher load levels (0.75 and 0.90), the shift becomes more pronounced.

- Aggregate-Interlock (V_{ci})

  Under short-term loading (dashed red), V_{ci} reaches its maximum after the member has already failed (i.e., beyond Δ_u).
  In contrast, with creep (solid red), the peak of V_{ci} is located before the overall failure point. Both the short-term and long-term V_{ci} curves drop to zero at $\Delta \approx 16\,\text{mm}$, reflecting full crack opening and loss of contact between crack faces.

- Stirrup Action (V_s)

  The stirrups yield at different displacements depending on creep. Under no creep (dashed green), yielding begins at $\Delta \approx 2.4\,\text{mm}$.
  After 50 years of creep (solid green), yielding is delayed to $\Delta \approx 3.1\,\text{mm}$ in all loading scenarios.
  With $f_v = \min(E_s\,\varepsilon_s,\ f_{yv})$, where

$$\varepsilon_s \ = \ \frac{\Delta_t\, l_t}{2\,\sin(\alpha_1)\,d}.$$

  For a precise Δ_t, the steel strain stress reaches the yielding stress f_{yv}. Since creep increases Δ_c, the total Δ is larger for the same applied V, so it means that obviously Δ will be greater with creep because $\Delta = \Delta_c + \Delta_t$.

- Dowel Action (V_d)

  The dowel contribution (blue curves) influences the post-peak branch of the total capacity. It plays no role in initiating failure but sustains residual shear after the V_{CLZ} and V_{ci} have degraded.

Summary of peak values after 50 Years :

Tab. 4.1 lists for each loading fraction, the short-term and 50-year creep-adjusted failure displacement Δ_u, total shear capacity $V_{\text{tot},u}$, the maximum capacity of the CLZ $V_{clz,\text{max}}$, and the maximum capacity of shear resisting by aggregate interlock $V_{ci,\text{max}}$.

Case	Δ_u [mm]	$V_{\text{tot},u}$ [kN]	$V_{clz,\text{max}}$ [kN]	$V_{ci,\text{max}}$ [kN]
Short-term (no creep)	6.3	995	513	270
50-year creep, $V/V_{u,0} = 0.60$	11.6	899	510	264
50-year creep, $V/V_{u,0} = 0.75$	11.6	862	490	265
50-year creep, $V/V_{u,0} = 0.90$	10.5	815	426	265

Table 4.1: Failure displacement and shear capacities (short-term vs. 50-year creep) for beam S1M.

Key observations:

- Failure displacement Δ_u.

  Under creep over 50 years , Δ_u increases from 6.3 mm (short-term) to 11.6 mm for $V/V_{u,0} = 0.60$ (+ 84%), to 11.6 mm for $V/V_{u,0} = 0.75$ (+ 84 %) and to 10.5 mm for $V/V_{u,0} = 0.90$ (+ 67%).

- Total shear capacity $V_{\text{tot},u}$.

  After 50 years of creep, $V_{\text{tot},u}$ decreases from 995 kN (short-term) to 899 kN for $V/V_{u,0} = 0.60$ (-10%), to 862 kN for $V/V_{u,0} = 0.75$ (-13%) and to 815 kN for $V/V_{u,0} = 0.90$ (-18%).

- CLZ capacity $V_{clz,\text{max}}$.

  The maximum CLZ values match those from Chapter 2, as expected, since V_{clz} is computed independently of other mechanisms.

- Aggregate-interlock capacity $V_{ci,\text{max}}$.

  A small reduction from 270 kN to about 265 kN occurs under all the load levels, indicating that long-term slip and crack opening marginally degrade V_{ci}.

Time-dependent degradation of shear Resistance over 50 years

Fig. 4.4, 4.5, and 4.6 plot the evolution of the total shear capacity $V_{\text{tot,u}}$ and its four component mechanisms (V_{clz}, V_{ci}, V_s, V_d) over a 50-year period of sustained loading.
In each plot, the abscissa is time (in days, up to $1.825 \times 10^4 \approx 50$ years), and the ordinate is shear force V (in kN).

Note that the value at each time step corresponds to the peak of $V_{\text{tot,creep}}$. It differs from the values reported in Tab. 4.1, which simply lists the maximum of each mechanism. Here, the value of each curve should be read at the displacement Δ that triggers member failure and the relative contribution of each mechanism at failure can be identified.

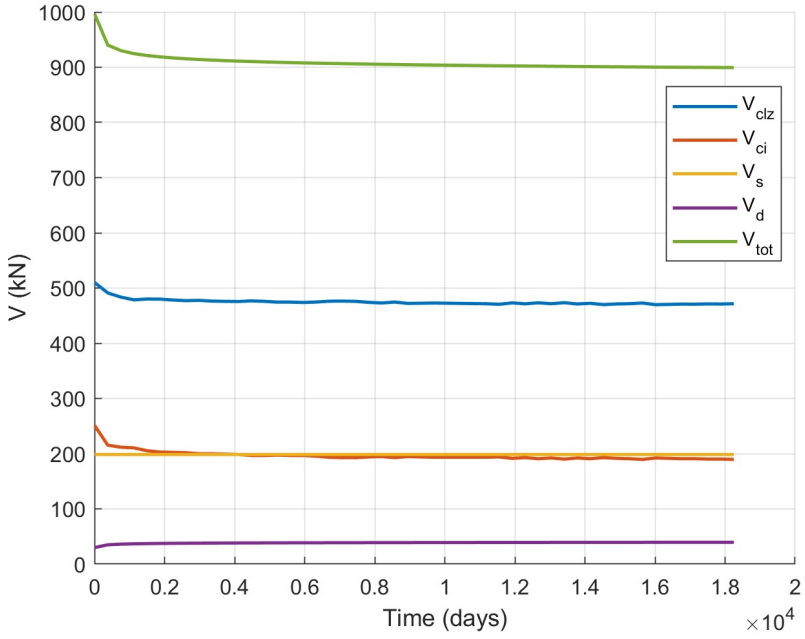

Figure 4.4: Time-dependent shear resistance components for $V/V_{u0} = 0.60$

In Fig. 4.4, for $V/V_{u0} = 0.60$, the total shear resistance $V_{\text{tot,u}}$ steadily declines, reaching 899 kN after 50 years (a 10% reduction). This long-term loss is primarily driven by reductions in shear resistance of the CLZ V_{clz} (from 510 kN to 471 kN at failure) and in the aggregate-interlock shear resistance V_{ci} (from 250 kN to 189 kN at failure). The stirrup contribution V_s (yellow) and dowel action V_d (purple) remain essentially unchanged over time, since none of them depends on the creep coefficient.

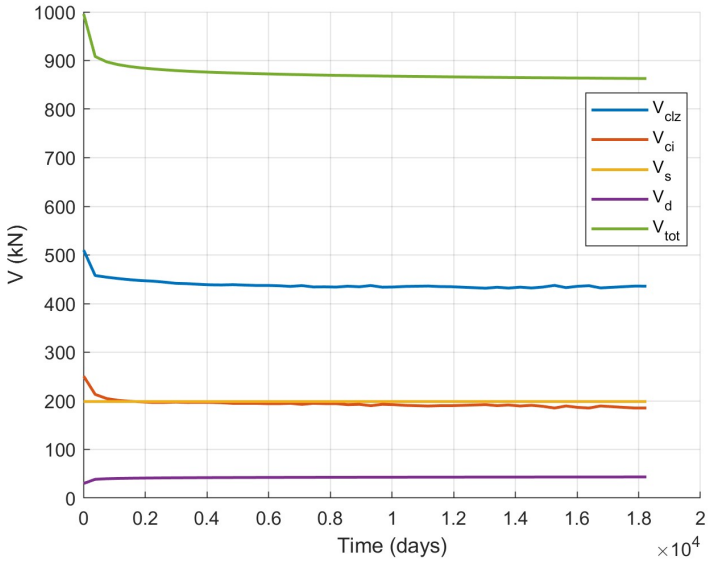

Figure 4.5: Time-dependent shear resistance components for $V/V_{u0} = 0.75$.

Fig. 4.5 ($V/V_{u0} = 0.75$) shows a two-phase reduction in $V_{\text{tot,u}}$: an initial sharp decrease from 995 kN down to $\approx$ 908 kN, followed by a slower decrease to 862 kN after 50 years (a 13% reduction overall).
The shear resistance of the CLZ again dominates the capacity loss, while aggregate interlock resistance contributes to a lesser extent.
Stirrup and dowel contributions remain constant.

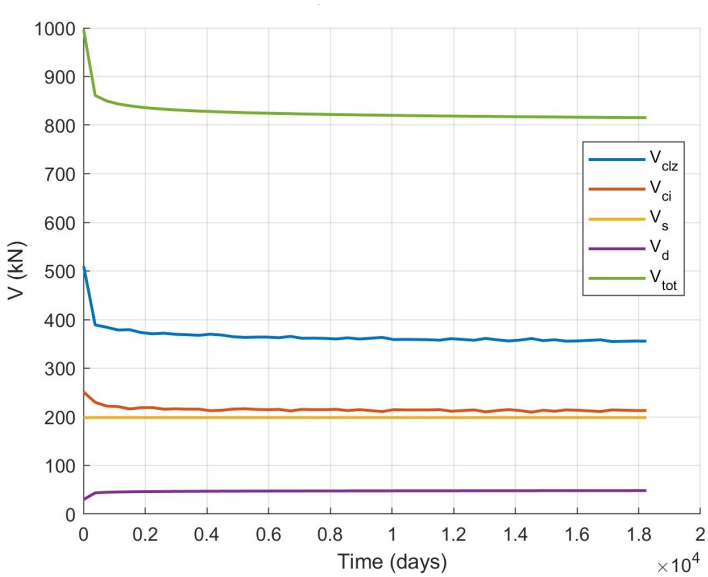

Figure 4.6: Time-dependent shear resistance components for $V/V_{u0} = 0.90$.

In Fig. 4.6 ($V/V_{u0} = 0.90$), the total shear capacity experiences an 18% reduction over 50 years, dropping from 995 kN to 815 kN. The two-phase pattern is again evident: a steep initial drop to ≈ 861 kN, followed by a gradual decrease to 815 kN.
The resistance of the CLZ accounts for most of the capacity loss, while V_{ci} makes a minor additional contribution.
The stirrup and dowel actions (V_s, V_d) remain nearly constant.

Extension to 100-Year Service Life

In many bridge design codes, the required service life can be as long as 100 years [14]. The previous subsection quantified the losses in total shear capacity $V_{\text{tot,u}}$ induced over 50 years and its component mechanisms for beam S1M under three sustained load fractions $V/V_{u0} = 0.60,\ 0.75,\ 0.90$. Here, the same simulations are extended up to $t = 100$ years ($\approx 36\,500$ days) in order to assess whether significant additional capacity degradation occurs between years 50 and 100.

Fig. 4.7 reproduces the same time-history plots of each mechanism and V_{tot} at the displacement that corresponds to the failure of the beam, now extended to $t = 100$ years.

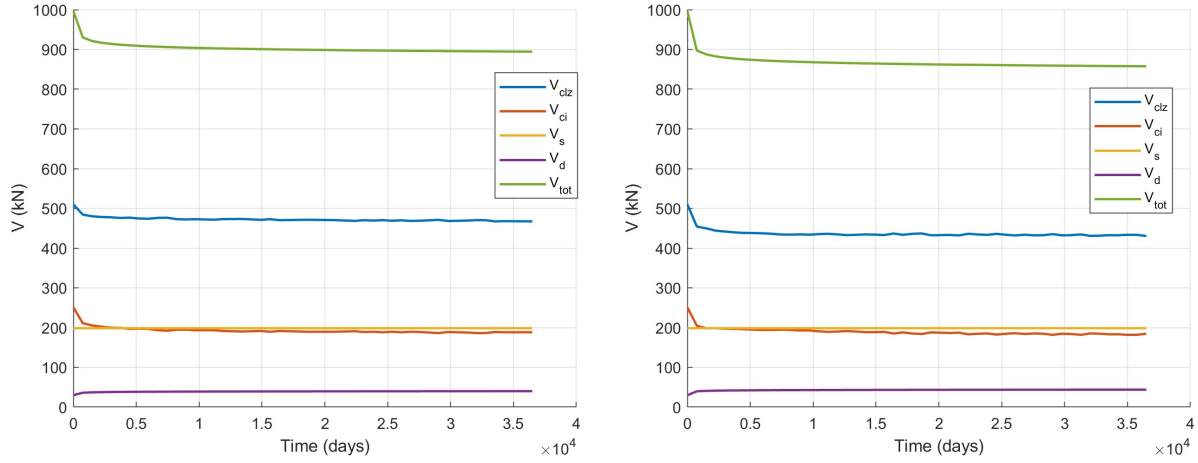

(a) $V/V_{u0} = 0.60$

(b) $V/V_{u0} = 0.75$

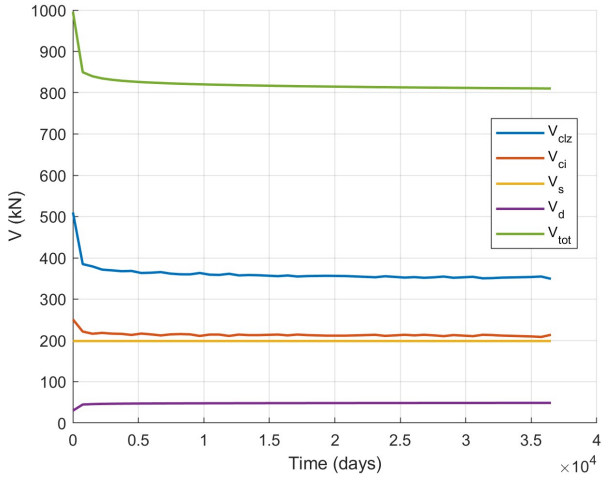

(c) $V/V_{u0} = 0.90$

Figure 4.7: Time-dependent shear resistance components over 100 years

Load Level	$V_{\text{tot},0}$ [kN]	$V_{\text{tot},50}$ [kN]	$V_{\text{tot},100}$ [kN]	$\Delta V_{\text{tot},\,50\to100}$[%]
$0.60\,V_{u0}$	995	899	894	0.6%
$0.75\,V_{u0}$	995	862	857	0.6%
$0.90\,V_{u0}$	995	815	810	0.6%

Table 4.2: Comparison of short-term, 50-year, and 100-year total shear capacities for S1M.

Key Observations:

- The 50-to-100 year loss is always small: ≈ 5 kN (0.6%) for all the sustained load levels.
- After 50 years, the majority of the shear-capacity reduction has already occurred. From year 50 to year 100, the curves $V_{CLZ}(t)$ and $V_{ci}(t)$ approach near-plateau values.

4.2.2 Constant-load service life assessment

Time of failure for sustained load levels

Previously, the beam was pushed to failure at each time to quantify the ultimate shear capacity.

Now, the aim is to hold these loading levels constant and determine how long the beam can sustain each level before failure. In other words, a plot of sustained load level V/V_{u0} versus time-to-failure is required. On the previous figures, $V_{\text{tot,u}}(t)$ is plotted as a function of time.
For a fixed load level, the time-to-failure is simply the time corresponding to the intersection of that horizontal load-level line with the $V_{\text{tot},u}$ versus time curve as shown on Fig. 4.8.

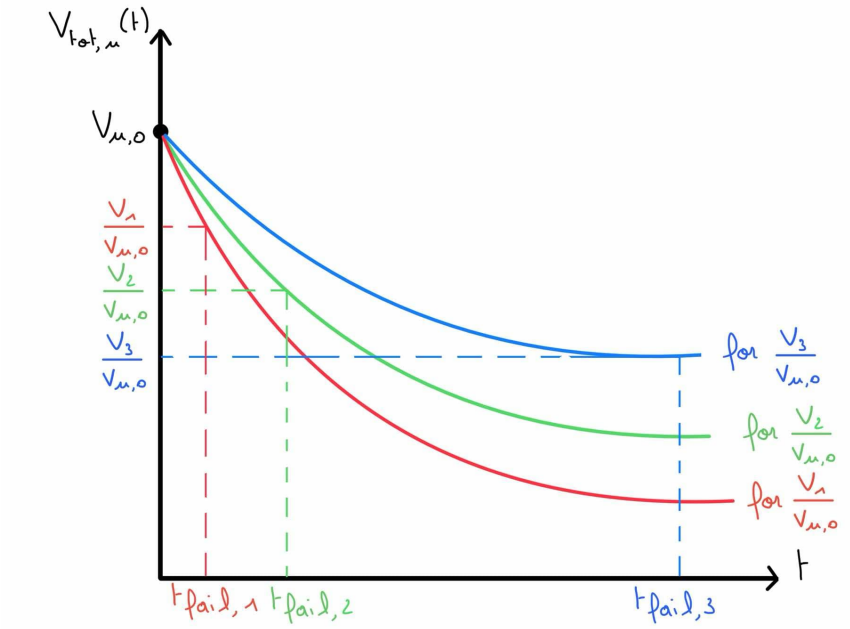

Figure 4.8: Time of failure

Fig. 4.9 shows the relationship between sustained load level V/V_{u0} (vertical axis) and time to failure (horizontal axis, in days, logarithmic scale). Each circular marker represents one computed data point from the numerical code. Vertical dashed lines at 1 year ($\approx$ 365 days), 50 years ($\approx$ 18 250 days), and 100 years ($\approx$ 36 500 days) are included to aid interpretation.

Below, four distinct regions in the plot are identified.

1. Very-short-term region (from t_0 up to 134 days, $V/V_{u0} \approx 0.95$):

   From the initial loading time t_0 ($\approx$7 days) up to about 134 days (when $V/V_{u0} = 0.95$), the curve is nearly a straight line in log linear coordinates.

2. Intermediate Short-Term Region (from 134 days to $\approx$1 year, $V/V_{u0} \approx 0.95 \rightarrow 0.88$):

   Between $t \approx 134$ days (at $V/V_{u0} = 0.95$) and $t \approx 365$ days (at $V/V_{u0} = 0.88$), the curve remains approximately linear in log space, but the slope is much steeper than in the prior region. A reduction of 7 % in sustained load (from 0.95 to 0.88) yields to an increase in lifetime from 134 days to 365 days.

3. Transition Region (from $\approx$1 year to 3972 days $\approx$11 years, $V/V_{u0} \approx 0.88 \rightarrow 0.85$):

   From 365 days up to about 3972 days ($\approx$ 11 years), corresponding to V/V_{u0} $\approx$0.88 to 0.85, the curve 'bends' gradually. The slope in log-linear space becomes less steep, indicating that small reductions in load (e.g. 0.88 to 0.87 to 0.86 to 0.85) yield progressively larger gains in lifetime (1 year to several years to $\approx$11 years).

4. Long-Term Region (from 3972 days to very large times, $V/V_{u0} \approx 0.85 \rightarrow 0.80$):

   Beyond $\approx$ 3972 days ($\approx$11 years, at $V/V_{u0} = 0.85$), the curve approximates again a straight line in ln-linear space, but with a very shallow slope. For example, decreasing load from $0.85\,V_{u0}$ to $0.83\,V_{u0}$ pushes failure time from $\approx$ 11 years to $\approx$325 years; further reduction to $0.82\,V_{u0}$ yields $\approx$ 1878 years. Small load decreases produce enormous lifetime gains.

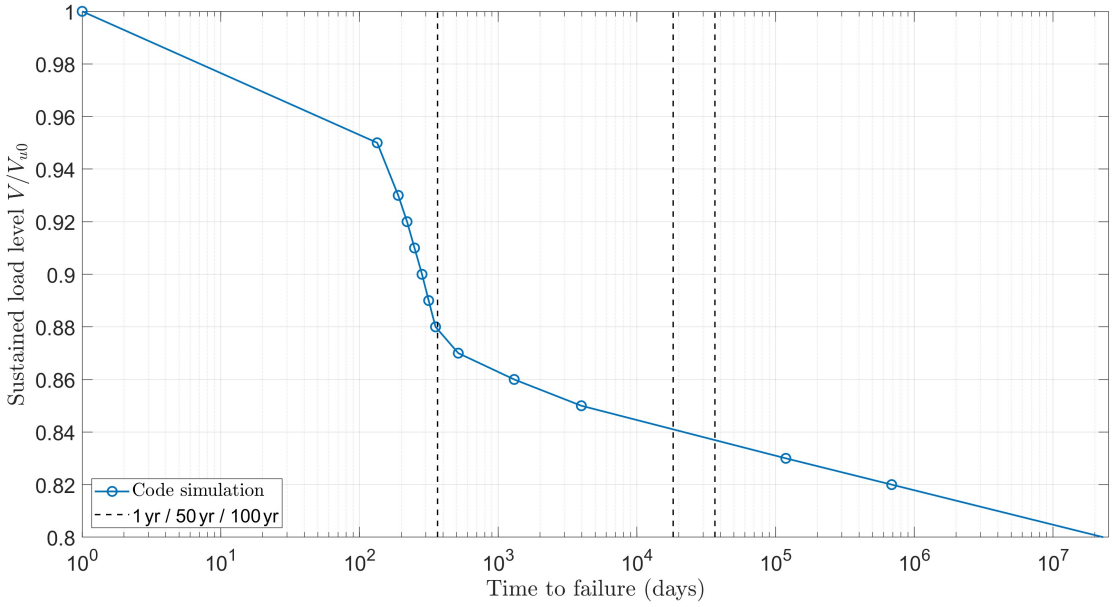

Figure 4.9: Sustained load level $V/V_{u,0}$ vs time of failure (in log scale)

Load Level V/V_{u0}	**Time to Failure** (days)
0.95	134
0.93	190
0.92	220
0.91	249
0.90	282
0.89	315
0.88	353
0.87	515
0.86	1303
0.85	3972
0.83	118 460
0.82	686 430

Table 4.3: Sustained Load Level vs. Time to Failure

Key observations :

- The failure occurs after 1 year for a sustained load level of $\approx 0.88 V/V_{u,0}$
- The failure occurs after 50 years for a sustained load level of $\approx 0.84 V/V_{u,0}$

It is important to emphasize that these times of failure are approximated values, it is impossible to predict the exact day of failure of a beam. It provides an idea and an estimate of the shear capacity loss by sustaining loads for a long time.

Time-dependent crack-width, total Deflection, and Concrete Loading Zone deformation

Fig. 4.10 shows the evolution of the critical crack-width w over a 50-year period for six different sustained load levels: $V/V_{u,0} = 0.60,\ 0.65,\ 0.70,\ 0.75,\ 0.80$, and 0.85. All of these load levels lie below the time-to-failure curve for 50 years except $V/V_{u,0} = 0.85$, which fails at approximately 3 972 days (≈11 years) (see Fig. 4.9).

The curves exhibit two clearly distinguishable regimes :

1. Rapid Early Growth (0-≈379 days).

   All six crack-width curves exhibit a steep increase during the first few hundred days following load application. For example, at $V/V_{u,0} = 0.80$, w grows from 1.21 mm at $t = t_0$ to about 2.70 mm by $t \approx 379$ days.

2. Long-Term Plateau

   After roughly ≈5 000-10 000 days, five of the six curves level off. By $t = 50$ years, the growth of crack-width has nearly stabilized for $V/V_{u,0} = 0.60$ through 0.75, with only minimal additional widening thereafter. However, the $V/V_{u,0} = 0.80$ curve continues to increase more appreciably even at late times. The $V/V_{u,0} = 0.85$ curve (blue) does not reach a plateau,

because the beam fails at about $t = 3\,972$ days (≈11 years), ultimately reaching a crack-width of $w = 5.03$ mm at failure.

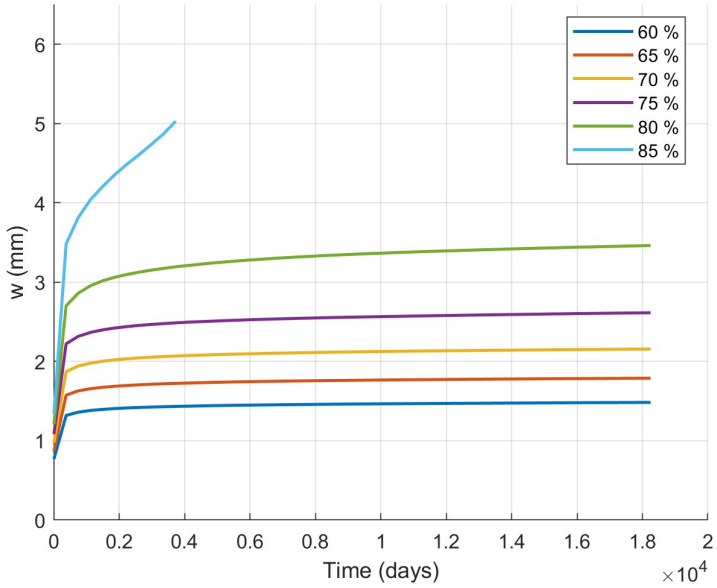

Figure 4.10: Time evolution of the crack-width $w(t)$ over 50 years

Tab. 4.4 summarizes the crack-width at the time of initial loading ($t = t_0$) and after 50 years ($t = 50$ y) for those load levels. The percentage increase $\left[(w_{50} - w_0)/w_0\right] \times 100\%$ highlights how creep magnifies crack opening over decades:

Load Level	$\mathbf{w_{t_0}}$ **[mm]**	$\mathbf{w_{t_{50}}}$ **[mm]**	**Increase (%)**
$0.60\,V/V_{u,0}$	0.77	1.48	92%
$0.65\,V/V_{u,0}$	0.86	1.79	108%
$0.70\,V/V_{u,0}$	0.97	2.15	121%
$0.75\,V/V_{u,0}$	1.08	2.61	142%
$0.80\,V/V_{u,0}$	1.21	3.46	186%

Table 4.4: Critical crack-width w at $t = t_0$ and $t = 50$ years for different sustained load levels.

Fig. 4.11 and 4.12 plot the total midspan deflection $\Delta(t)$ and the CLZ displacement $\Delta_c(t)$ for the same six load levels over 50 years.

Both Δ and Δ_c mirror the two-stages behaviour seen in crack-width.

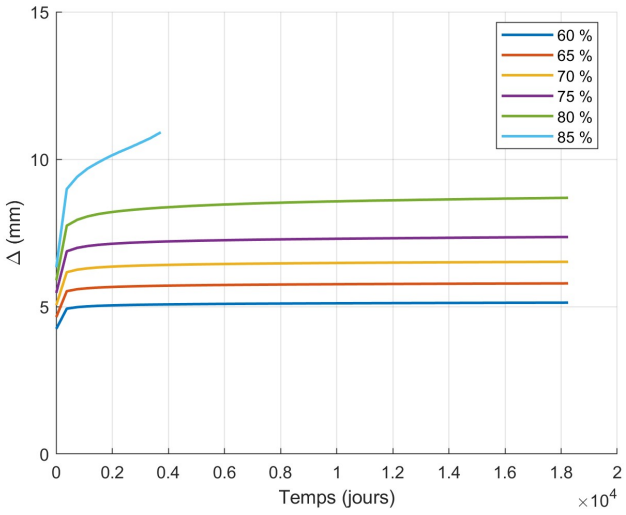

Figure 4.11: Time evolution of the total midspan deflection $\Delta(t)$ over 50 years

Load Level	$\boldsymbol{\Delta_{t_0}}$ **[mm]**	$\boldsymbol{\Delta_{t_{50}}}$ **[mm]**	**Increase (%)**
$0.60\,V/V_{u,0}$	4.25	5.13	20.7%
$0.65\,V/V_{u,0}$	4.65	5.79	24.5%
$0.70\,V/V_{u,0}$	5.05	6.52	29.1%
$0.75\,V/V_{u,0}$	5.47	7.36	34.6%
$0.80\,V/V_{u,0}$	5.89	8.69	47.6%

Table 4.5: Total deflection Δ at $t = t_0$ and $t = 50$ years for different sustained load levels.

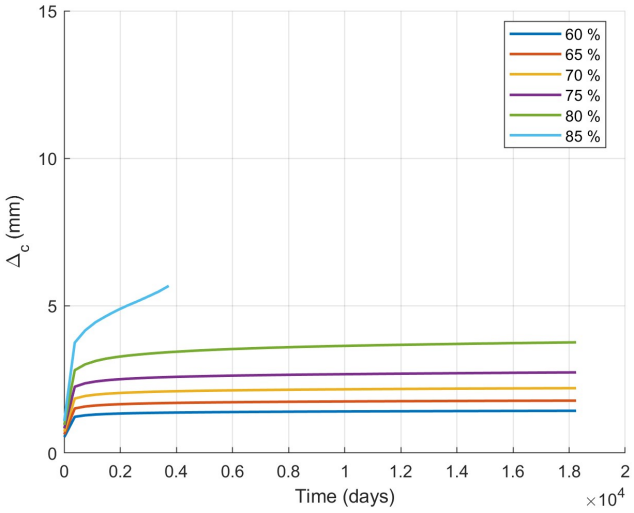

Figure 4.12: Time evolution of the CLZ displacement $\Delta_c(t)$ over 50 years

Load Level	Δ_{c,t_0} **[mm]**	$\Delta_{c,t_{50}}$ **[mm]**	**Increase (%)**
$0.60\,V/V_{u,0}$	0.54	1.43	164.8%
$0.65\,V/V_{u,0}$	0.63	1.78	182.5%
$0.70\,V/V_{u,0}$	0.73	2.20	201.4%
$0.75\,V/V_{u,0}$	0.83	2.73	228.9%
$0.80\,V/V_{u,0}$	0.95	3.75	294.7%

Table 4.6: CLZ displacement Δ_c at $t = t_0$ and $t = 50$ years for different sustained load levels.

Summary of Key Observations:

- *Crack-Width Growth:*
  w increases from 165% (for $V/V_{u,0} = 0.60$) to 255 % (for $V/V_{u,0} = 0.80$). At $0.85\,V/V_{u,0}$ the beam fails at ≈11 years with $w = 5.03$ mm.
- *Deflection Increase:*
  Sustained loading elevates Δ by 21 - 48 % after 50 years for $V/V_{u,0} = 0.60$-0.80. At $0.85\,V/V_{u,0}$, Δ reaches 10.91 mm at failure.
- *CLZ Deformation:*
  The CLZ displacement Δ_c increases by 165 -295 % after 50 years for $V/V_{u,0} = 0.60$-0.80. At $0.85\,V/V_{u,0}$, $\Delta_c = 5.67$ mm at failure.
- *Failure at* $0.85\,V/V_{u,0}$*:*
  Because the beam fails at ≈3 972 days, the $0.85\,V/V_{u,0}$ curves terminate at that time rather than extending to 50 years. The final values at failure are $w = 5.03$ mm, $\Delta = 10.91$ mm, $\Delta_c = 5.67$ mm.

4.2.3 Conclusion

Over a period of 50 years, the failure displacement Δ_u measured when the beam is pushed to failure after being subject to various load levels increases by approximately 85 %. The shear capacity decreases by 10 % for $V/V_{u,0} = 0.6$ up to 19 % for $V/V_{u,0} = 0.9$

When considering time-dependency under constant loading, the failure of the beam S1M occurs after 50 years by sustaining a load level $V/V_{u,0} = 0.84$ as shown on Fig.4.9. It represents a loss in shear capacity of 16% at 50 years under sustained loading.

In term of crack-width(w), total deflection (Δ) and Concrete Loading Zone displacement (Δ_c), the effect of creep leads to high increases when the load is sustained for 50 years even if the failure is not reached.
It is even more important to look for the range corresponding to the service loads such as $V/V_{u,0} = 0.6$ and $V/V_{u,0} = 0.65$.
The crack-width increases by 92% for $V/V_{u,0} = 0.6$ and 108 % for $V/V_{u,0} = 0.65$, the total deflection increases by 21% for $V/V_{u,0} = 0.6$ and ≈ 25% for $V/V_{u,0} = 0.65$ and by 165% for $V/V_{u,0} = 0.6$ and 182% for $V/V_{u,0} = 0.65$.

These results demonstrate that, even when the beam does not fail under a given sustained load, creep can dramatically widen cracks and increase both total and CLZ deflections over practical design lifetimes. For serviceability, it is important that these parameters remain within an acceptable range.

4.3 Parametric and Comparative studies

4.3.1 Shear reinforcement

In this section, the changing parameter is the shear reinforcement. In the basic case, $\rho_v = 0.1\%$ and in this section, the case without shear reinforcement is tested :

1. $\rho_v = 0.1\%$ (basic case, done in Section 4.2)
2. $\rho_v = 0\%$ (without any shear reinforcement)

Results presented in this section correspond to the deep beam S0M tested by *Prof. Mihaylov* at the University of Toronto as part of his PhD research [13].
Its characteristic properties are listed in Tab. 4.7.

Parameter	Value (unit)
f_{cm}	33 MPa
h	1200 mm
d	1095 mm
a	1700 mm
b	400 mm
A_s	3060 mm^2
f_y	652 MPa
E_r	200,000 MPa
n_b	6
a_g	20 mm
ρ_v	0%
f_{yv}	490 MPa
E_v	200,000 MPa
l_{b1}	300 mm
l_{b2}	150 mm
V/P	0.50
l_f	0 mm
L	3400 mm
A_{st}	3060 mm^2

Table 4.7: Characteristic properties of beam S1M

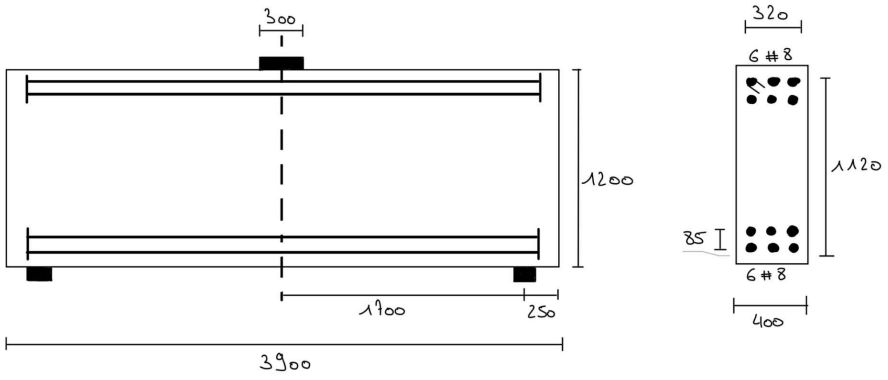

Figure 4.13: Beam S0M

This beam has exactly the same dimensions than S1M , the only major difference is the shear reinforcement ratio $\rho_v = 0\%$ in this case.

Consequently, the total shear resistance V_{tot} is reduced to the sum of three mechanisms :

$$V_{tot} = V_{CLZ} + V_{ci} + V_d \tag{4.5}$$

Fig.4.14 shows, for each sustained load level, the individual contributions of the four shear-resisting mechanisms : V_{clz} (Shear resistance of the CLZ), V_{ci} (aggregate-interlock), V_d (dowel action), and $V_s = 0$ (stirrup action) plotted against the combined displacement $\Delta = \Delta_c + \Delta_t$

In each plot, dashed lines represent the short-term (no creep) response, while solid lines correspond to the long-term behavior after 50 years of sustained loading.

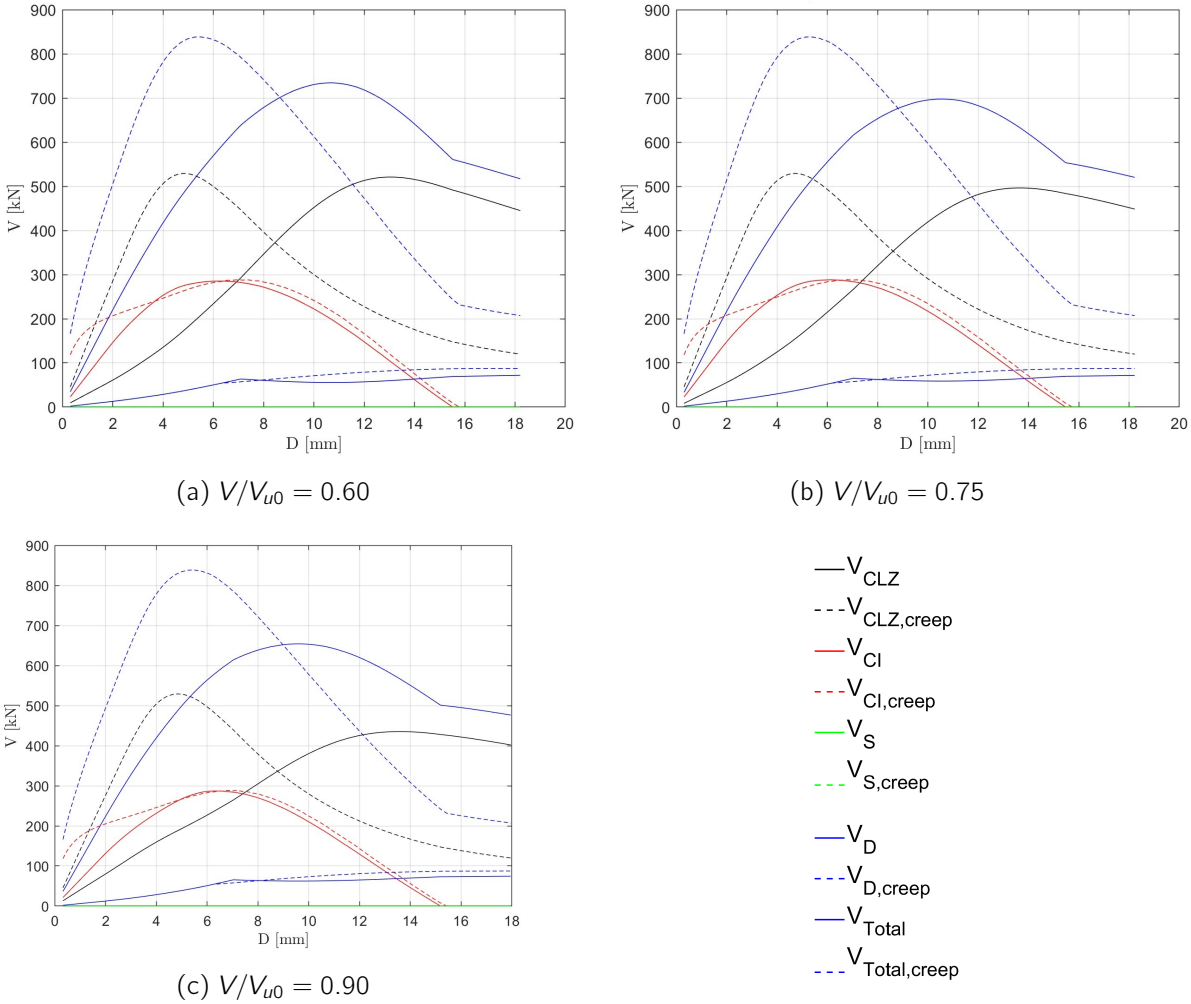

(a) $V/V_{u0} = 0.60$

(b) $V/V_{u0} = 0.75$

(c) $V/V_{u0} = 0.90$

Figure 4.14: Shear-resisting contributions versus Δ at 50 years for the beam S0M

Comparison with the curves of S1M :

The shape of the curves are the same than the ones observed on Fig. 4.1,4.2 and 4.3.

The main difference is that because of $V_s = 0$, other mechanisms are even more important to replace the stirrup resistance. As said before, the failure is mainly triggered by the resistance of the CLZ so instinctively it is this mechanism that is supposed to replace V_s.

Here is the comparison of the proportion of V_{clz} that contributes to the total shear resistance for each beam :

Case	V_{CLZ}/V_{tot} for S1M [%] S	V_{CLZ}/V_{tot} for S0M [%]
Short-term (no creep)	51.5	63.1
50-year creep, $V/V_{u,0} = 0.60$	56.7	70.9
50-year creep, $V/V_{u,0} = 0.75$	56.8	71.1
50-year creep, $V/V_{u,0} = 0.90$	52.2	66.5

Table 4.8: Proportion of V_{CLZ} contributing to the total shear resistance V_{tot}

Case	Δ_u [mm]	$V_{\text{tot},u}$ [kN]	$V_{clz,\text{max}}$ [kN]	$V_{ci,\text{max}}$ [kN]
Short-term (no creep)	5.4	838	529	288
50-year creep, $V/V_{u,0} = 0.60$	10.7	734	521	285
50-year creep, $V/V_{u,0} = 0.75$	10.5	697	496	288
50-year creep, $V/V_{u,0} = 0.90$	9.6	654	435	286

Table 4.9: Failure displacement and shear capacities (short-term vs. 50-year creep) for beam S0M.

Key observations:

- Failure displacement Δ_u.

  Under creep, Δ_u increases from 5.4 mm (short-term) to 10.7 mm for $V/V_{u,0} = 0.60$ (+ 98%), to 10.5 mm for $V/V_{u,0} = 0.75$ (+ 94 %) and to 9.6 mm for $V/V_{u,0} = 0.90$ (+ 77%). By comparing with the results described in Section 4.2.1, the augmentation of the failure displacement is more important for S0M than for S1M.

  It can be explained with Tab. 4.8, it is shown that the shear mechanism V_{CLZ} takes a more important part in the total shear resistance. As said few times, this mechanism is the mechanism that is the most impacted by the effect of creep so it is not surprising to see that the augmentation of the failure displacement with creep compared to short-term is more important for S0M than for S1M.

- Total shear capacity $V_{\text{tot},u}$.

  After 50 years of creep, $V_{\text{tot},u}$ decreases from 838 kN (short-term) to 734 kN for $V/V_{u,0} = 0.60$ (-12,5%), to 697 kN for $V/V_{u,0} = 0.75$ (-17%) and to 654 kN for $V/V_{u,0} = 0.90$(-22%). By comparing with the results described in Section 4.2.1, the decrease in total shear resistance is more important for S0M than for S1M.

It is exactly the same explanation than the one provided for failure displacement. The CLZ resistance contributes more and so creep effect is more important for S0M leading on a more important decrease of the total shear resistance than for S1M.

Fig. 4.15 plots the evolution of the total shear capacity V_{tot} and its four component mechanisms (V_{clz}, V_{ci}, V_s, V_d) over a 50-year period of sustained loading for the three different load levels In each plot, the abscissa is time (in days, up to $1.825 \times 10^4 \approx 50$ years), and the ordinate is shear force V (in kN)

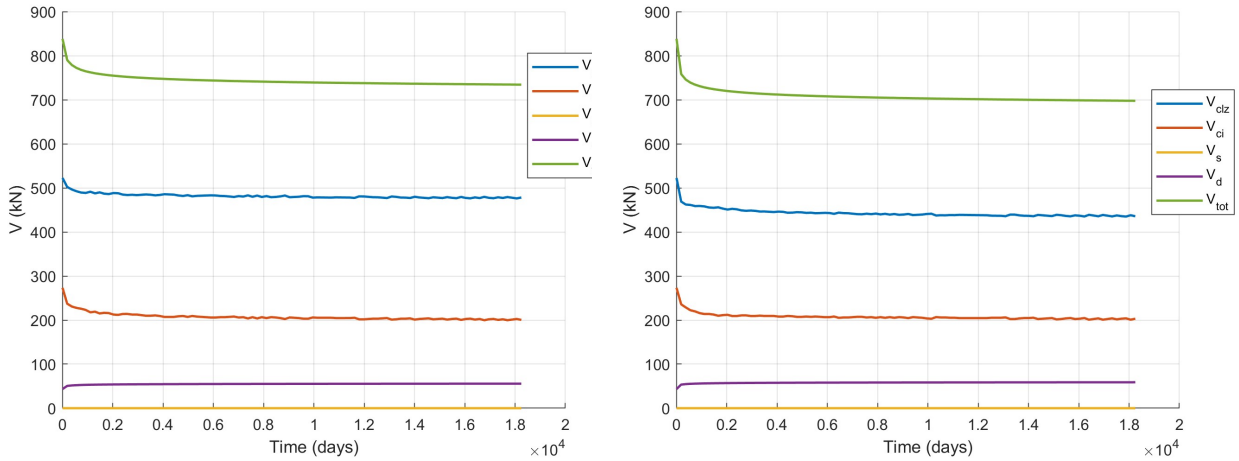

(a) $V/V_{u,0} = 0.60$ (b) $V/V_{u,0} = 0.75$

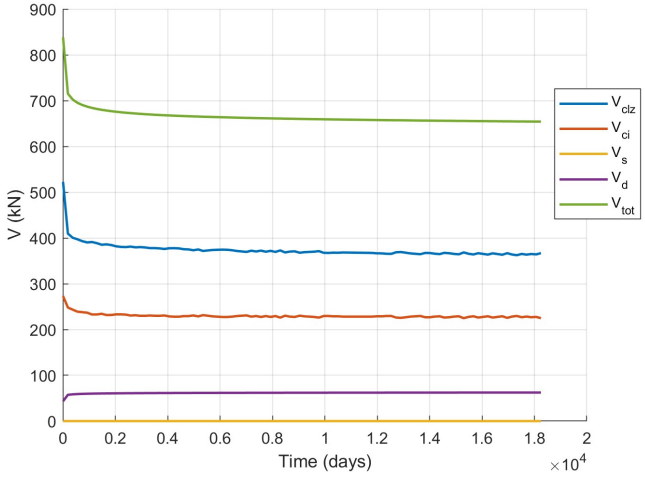

(c) $V/V_{u,0} = 0.90$

Figure 4.15: Time-dependent shear resistance components for the beam S0M

Fig. 4.16 shows the relationship between sustained load level V/V_{u0} (vertical axis) and time to failure (horizontal axis, in days, logarithmic scale) for the beam S0M. Each circular marker represents one computed data point from the numerical code. Vertical dashed lines at 1 year ($\approx$ 365 days), 50 years ($\approx$ 18 250 days), and 100 years ($\approx$ 36 500 days) are included to aid interpretation.

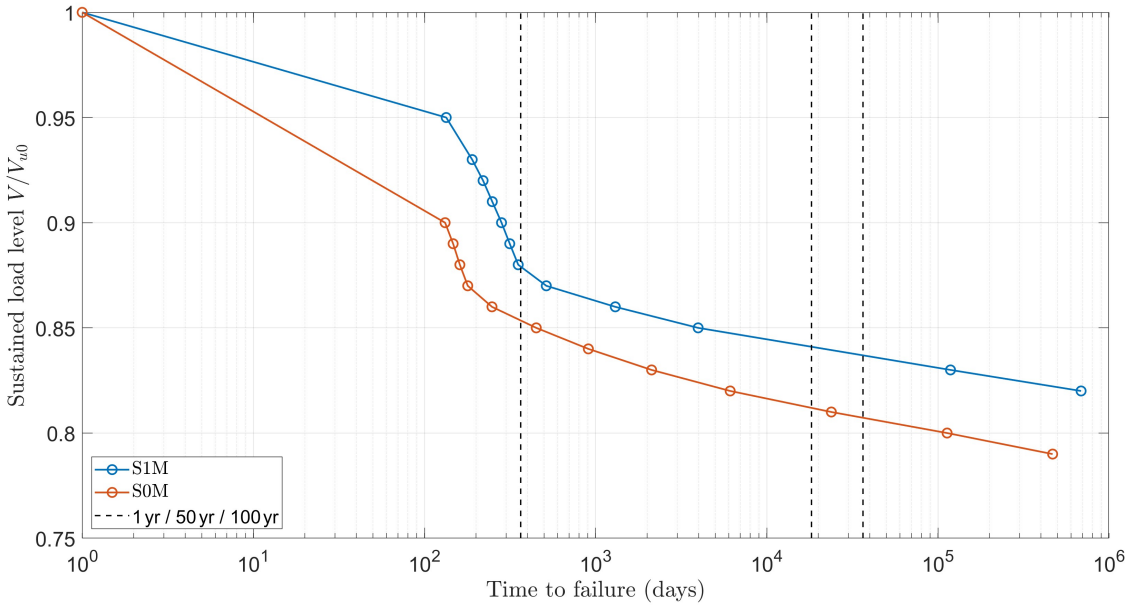

Figure 4.16: Sustained load level $V/V_{u,0}$ vs time of failure (in log scale)

Load Level V/V_{u0}	**Time to Failure (days)**
0.9	132
0.89	147
0.88	161
0.87	179
0.86	248
0.85	450
0.84	907
0.83	2124
0.82	6114
0.81	23840
0.80	113 170
0.79	468 090

Table 4.10: Sustained Load Level vs. Time to Failure for S0M

Comparison with S1M :

It can be very interesting to compare the two curves plotted on 4.16 to see the impact of the stirrups on the time before failure.

- For a sustained load level of $V/V_{u0} = 0.9$, the time of failure of the beam S1M is 282 days against 132 days for the beam S0M
- For a sustained load level of $V/V_{u0} = 0.85$, the time of failure of the beam S1M is 3972 days ($\approx$ 11 years) against 450 days for the beam S0M
- For a sustained load level of $V/V_{u0} = 0.80$, the time of failure of the beam S1M is greater than 10^7 days (27 397 years) against 113 170 days (310 years) for the beam S0M.
- For a failure of the beam at 50 years, a level of 0.84 $V/_{u,0}$ has to be sustained for S1M and a level of $\approx$ 0.815 $V/_{u,0}$ for S0M.

Fig. 4.17 shows the evolution of the critical crack-width w for the beam S0M over a 50-year period for six different sustained shear-load levels: $V/V_{u,0} = 0.60,\ 0.65,\ 0.70,\ 0.75,\ 0.80$, and 0.85. For all these load levels the failure doesn't occur over 50 years except $V/V_{u,0} = 0.85$, which fails at approximately 450 days (see Fig. 4.16).

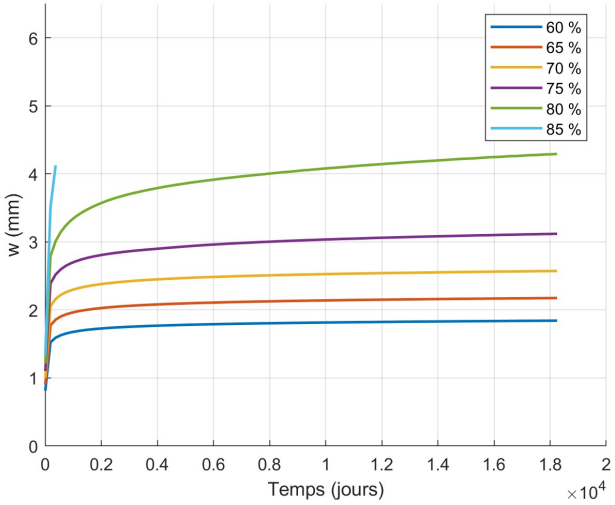

Figure 4.17: Time evolution of the crack-width $w(t)$ over 50 years

Load Level	$\mathbf{w_{t_0}}$ **[mm]**	$\mathbf{w_{t_{50}}}$ **[mm]**	**Increase (%)**
$0.60\,V/V_{u,0}$	0.81	1.84	127 %
$0.65\,V/V_{u,0}$	0.9	2.17	141%
$0.70\,V/V_{u,0}$	1	2.57	157%
$0.75\,V/V_{u,0}$	1.1	3.12	184 %
$0.80\,V/V_{u,0}$	1.21	4.29	255%

Table 4.11: Critical crack-width w at $t = t_0$ and $t = 50$ years for various sustained load levels.

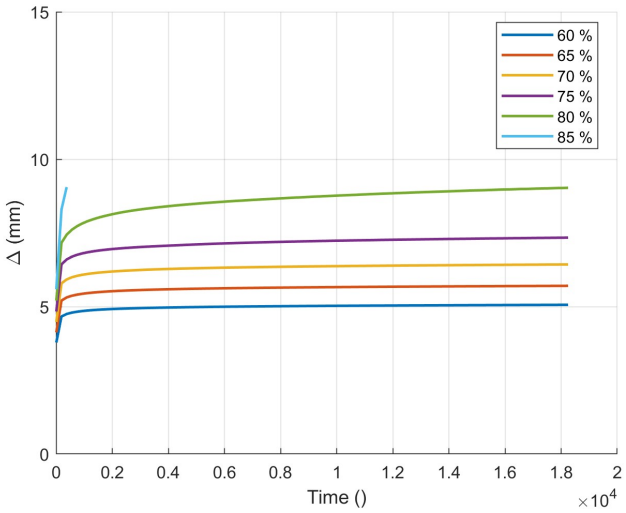

Figure 4.18: Time evolution of the total mid-span deflection $\Delta(t)$ over 50 years

Load Level	$\boldsymbol{\Delta_{t_0}}$ **[mm]**	$\boldsymbol{\Delta_{t_{50}}}$ **[mm]**	**Increase (%)**
$0.60\,V/V_{u,0}$	3.78	5.06	33.9 %
$0.65\,V/V_{u,0}$	4.13	5.7	38%
$0.70\,V/V_{u,0}$	4.48	6.43	43.5%
$0.75\,V/V_{u,0}$	4.83	7.34	52%
$0.80\,V/V_{u,0}$	5.2	9.03	73.7%

Table 4.12: Total deflection Δ at $t = t_0$ and $t = 50$ years for different sustained load levels.

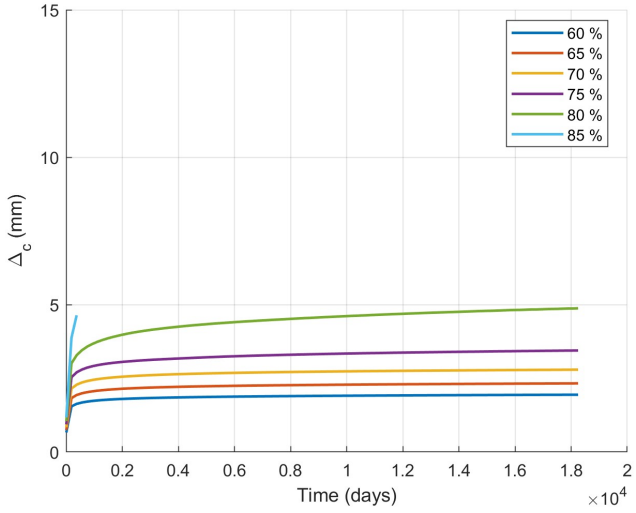

Figure 4.19: Time evolution of the CLZ displacement $\Delta_c(t)$ over 50 years

Load Level	$\mathbf{\Delta_{c,t_0}}$ **[mm]**	$\mathbf{\Delta_{c,t_{50}}}$ **[mm]**	**Increase (%)**
$0.60\,V/V_{u,0}$	0.66	1.94	193.9%
$0.65\,V/V_{u,0}$	0.75	2.33	210.7%
$0.70\,V/V_{u,0}$	0.84	2.79	232.1 %
$0.75\,V/V_{u,0}$	0.94	3.44	266 %
$0.80\,V/V_{u,0}$	1.05	4.87	364 %

Table 4.13: CLZ displacement Δ_c at $t = t_0$ and $t = 50$ years for different sustained load levels.

Comparison with S1M :

- *Crack-Width Growth:*

  For S1M , creep causes an increase between 92 % (for $0.60\,V/V_{u,0}$) and 186% (for $0.80\,V/V_{u,0}$) over 50 years while for S0M it goes from 127 % (for $0.60\,V/V_{u,0}$) to 255 % (for $0.80\,V/V_{u,0}$). The beam fails at w=5.03 mm at $0.85\,V/V_{u,0}$ for S1M and at w= 4.12 mm for S0M.

- *Deflection Increase:*

  Sustained loading elevates Δ by 21 to 48 % after 50 years for $V/V_{u,0} = 0.60$-0.80 for the beam S1M while it increases Δ by 34 to 73.7 % for S0M.
  At $0.85\,V/V_{u,0}$, Δ reaches 10.91 mm at failure for the beam S1M and 9.07 mm for S0M.

- *CLZ Deformation:*

  The CLZ displacement Δ_c increases by 165 -295 % after 50 years for $V/V_{u,0} = 0.60$-0.80 for the beam S1M and by 194 to 364 % for S0M.
  At $0.85\,V/V_{u,0}$, $\Delta_c = 5.67$ mm at failure for the beam S1M and $\Delta_c = 4,66$ mm for the beam S0M.

4.3.2 Support and loading plate width

In this section, the changing parameters are the distances lb_1 and lb_2.

As shown on Fig. 4.20, lb_1 corresponds to the width of the loading plate while lb_2 corresponds to the width of the support.
Initially, for the beam S1M, these parameters had the following values :

- lb_1=300 mm
- lb_2=150 mm

Here, the aim is to see the effect of an increase of these parameters on the capacity of the beam and so previous values are increased with a factor 1.5 such as :

- lb_1=450 mm
- lb_2=225 mm

First, it is important to know the influence of this parameter on *the 2PKT model*.

lb_1 appears in some equations in the CLZ :

$$\varepsilon_{max} = \frac{\Delta_c \, \tan\alpha_{CLZ}}{3 \, b \, l_{b1e}} \tag{4.6}$$

$$V_{CLZ} = \sigma_{avg} \, b \, l_{b1e} \, \sin^2\alpha_{CLZ}. \tag{4.7}$$

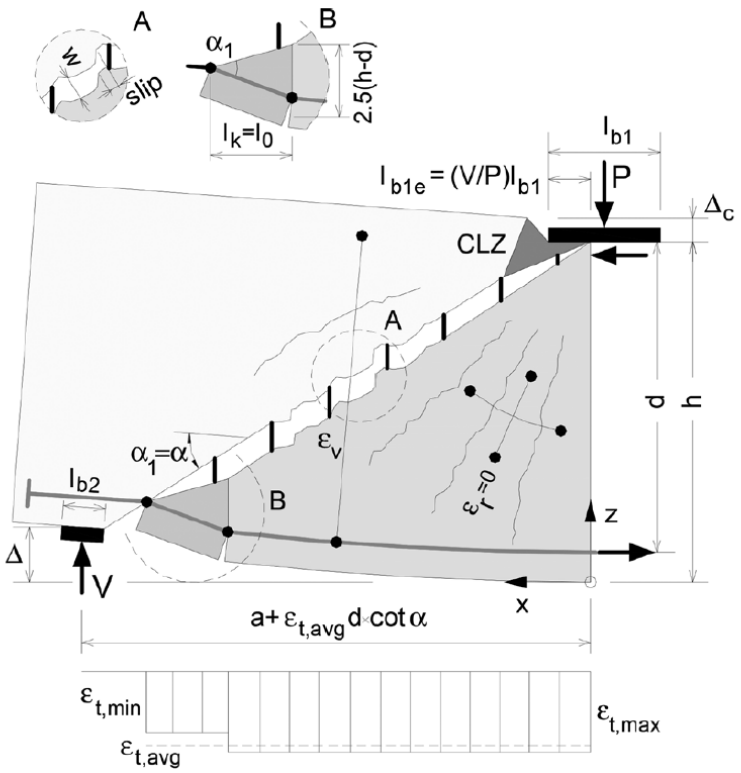

Figure 4.20: Geometric parameters of the *2PKT model* (adapted from [1])

Here is what happens in the CLZ by plotting the $V_{CLZ} - \Delta_c$ relationship.

The short-term shear capacity of the CLZ is higher by increasing the width of the loading plate (790 KN >< 513 kN).

Compared to the short-term shear capacity, there is a decrease of :

- ≈ 0 for $V/V_{u,0} = 0.60$
- 4 % for $V/V_{u,0} = 0.75$
- 14 % for $V/V_{u,0} = 0.90$

The ultimate displacements of the CLZ with this increase of the width of the loading plate are much bigger than the ones observed in Section 2.2.2 :

- For $V/V_{u,0} = 0.60$: 12.8 mm for $lb_1 = 450\,mm$ and 7.5 mm $lb_1 = 300\,mm$
- For $V/V_{u,0} = 0.75$: 14.14 mm $lb_1 = 450\,mm$ and 8.6 mm $lb_1 = 300\,mm$
- For $V/V_{u,0} = 0.90$) : 14.88 mm $lb_1 = 450\,mm$ and 8.9 mm $lb_1 = 300\,mm$

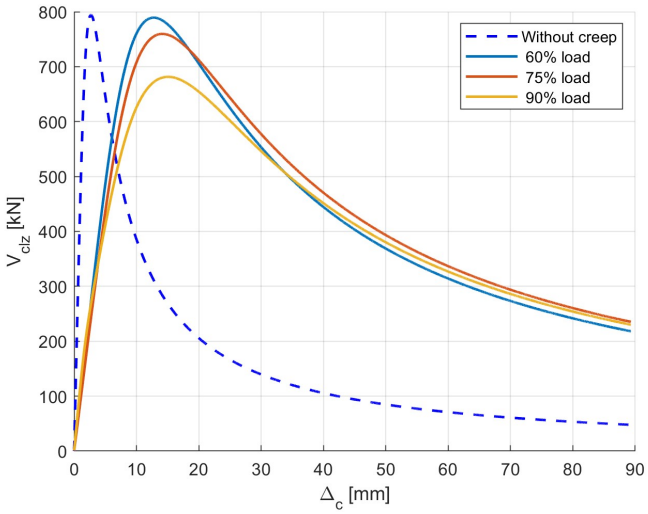

Figure 4.21: V_{CLZ}-Δ_c response for $lb_1 = 450\,mm$ and $lb_2 = 225\,mm$

Load condition	Δ_{cu} [mm]	$V_{CLZ,\max}$ [kN]
Short-term (no creep)	2.96	790
$V/V_{u,0} = 0.60$	12.8	789
$V/V_{u,0} = 0.75$	14.14	759
$V/V_{u,0} = 0.90$	14.88	681

Table 4.14: Displacement capacity Δ_{cu} and shear resistance $V_{CLZ,\max}$

Fig. 4.22 shows, for each sustained load level, the individual contributions of the four shear-resisting mechanisms : V_{clz} (shear resistance of the CLZ), V_{ci} (aggregate-interlock), V_d (dowel action), and ($V_s = 0$) (stirrup action) plotted against the combined displacement $\Delta = \Delta_c + \Delta_t$

In each plot, dashed lines represent the short-term (no creep) response, while solid lines correspond to the long-term behavior after 50 years of sustained loading.

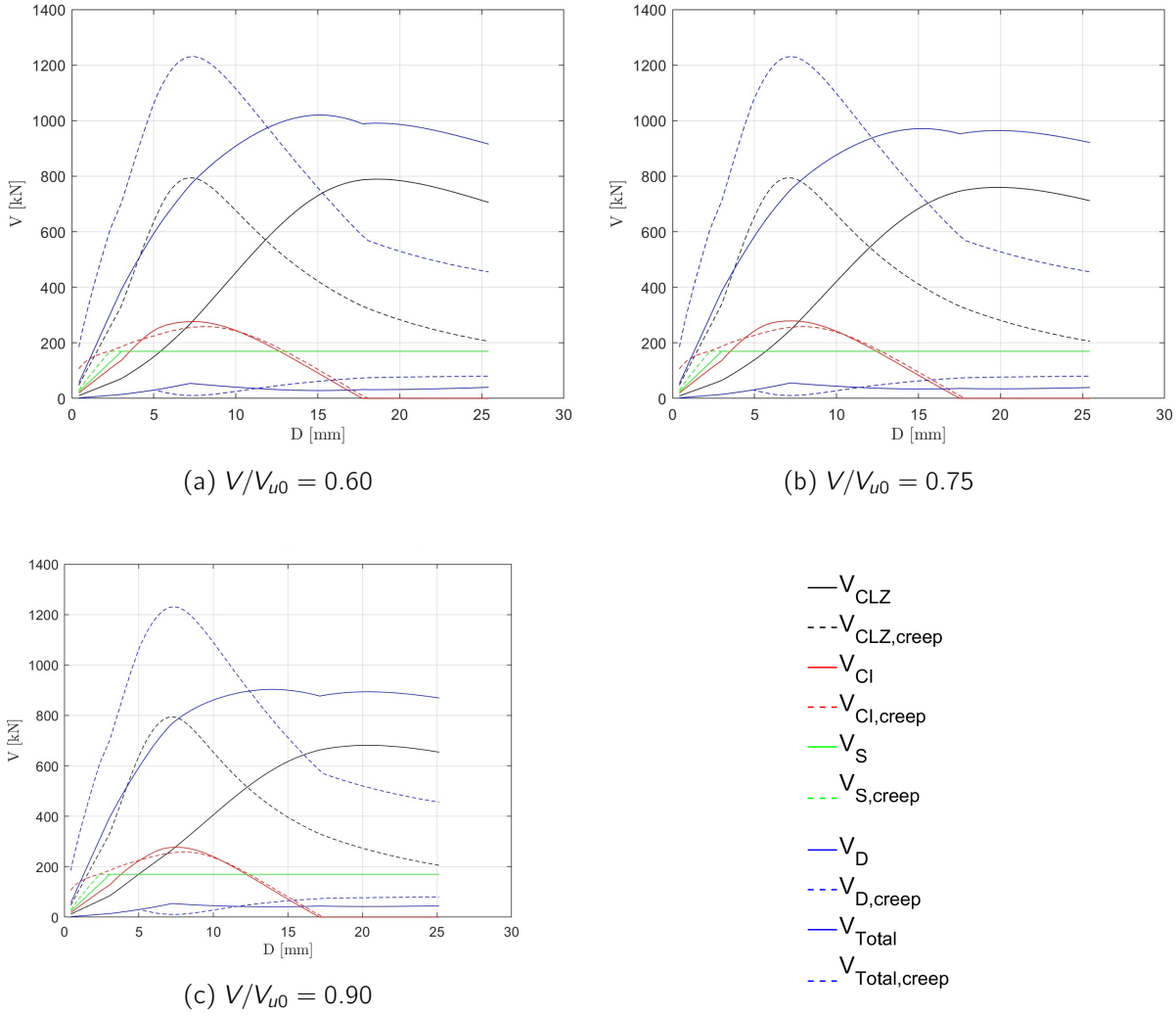

(a) $V/V_{u0} = 0.60$

(b) $V/V_{u0} = 0.75$

(c) $V/V_{u0} = 0.90$

Figure 4.22: Shear-resisting contributions versus Δ for $lb_1 = 450\,mm$ and $lb_2 = 225\,mm$

Case	Δ_u [mm]	$V_{\text{tot},u}$ [kN]	$V_{clz,\max}$ [kN]	$V_{ci,\max}$ [kN]
Short-term (no creep)	7.2	1230	790	257
50-year creep, $V/V_{u,0} = 0.60$	15	1020	789	276
50-year creep, $V/V_{u,0} = 0.75$	15	971	759	279
50-year creep, $V/V_{u,0} = 0.90$	13.9	903	681	280

Table 4.15: Failure displacement and shear capacities (short-term vs. 50-year creep) for $lb_1 = 450\,mm$ and $lb_2 = 225\,mm$

Key observations:

- Failure displacement Δ_u.

  Under creep, Δ_u increases from 7.2 mm (short-term) to 15 mm for $V/V_{u,0} = 0.60$ (+ 108%), to 15 mm for $V/V_{u,0} = 0.75$ (+ 108 %) and to 13.9 mm for $V/V_{u,0} = 0.90$ (+ 93%). By comparing with the results described in Section 4.2.1, the increase of the failure displacement is $\approx 25\%$ more important for with this increase of the widths of the loading plate and the support .

- Total shear capacity $V_{\text{tot},u}$.

  After 50 years of creep, $V_{\text{tot},u}$ decreases from 1230 kN (short-term) to 1020 kN for $V/V_{u,0} = 0.60$ (-17%), to 971 kN for $V/V_{u,0} = 0.75$ (-21%) and to 903 kN for $V/V_{u,0} = 0.90$ (-17.5%). By comparing with the results described in Section 4.2.1, the decrease in total shear resistance is $\approx 7 - 8$ % more important for $V/V_{u,0} = 0.60$ and $V/V_{u,0} = 0.75$ and is the same for $V/V_{u,0} = 0.90$.

Fig. 4.23 plot the evolution of the total shear capacity V_{tot} and its four component mechanisms (V_{clz}, V_{ci}, V_s, V_d) over a 50-year period of sustained loading.
In each plot, the abscissa is time (in days, up to $1.825 \times 10^4 \approx 50$ years), and the ordinate is shear force (kN)

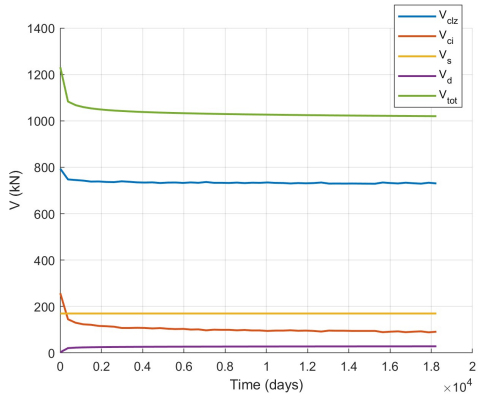

(a) $V/V_{u0} = 0.60$

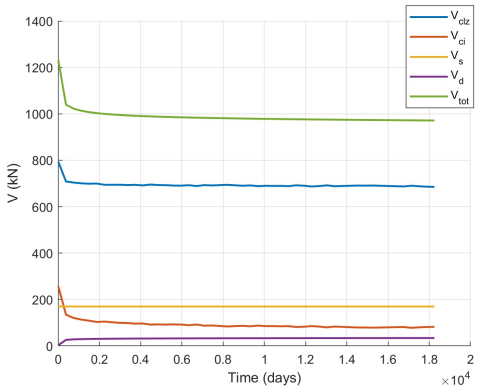

(b) $V/V_{u0} = 0.75$

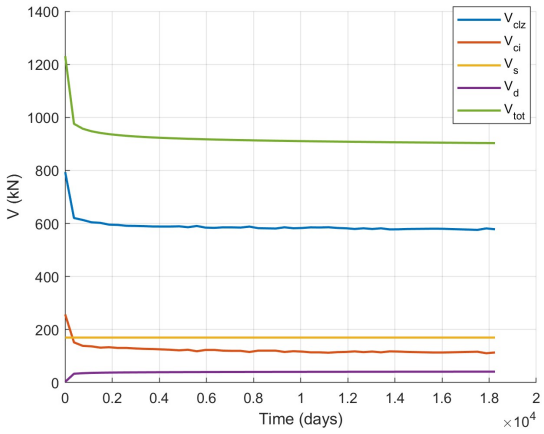

(c) $V/V_{u0} = 0.90$

Figure 4.23: Time-dependent shear resistance components for the beam S1M with $lb_1 = 450\,mm$ and $lb_2 = 225\,mm$

Fig. 4.24 shows the relationship between sustained load level V/V_{u0} (vertical axis) and time to failure (horizontal axis, in days, logarithmic scale) by comparing the reference case ($lb_1 = 300\,mm$ and $lb_2 = 150\,mm$) to the present configuration ($lb_1 = 450\,mm$ and $lb_2 = 225\,mm$). Each circular marker represents one computed data point from the numerical code. Vertical dashed lines at 1 year ($\approx$ 365 days), 50 years ($\approx$ 18 250 days), and 100 years ($\approx$ 36 500 days) are included to aid interpretation.

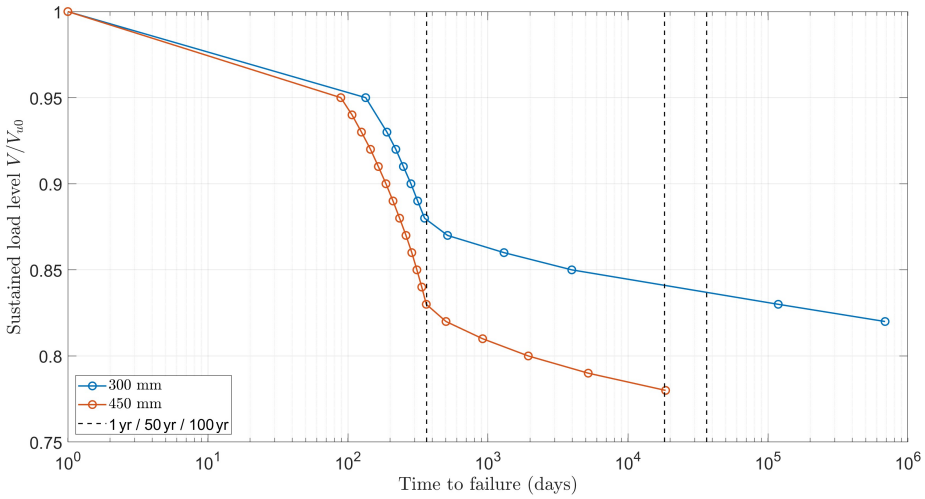

Figure 4.24: Sustained load level $V/V_{u,0}$ vs time of failure (in log scale)

Load Level $V/V_{u,0}$	**Time to Failure (days)**
0.95	89
0.94	107
0.93	125
0.92	145
0.91	165
0.90	187
0.89	210
0.88	234
0.87	260
0.86	286
0.85	311
0.84	337
0.83	363
0.82	502
0.81	917
0.80	1943
0.79	5206
0.78	18584

Table 4.16: Load levels and corresponding time to failure for beam S1M with $lb_1 = 450\,mm$ and $lb_2 = 225\,mm$.

Comparison with $lb_1 = 300\,mm$ and $lb_2 = 150\,mm$

A comparative analysis of the two curves plotted on Fig. 4.24 reveals :

- The very-short term region is almost similar for the two cases. In both cases the curve is nearly a straight line in log coordinates from t_0 up to 134 days for the case $lb_1 = 300\,mm$ and up to 89 days for $lb_1 = 450\,mm$ corresponding to the times of failure for a load level of $V/V_{u0} = 0.95$.
- The main difference between the 2 curves appears for the intermediate short-term region that goes in both cases from $\approx$ 134 days to $\approx$ 1 year (represented by the first vertical dashed line on Fig. 4.24).
  In fact, a time of failure of one year occurs by sustaining a load level of $V/V_{u0} = 0.88$ for $lb_1 = 300\,mm$ and by keeping constant load level of $V/V_{u0} = 0.83$, this a big difference.
- The gap between the two curves continues to increase. A time of failure of 50 years corresponds to a sustained load level $\approx V/V_{u0} = 0.845$ for the case $lb_1 = 300\,mm$ while the deep beam fails after 50 years for a sustained level of $V/V_{u0} = 0.78$ for $lb_1 = 450\,mm$.
- In the very long-term region, it was impossible to find some points that correspond to load levels $V/V_{u0} = 0.77$,$V/V_{u0} = 0.76$ and after for the present case because of a phenomenon observed on Fig. 4.25a and 4.25b that will be described right after.

It is impossible to compute the time of failure at very long term for levels $V/V_{u0} = 0.76$ and $V/V_{u0} = 0.77$ because of these jumps of V_{CLZ} and V_{ci} illustrated on Fig. 4.25a and 4.25b.
In fact, V_{CLZ} increases and V_{ci} goes to 0 and these phenomena impact the curve $V_{tot} - t$ leading to a slope almost constant and the impossibility to find some corresponding time for these levels.
It happens after 29 797 days $\approx$ 81 years for $V/V_{u0} = 0.76$ and after 26 073 days $\approx$ 71 years for $V/V_{u0} = 0.77$.

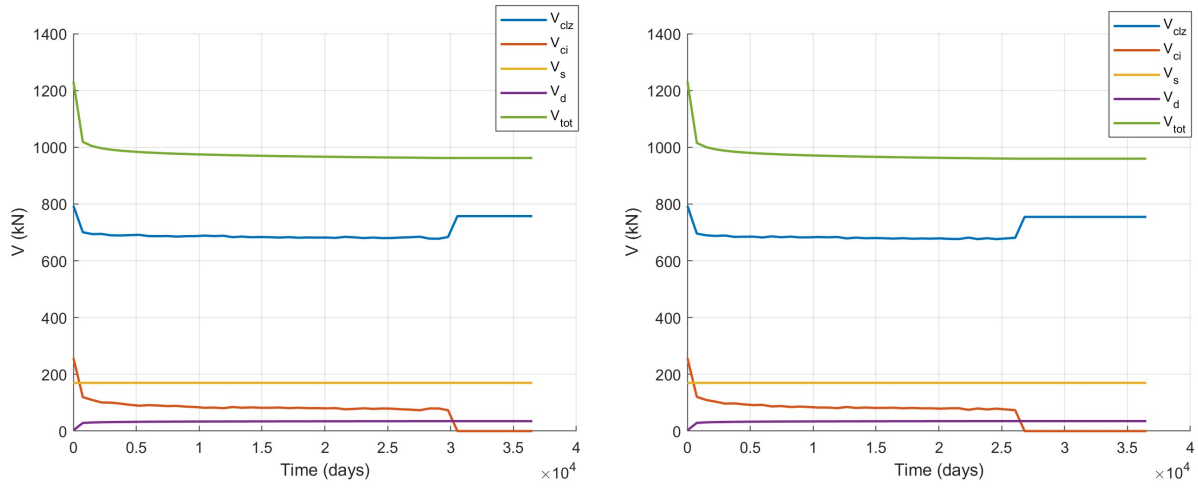

(a) $V/V_{u0} = 0.76$ (b) $V/V_{u0} = 0.77$

Figure 4.25: Time-dependent shear resistance components for the beam S1M with $lb_1 = 450\,mm$ and $lb_2 = 225\,mm$

Then, it is interesting to plot the curves of the different mechanisms with Δ at these fixed times to see exactly what happens and it is shown on Fig. 4.26 and 4.27.

As explained earlier, to compute the relationship $V - t$, at each time, the shear value of each mechanism is taken at the failure of the beam corresponding to the maximum of the curve $V_{tot} - \Delta$. The problem is that at these two specific times mentioned just before, there is a change of the maximum as shown on Fig. 4.26 and 4.27.

For the times before, the maximum corresponds always to the first value highlighted on the plots and after V_{tot} decreases. For these cases, it finds another maximum a little later.

This new maximum corresponds to a higher V_{CLZ} because $V_{CLZ} - \Delta$ is almost at the maximum that is why there is a jump of V_{CLZ} on Fig.4.25a and 4.25b.

This new maximum corresponds also to a value of the aggregate mechanism V_{ci} equals to zero, that is why there is a drop to 0 illustrated on Fig.4.25a and 4.25b.

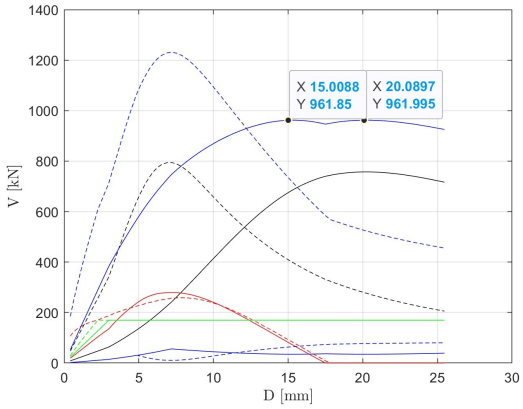

Figure 4.26: Shear-resisting contributions versus Δ for $V/V_{u0} = 0.76$ at t= 29 797 days

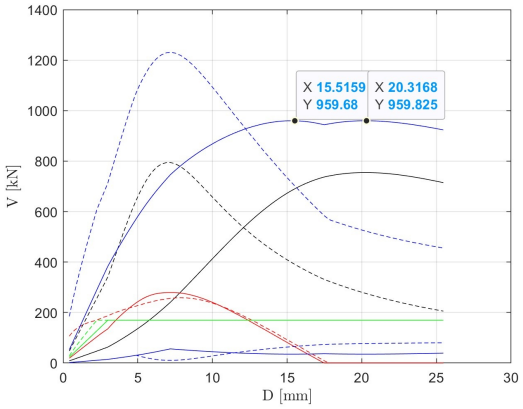

Figure 4.27: Shear-resisting contributions versus Δ for $V/V_{u0} = 0.77$ at t= 26 073 days

Fig. 4.28 shows the evolution of the crack-width w for the present case over a 50-year period for five different sustained load levels: $V/V_{u,0} = 0.60,\ 0.65,\ 0.70,\ 0.75,\ 0.80$. For all these load levels, the failure doesn't occur over 50 years except $V/V_{u,0} = 0.80$, which fails at approximately 1943 days (see Tab. 4.16).

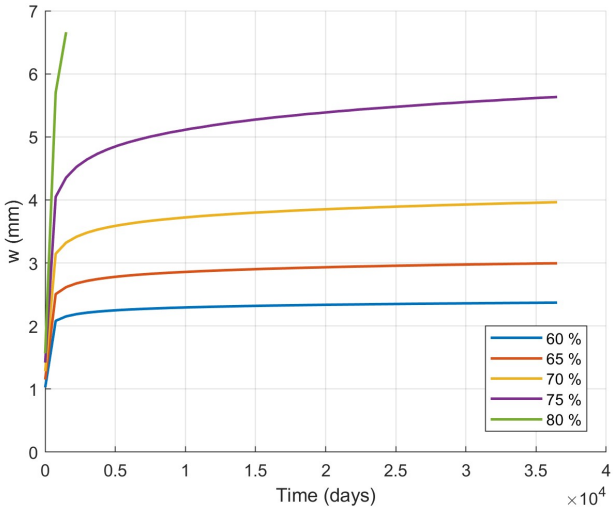

Figure 4.28: Time evolution of the crack-width $w(t)$ over 50 years

Load Level	$\mathbf{w_{t_0}}$ **[mm]**	$\mathbf{w_{t_{50}}}$ **[mm]**	**Increase (%)**
$0.60\,V/V_{u,0}$	1.02	2.37	132 %
$0.65\,V/V_{u,0}$	1.15	2.99	160%
$0.70\,V/V_{u,0}$	1.28	3.96	209%
$0.75\,V/V_{u,0}$	1.42	5.63	296%

Table 4.17: Critical crack-width w at $t = t_0$ and $t = 50$ years for various sustained load levels.

Fig. 4.29 and 4.30 plot the total midspan deflection $\Delta(t)$ and the concrete loading zone (CLZ) displacement $\Delta_c(t)$ for the same five load levels over 50 years.

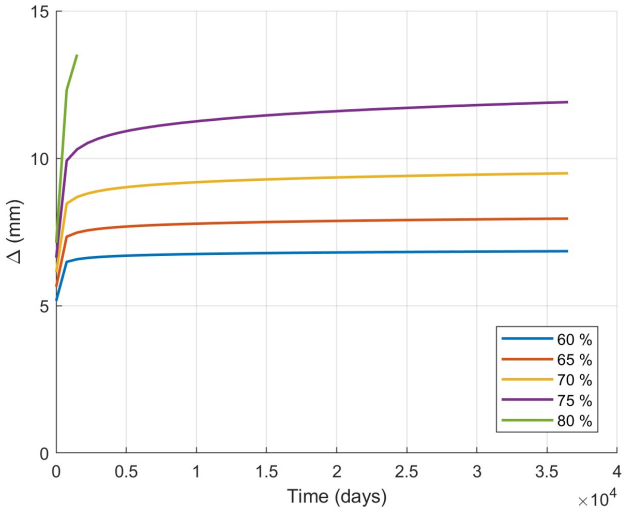

Figure 4.29: Time evolution of the total mid-span deflection $\Delta(t)$ over 50 years

Load Level	$\mathbf{\Delta_{t_0}}$ **[mm]**	$\mathbf{\Delta_{t_{50}}}$ **[mm]**	**Increase (%)**
$0.60\,V/V_{u,0}$	5.16	6.85	32.5 %
$0.65\,V/V_{u,0}$	5.64	7.95	41%
$0.70\,V/V_{u,0}$	6.13	9.49	54%
$0.75\,V/V_{u,0}$	6.62	11.9	79%

Table 4.18: Total deflection Δ at $t = t_0$ and $t = 50$ years for different sustained load levels.

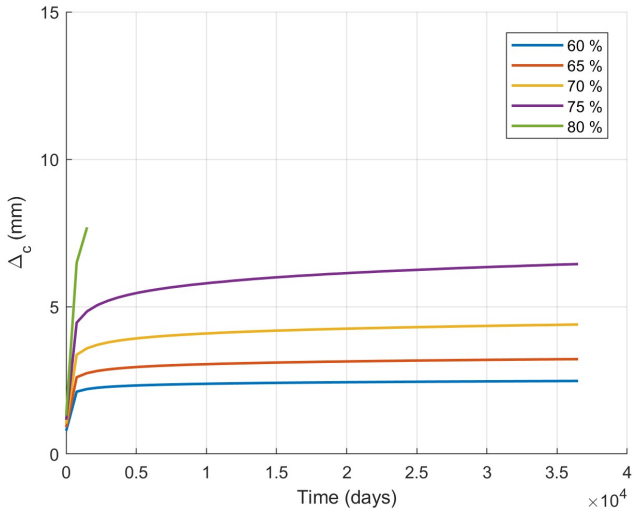

Figure 4.30: Time evolution of the CLZ displacement Δ_c over 50 years

Load Level	$\boldsymbol{\Delta_{c,t_0}}$ **[mm]**	$\boldsymbol{\Delta_{c,t_{50}}}$ **[mm]**	**Increase (%)**
$0.60\,V/V_{u,0}$	0.79	2.48	213%
$0.65\,V/V_{u,0}$	0.9	3.22	257%
$0.70\,V/V_{u,0}$	1.03	4.39	326 %
$0.75\,V/V_{u,0}$	1.16	6.44	455 %

Table 4.19: CLZ displacement Δ_c at $t = t_0$ and $t = 50$ years for different sustained load levels.

Comparison with the basic case ($lb_1 = 300\,mm, lb_2 = 150\,mm$)

- *Crack-Width Growth:*

  For the basic case, creep causes an increase between 92 % (for $0.60\,V/V_{u,0}$) and 142% (for $0.75\,V/V_{u,0}$) over 50 years while for this case it goes from 132 % (for $0.60\,V/V_{u,0}$) to 296 % (for $0.80\,V/V_{u,0}$).
  The beam fails at w=6.66 mm at $0.80\,V/V_{u,0}$.

- *Deflection Increase:*

  Sustained loading elevates Δ by 21 to 35 % after 50 years for $V/V_{u,0} = 0.60$-0.75 for the basic case while it increases Δ by 32.5 to 79% for S0M. At $0.80\,V/V_{u,0}$, Δ reaches 13.51 mm at failure.

- *CLZ Deformation:*

  The CLZ displacement Δ_c increases by 165 -229 % after 50 years for $V/V_{u,0} = 0.60$-0.75 for the basic case and by 213 to 455 % for the present case. At $0.80\,V/V_{u,0}$, Δ_c reaches 7,69 mm at failure.

4.3.3 Size of the member (a/d)

In this section, the changing parameter is the size of the member depending on the ratio a/d.The effective depth of the beam is held constant while the shear-span a is varied to change the a/d ratio.

The basic case studied in Section 4.2 has a ratio a/d=1.55 and in this section, two cases are considered :

- a/d=1
- a/d=2.28

First, the short-term predictions for each shear-resisting mechanism as a/d varies is considered. Fig. 4.31 from *Mihaylov and al.* illustrates this dependency clearly.
As a/d decreases, V_{CLZ} and the aggregate-interlock resistance V_{ci} contribute increasingly to the total shear capacity.

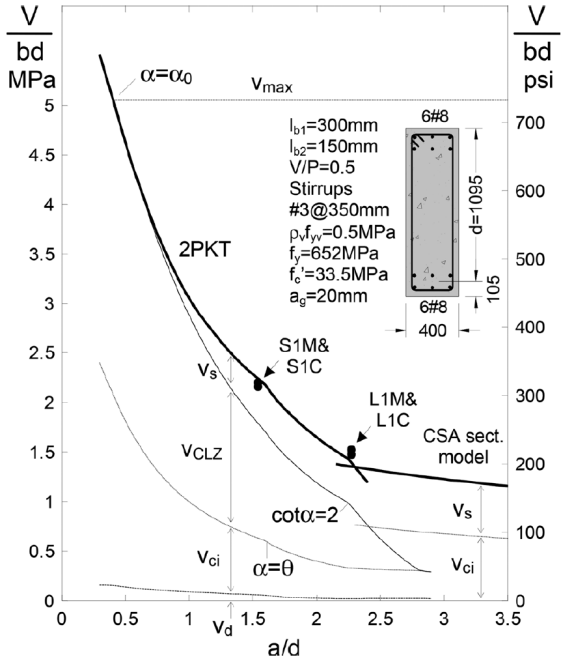

Figure 4.31: Size effect in deep beams (adapted from [1])

a/d=1

Here is the impact of reducing the a/d ratio to the value of 1.

In this case :

- a=1095 mm
- d=1095 mm

As expected, the short-term shear resistance of the concrete loading zone is higher by reducing the a/d ratio and compared to this short-term capacity there is a decrease :

- $\approx$ 2% for $V/V_{u,0} = 0.60$ ($\approx$ 0% for a/d=1.55)
- 6.4 % for $V/V_{u,0} = 0.75$ ($\approx$ 5% for a/d=1.55)

- 18 % for $V/V_{u,0} = 0.90$ ($\approx$ 17% for a/d=1.55)

This decrease due to creep is higher with a/d=1 than a/d=1.55 because the short-term resistance of the CLZ is higher so the CLZ carries higher stresses and, with this effect of integration of the fibers studied in Chap.2, the decrease in strength is more important.

Because the a/d ratio is lower, the ultimate displacements are also lower than the ones observed for the basic case (a/d=1.55) in Section 2.2.2 :

- For $V/V_{u,0} = 0.60$: 5.76 mm for $a/d = 1$ and 7.5 mm for $a/d = 1.55$
- For $V/V_{u,0} = 0.75$: 6.39 mm $a/d = 1$ and 6.39 mm $a/d = 1.55$
- For $V/V_{u,0} = 0.90$) : 6.57 mm $a/d = 1$ and 8.9 mm $a/d = 1.55$

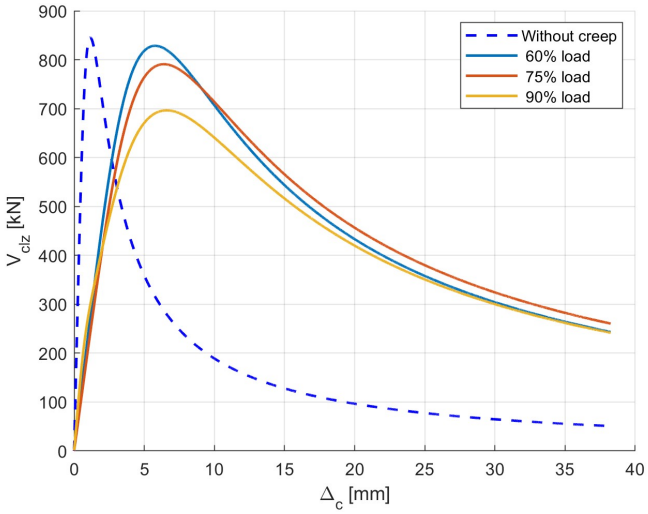

Figure 4.32: V_{CLZ}-Δ_c response for a/d=1

Load condition	Δ_{cu} [mm]	$V_{CLZ,\max}$ [kN]
Short-term (no creep)	2.96	844
$V/V_{u,0} = 0.60$	5.76	828
$V/V_{u,0} = 0.75$	6.39	790
$V/V_{u,0} = 0.90$	3.57	696

Table 4.20: Displacement capacity Δ_{cu} and shear resistance $V_{CLZ,\max}$ for a/d=1

Fig. 4.33 shows, for each sustained load level, the individual contributions of the four shear-resisting mechanisms : V_{clz} (Shear resistance of the CLZ), V_{ci} (aggregate-interlock), V_d (dowel action), and ($V_s = 0$) (stirrup action) plotted against the combined displacement $\Delta = \Delta_c + \Delta_t$

In each plot, dashed lines represent the short-term (no creep) response, while solid lines correspond to the long-term behavior after 50 years of sustained loading.

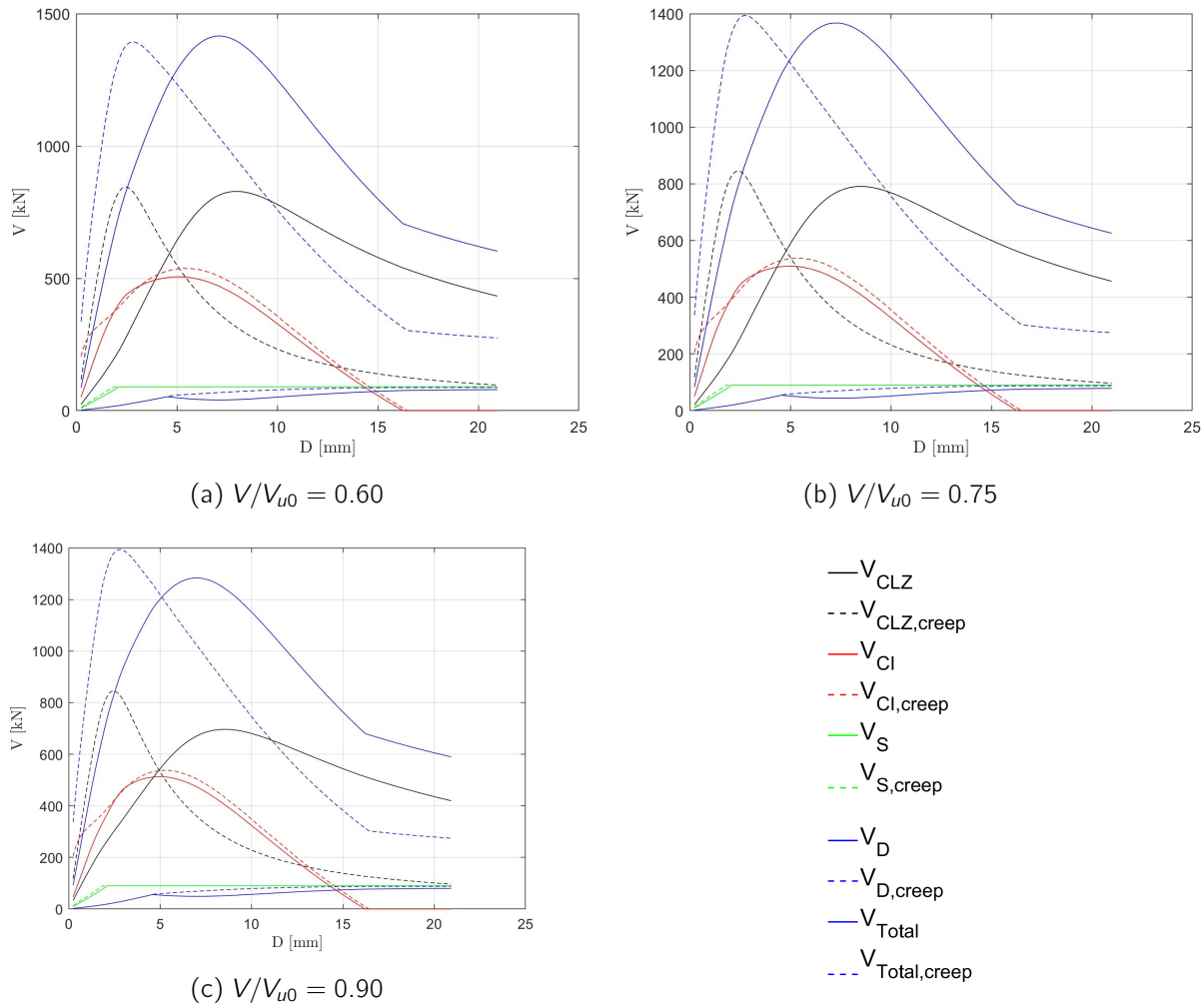

(a) $V/V_{u0} = 0.60$

(b) $V/V_{u0} = 0.75$

(c) $V/V_{u0} = 0.90$

Figure 4.33: Shear-resisting contributions versus Δ after 50 years for a/d=1

Case	Δ_u [mm]	$V_{\text{tot},u}$ [kN]	$V_{clz,\max}$ [kN]	$V_{ci,\max}$ [kN]
Short-term (no creep)	2.73	1393	844	538
50-year creep, $V/V_{u,0} = 0.60$	6.98	1415	828	505
50-year creep, $V/V_{u,0} = 0.75$	7.13	1366	790	509
50-year creep, $V/V_{u,0} = 0.90$	6.94	1283	696	513

Table 4.21: Failure displacement and shear capacities (short-term vs. 50-year creep) for $a/d = 1$

Key observations:

- Failure displacement Δ_u

  Under creep, Δ_u increases from 2.73 mm (short-term) to 6.98 mm for $V/V_{u,0} = 0.60$ (+ 156%), to 7.13 mm for $V/V_{u,0} = 0.75$ (+ 161 %) and to 6.94 mm for $V/V_{u,0} = 0.90$ (+ 154%).

- Total shear capacity $V_{\text{tot},u}$

  After 50 years of creep, $V_{\text{tot},u}$ increases from 1393 kN (short-term) to 1415 kN for $V/V_{u,0} = 0.60$, decreases to 1366 kN for $V/V_{u,0} = 0.75$ (-2%) and to 1283 kN for $V/V_{u,0} = 0.90$ (-8%).
  It might be surprising because in this case, creep has a positive impact on the shear capacity of the beam. In fact, the decreases are much less important than for the reference case and even more there is an increase in term of shear capacity for $V/V_{u,0} = 0.60$.

  It can be explained by the fact that the stiffness in the CLZ and in the aggregate interlock mechanism is about the same. This allows these mechanisms to interact constructively as their peaks are close and it contributes more to the total shear resistance and so it leads to a positive effect for the shear capacity of the beam.

Fig. 4.34 plots the evolution of the total shear capacity V_{tot} and its four component mechanisms (V_{clz}, V_{ci}, V_s, V_d) over a 50-year period of sustained loading.
In each plot, the abscissa is time (in days, up to $1.825 \times 10^4 \approx 50$ years), and the ordinate is shear force V (kN).

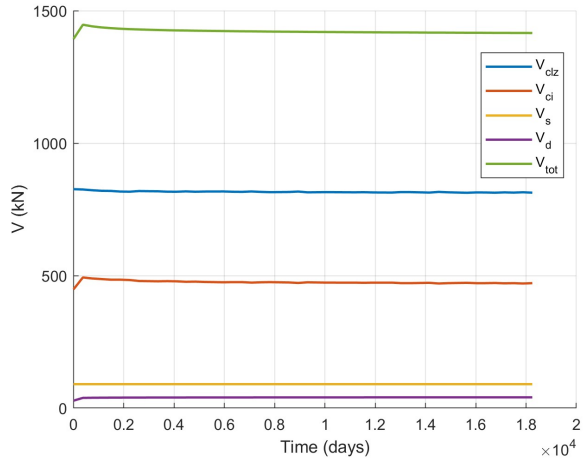

(a) $V/V_{u0} = 0.60$

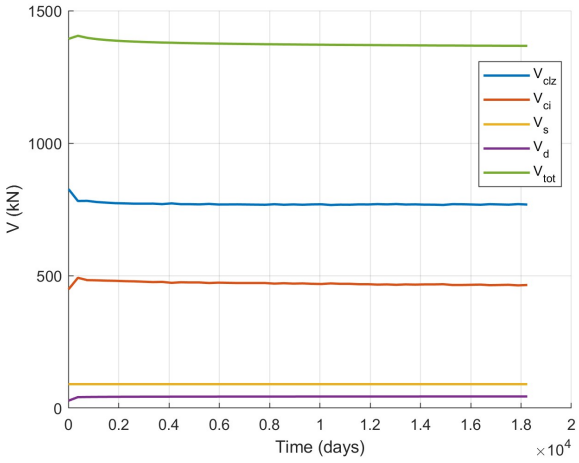

(b) $V/V_{u0} = 0.75$

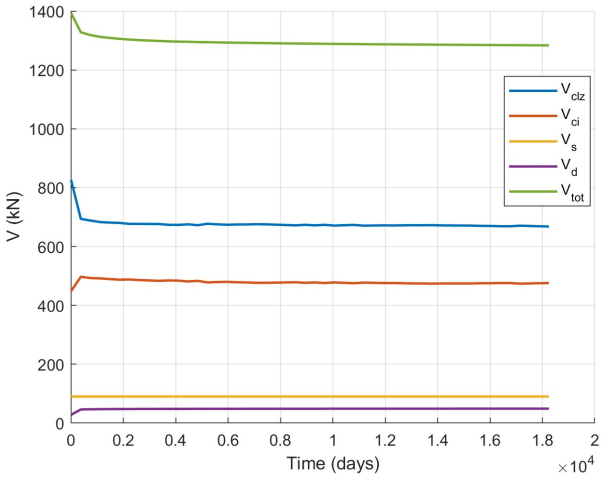

(c) $V/V_{u0} = 0.90$

Figure 4.34: Time-dependent shear resistance components for a/d=1

As shown by these figures, even for $V/V_{u,0} = 0.9$, it is impossible to find a time of failure at 50 years because the shear capacity at 50 years is $V_{tot,u} = 1283\,kN$ and it corresponds to a ratio $V_{tot,u}/V_{u,0} = 0.92$ so there is no time of failure for $V/V_{u,0} = 0.9$ over 50 years.

Therefore, it is not interesting to get a time of failure-load level relationship because just very, very high load levels will lead to failure.

Fig. 4.35 shows the evolution of the critical crack-width w for the present case $a/d = 1$ over a 50-year period for six different sustained shear-load levels. For all these load levels, the beam doesn't fail as discussed before but it is still interesting to see for service-life loading what is the increased case by the effect of creep on the crack-width.

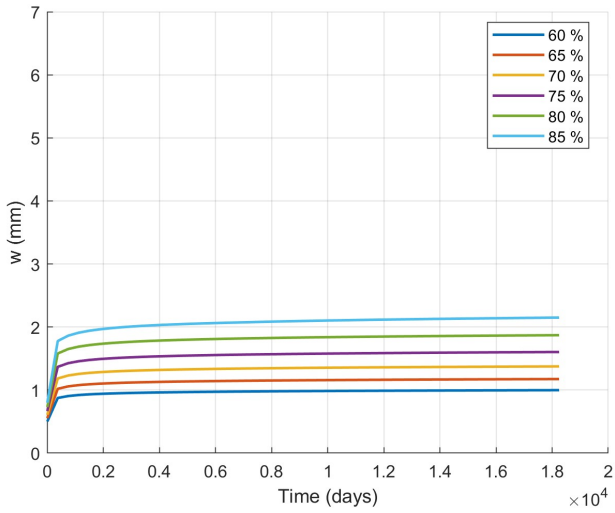

Figure 4.35: Time evolution of the crack-width $w(t)$ for a/d=1

Load Level	$\mathbf{w_{t_0}}$ **[mm]**	$\mathbf{w_{t_{50}}}$ **[mm]**	**Increase (%)**
$0.60\,V/V_{u,0}$	0.5	1	100%
$0.65\,V/V_{u,0}$	0.55	1.17	112.7 %
$0.70\,V/V_{u,0}$	0.61	1.38	126.2%
$0.75\,V/V_{u,0}$	0.67	1.6	138.9%
$0.80\,V/V_{u,0}$	0.73	1.87	156.2%
$0.85\,V/V_{u,0}$	0.8	2.15	168.8%

Table 4.22: Critical crack-width w at $t = t_0$ and $t = 50$ years for various sustained load levels.

Fig. 4.36 and 4.37 plot the total mid-span deflection $\Delta(t)$ and the concrete loading zone (CLZ) displacement $\Delta_c(t)$ for the same five load levels over 50 years.

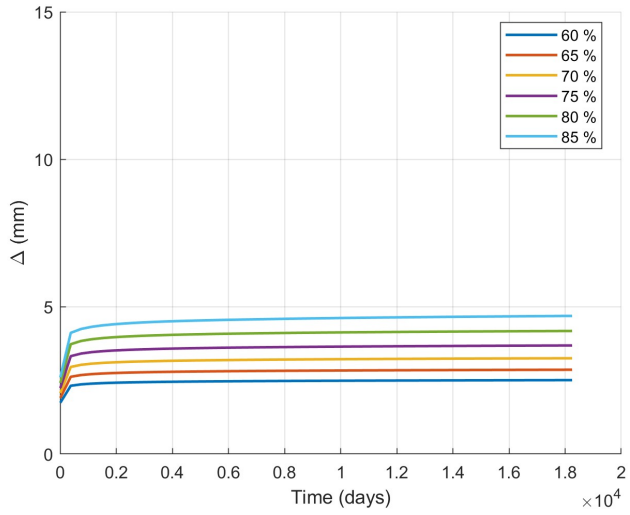

Figure 4.36: Time evolution of the total deflection Δ for a/d=1

Load Level	Δ_{t_0} **[mm]**	$\Delta_{t_{50}}$ **[mm]**	**Increase (%)**
$0.60\,V/V_{u,0}$	1.74	2.51	44.3%
$0.65\,V/V_{u,0}$	1.9	2.86	50.5%
$0.70\,V/V_{u,0}$	2.06	3.25	57.8%
$0.75\,V/V_{u,0}$	2.23	3.68	65 %
$0.80\,V/V_{u,0}$	2.41	4.17	73.3%
$0.85\,V/V_{u,0}$	2.6	4.69	80.4 %

Table 4.23: Total deflection Δ at $t = t_0$ and $t = 50$ years for different sustained load levels.

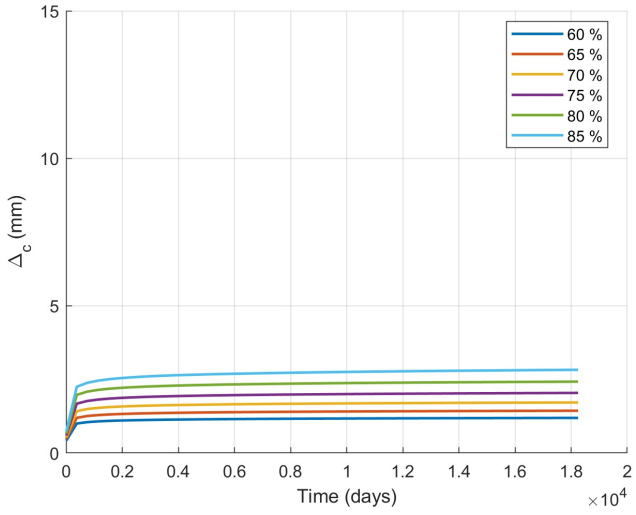

Figure 4.37: Time volution of the CLZ displacement Δ_c for a/d=1

Load Level	Δ_{c,t_0} **[mm]**	$\Delta_{c,t_{50}}$ **[mm]**	**Increase (%)**
$0.60\,V/V_{u,0}$	0.42	1.19	183.3 %
$0.65\,V/V_{u,0}$	0.47	1.43	204.3 %
$0.70\,V/V_{u,0}$	0.53	1.71	222.6 %
$0.75\,V/V_{u,0}$	0.59	2.04	245.8 %
$0.80\,V/V_{u,0}$	0.66	2.42	266.7 %
$0.85\,V/V_{u,0}$	0.74	2.82	281.1 %

Table 4.24: CLZ displacement Δ_c at $t = t_0$ and $t = 50$ years for different sustained load levels.

Comparison with the basic case ($a/d = 1.55$) :

- *Crack-Width Growth:*

  For the basic case ($a/d = 1.55$), creep causes an increase between 92 % (for $0.60\,V/V_{u,0}$) and 186% (for $0.80\,V/V_{u,0}$) over 50 years while for this case ($a/d = 1$) it goes from 100 % (for $0.60\,V/V_{u,0}$) to 156,2% (for $0.80\,V/V_{u,0}$).
  The beam fails at w=5.03 mm after $\approx$ 11 years at $0.85\,V/V_{u,0}$ for $a/d = 1.55$ while for $a/d = 1$, it does not fail for this level.

- *Deflection Increase:*

  Sustained loading elevates Δ by 21 to 48 % after 50 years for $V/V_{u,0}$ = 0.60-0.80 for the basic case ($a/d = 1.55$) while it increases Δ by 44 to 80 % for $a/d = 1$. At $0.85\,V/V_{u,0}$, Δ reaches 10.9 mm at failure for $a/d = 1.55$ while for $a/d = 1$, it does not fail for this level.

- *CLZ Deformation:*

  The CLZ displacement Δ_c increases by 165 -295 % after 50 years for $V/V_{u,0}$ = 0.60-0.80 for the basic case ($a/d = 1.55$) and by 183 to 267 % for the present case $a/d = 1$. At $0.85\,V/V_{u,0}$, Δ_c reaches 5.67 mm at failure for $a/d = 1.55$ while for $a/d = 1$, it does not for this level.

a/d=2.28

Here is the impact of increasing the a/d ratio to the value of 2.28.

In this case :

- a=2500 mm
- d=1095 mm

This ratio corresponds to the transition between deep beam and slender beam as shown on Fig.4.31.

As expected, the short-term shear resistance of the CLZ is lower by increasing the a/d ratio and compared to this short-term capacity there is a decrease :

- $\approx$ 0% for $V/V_{u,0} = 0.60$ ($\approx$ 0% for a/d=1.55)

- 4.5 % for $V/V_{u,0} = 0.75$ ($\approx$ 5% for a/d=1.55)
- 15.5 % for $V/V_{u,0} = 0.90$ ($\approx$ 17% for a/d=1.55)

This is the opposite behaviour compared to the case with $a/d = 1$. The reduction in shear resistance due to creep is less pronounced for $a/d = 2.28$ than for $a/d = 1.55$, because the short-term contribution of the CLZ is lower. As a result, the CLZ carries less stress, and due to the fiber integration effect discussed in Chapter 2, the overall decrease in shear resistance is smaller than in the reference case.

The ultimate displacements of the CLZ are greater than the ones observed for the basic case (a/d=1.55) in Section 2.2.2 :

- For $V/V_{u,0} = 0.60$: 12.5 mm for $a/d = 2.28$ and 7.5 mm for $a/d = 1.55$
- For $V/V_{u,0} = 0.75$: 14,04 mm $a/d = 2.28$ and 6.39 mm $a/d = 1.55$
- For $V/V_{u,0} = 0.90$) : 15.18 mm $a/d = 2.28$ and 8.9 mm $a/d = 1.55$

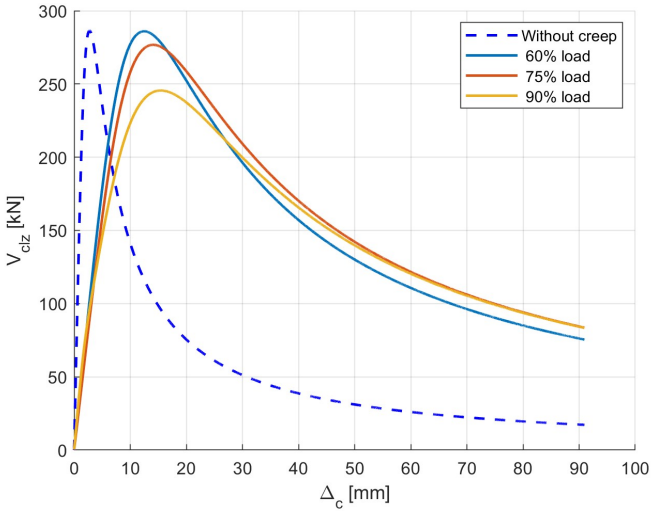

Figure 4.38: V_{CLZ}-Δ_c response for a/d=2.28

Load condition	Δ_{cu} [mm]	$V_{CLZ,\max}$ [kN]
Short-term (no creep)	2.88	286
$V/V_{u,0} = 0.60$	12.5	286
$V/V_{u,0} = 0.75$	14.04	276
$V/V_{u,0} = 0.90$	15.18	245

Table 4.25: Displacement capacity Δ_{cu} and shear resistance $V_{CLZ,\max}$

Fig. 4.39 shows, for each sustained load level, the individual contributions of the four shear-resisting

mechanisms : V_{clz} (Shear resistance of the CLZ), V_{ci} (aggregate-interlock), V_d (dowel action), and ($V_s = 0$) (stirrup action) plotted against the combined displacement $\Delta = \Delta_c + \Delta_t$

In each plot, dashed lines represent the short-term (no creep) response, while solid lines correspond to the long-term behavior after 50 years of sustained loading.

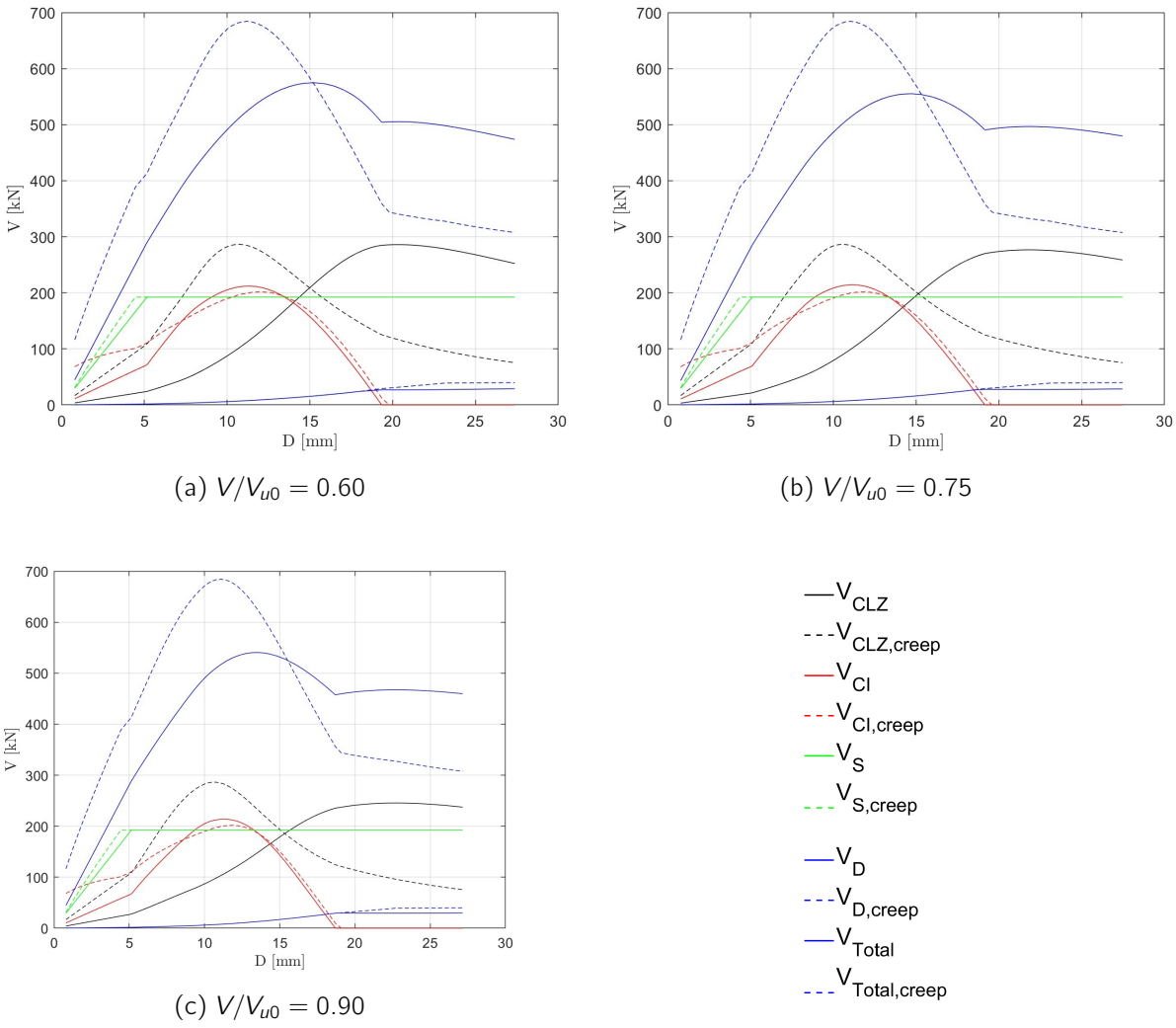

(a) $V/V_{u0} = 0.60$

(b) $V/V_{u0} = 0.75$

(c) $V/V_{u0} = 0.90$

Figure 4.39: Shear-resisting contributions versus Δ for a/d=2.28

Case	Δ_u [mm]	$V_{\text{tot},u}$ [kN]	$V_{clz,\max}$ [kN]	$V_{ci,\max}$ [kN]
Short-term (no creep)	11.13	684	286	201
50-year creep, $V/V_{u,0} = 0.60$	15.22	574	286	212
50-year creep, $V/V_{u,0} = 0.75$	14.73	555	276	214
50-year creep, $V/V_{u,0} = 0.90$	13.49	540	245	214

Table 4.26: Failure displacement and shear capacities (short-term vs. 50-year creep) for $a/d = 2.28$

Key observations:

- Failure displacement Δ_u.

  Under creep, Δ_u increases from 11.13 mm (short-term) to 15.22 mm for $V/V_{u,0} = 0.60$ (+ 37%), to 14.73 mm for $V/V_{u,0} = 0.75$ (+ 32 %) and to 13.49 mm for $V/V_{u,0} = 0.90$ (+ 21%).

- Total shear capacity $V_{\text{tot},u}$.

  After 50 years of creep, $V_{\text{tot},u}$ decreases from 684 kN (short-term) to 574 kN for $V/V_{u,0} = 0.60$ (-16%), decreases to 555 kN for $V/V_{u,0} = 0.75$ (-19%) and to 540 kN for $V/V_{u,0} = 0.90$ (-21%). The aggregate interlock and CLZ mechanisms reach their peaks for some very different displacements Δ and that leads to a higher decrease of the shear capacity over 50 years when the beam is pushed to failure.

Fig. 4.40 plots the evolution of the total shear capacity V_{tot} and its four component mechanisms (V_{clz}, V_{ci}, V_s, V_d) over a 50-year period of sustained loading for the considered $a/d = 2.28$.
In each plot, the abscissa is time (in days, up to $1.825 \times 10^4 \approx 50$ years), and the ordinate is shear force V (kN)

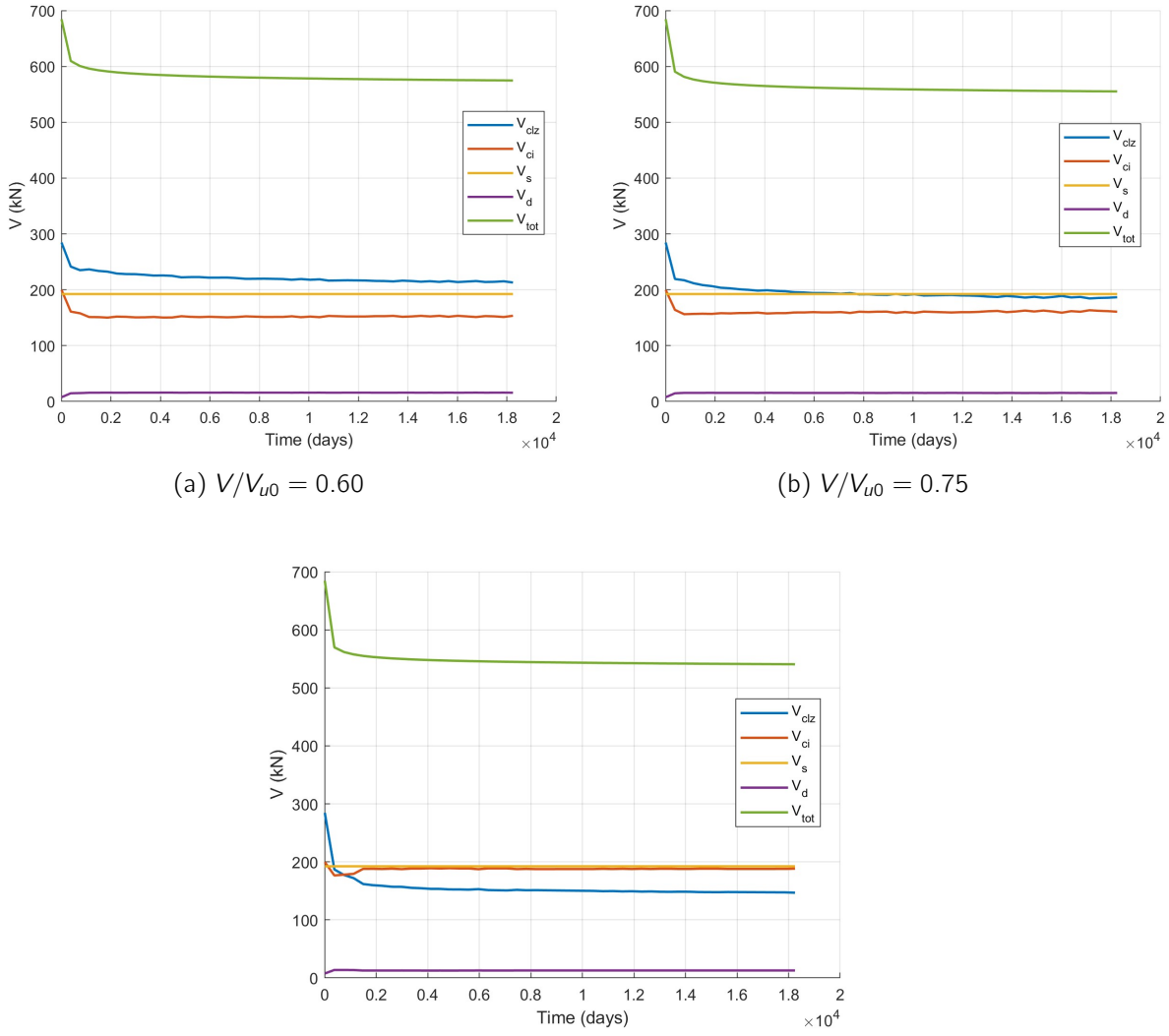

(a) $V/V_{u0} = 0.60$

(b) $V/V_{u0} = 0.75$

(c) $V/V_{u0} = 0.90$

Figure 4.40: Time-dependent shear resistance components for a/d=2.28

Fig. 4.41 shows the relationship between sustained load level V/V_{u0} (vertical axis) and time to failure (horizontal axis, in days, logarithmic scale) by comparing the reference case ($a/d = 1.55$) to the present configuration ($a/d = 2.28$) . Each circular marker represents one computed data point from the numerical code. Vertical dashed lines at 1 year ($\approx$ 365 days), 50 years ($\approx$ 18 250 days), and 100 years ($\approx$ 36 500 days) are included to aid interpretation.

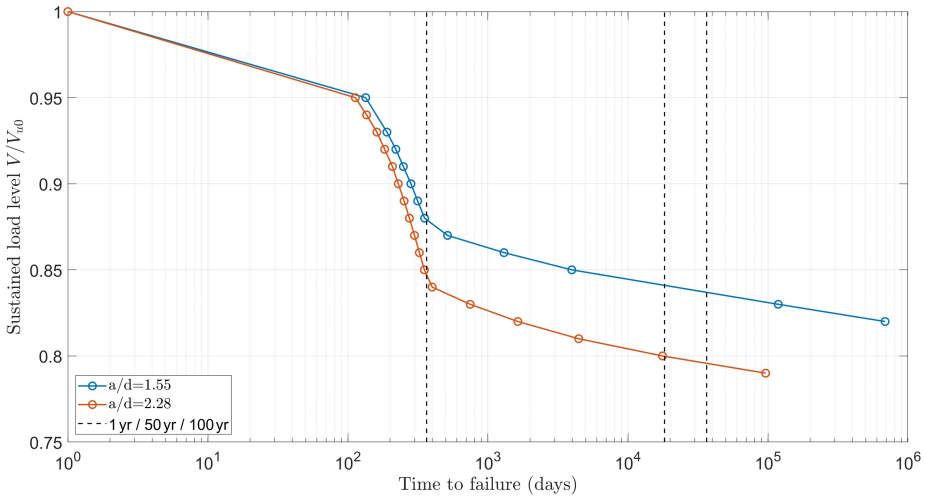

Figure 4.41: Sustained load level $V/V_{u,0}$ vs time of failure

Load Level $V/V_{u,0}$	**Time to Failure (days)**
0.95	113
0.94	136
0.93	161
0.92	183
0.91	208
0.90	229
0.89	252
0.88	275
0.87	299
0.86	324
0.85	352
0.84	400
0.83	747
0.82	1636
0.81	4451
0.80	17669
0.79	96314

Table 4.27: Load levels and corresponding time to failure for beam S1M with a/d=2.28

A comparative analysis of the two curves plotted on Fig.4.41 :

- The very-short term region is almost similar for the two cases, in both cases the curve is nearly a straight line in log coordinates from t_0 up to 134 days for the case $a/d = 1.55$ and up to 113 days for $a/d = 2.28$ corresponding to the times of failure for a load level of $V/V_{u0} = 0.95$.
- The big difference between the 2 curves appears for the intermediate short-term region that goes in both cases from $\approx$ 134 days to $\approx$ 1 year (represented by the first vertical dashed line on Fig. 4.41).
  In fact, a time of failure of one year occurs by sustaining a load level of $V/V_{u0} = 0.88$ for $a/d = 1.55$ and by keeping constant load level of $\approx V/V_{u0} = 0.85$ for $a/d = 2.28$.
- The gap between the two curves remains approximately constant until very large times. A time of failure of 50 years corresponds to a sustained load level $\approx V/V_{u0} = 0.845$ for the case $a/d = 1.55$ while the deep beam fails after 50 years for a sustained level of approximately $V/V_{u0} = 0.80$ for $a/d = 2.28$.

Fig. 4.42 shows the evolution of the critical crack-width w for the present case $a/d = 2.28$ over a 50-year period for five different sustained shear-load levels: $V/V_{u,0} = 0.60,\ 0.65,\ 0.70,\ 0.75,\ 0.80,$. All of these load levels lie below the time-to-failure curve for 50 years except for $V/V_{u,0} = 0.80$, which corresponds to a failure of approximately 17 669 days.

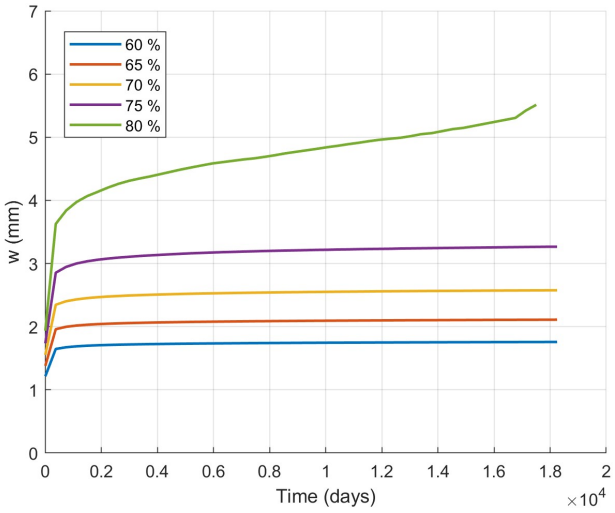

Figure 4.42: Time evolution of the crack-width $w(t)$ for a/d=2.28

Load Level	$\mathbf{w_{t_0}}$ **[mm]**	$\mathbf{w_{t_{50}}}$ **[mm]**	**Increase (%)**
$0.60\,V/V_{u,0}$	1.21	1.76	45.5%
$0.65\,V/V_{u,0}$	1.38	2.11	52.9%
$0.70\,V/V_{u,0}$	1.55	2.57	65.8%
$0.75\,V/V_{u,0}$	1.73	3.26	88.4%

Table 4.28: Critical crack-width w at $t = t_0$ and $t = 50$ years for various sustained load levels.

Fig. 4.43 and 4.44 plot the total mid-span deflection $\Delta(t)$ and the concrete loading zone (CLZ) displacement $\Delta_c(t)$ for the same five load levels over 50 years.

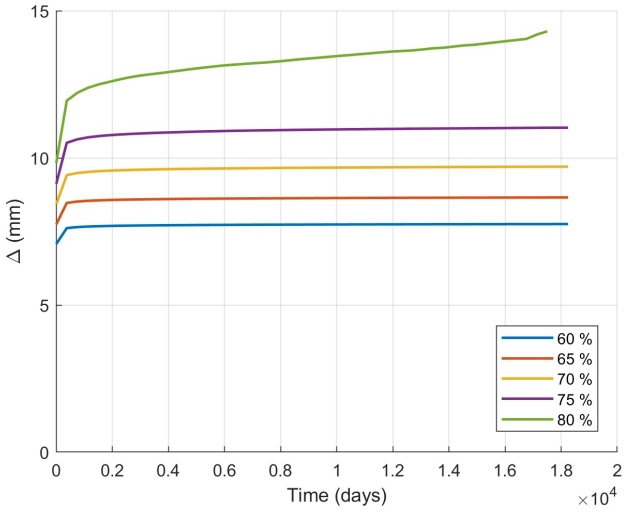

Figure 4.43: Time evolution of the total deflection Δ for a/d=2.28

Load Level	Δ_{t_0} **[mm]**	$\Delta_{t_{50}}$ **[mm]**	**Increase (%)**
$0.60\,V/V_{u,0}$	7.07	7.75	9.6%
$0.65\,V/V_{u,0}$	7.74	8.66	11.9 %
$0.70\,V/V_{u,0}$	8.42	9.7	15.2%
$0.75\,V/V_{u,0}$	9.12	11.03	20.9 %

Table 4.29: Total deflection Δ at $t = t_0$ and $t = 50$ years for different sustained load levels.

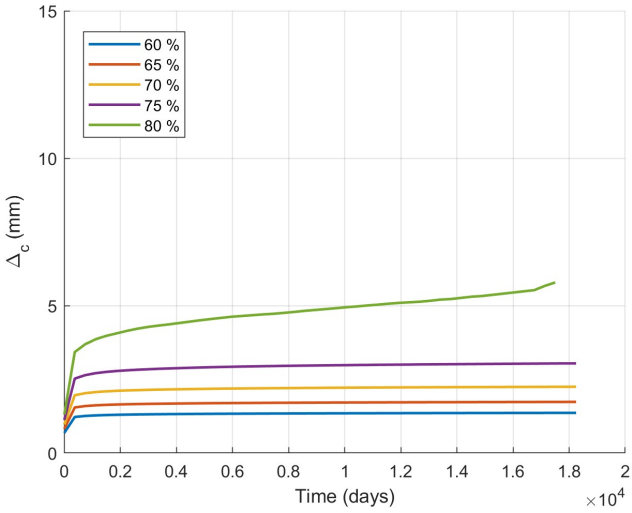

Figure 4.44: Time evolution of the CLZ displacement Δ_c for a/d=2.28

Load Level	Δ_{c,t_0} **[mm]**	$\Delta_{c,t_{50}}$ **[mm]**	**Increase (%)**
$0.60\,V/V_{u,0}$	0.68	1.32	94,1%
$0.65\,V/V_{u,0}$	0.82	1.73	110%
$0.70\,V/V_{u,0}$	0.96	2.25	134.4%
$0.75\,V/V_{u,0}$	1.12	3.04	171.4%

Table 4.30: CLZ displacement Δ_c at $t = t_0$ and $t = 50$ years for different sustained load levels.

Comparison with the basic case ($a/d = 1.55$)

- *Crack-Width Growth:*

  For the basic case ($a/d = 1.55$), creep causes an increase between 92 % (for $0.60\,V/V_{u,0}$) and 142% (for $0.75\,V/V_{u,0}$) over 50 years while for this case it goes from 45 % (for $0.60\,V/V_{u,0}$) to 88% (for $0.80\,V/V_{u,0}$).
  The beam fails at w=5.51 mm at $0.80\,V/V_{u,0}$ as shown on Fig. 4.42.

- *Deflection Increase:*

  Sustained loading elevates Δ by 21 to 35 % after 50 years for $V/V_{u,0} = 0.60$-0.75 for the basic case ($a/d = 1.55$) while it increases Δ by 9.6 to 20.9% for $a/d = 2.28$. At $0.80\,V/V_{u,0}$, Δ reaches 14.3 mm at failure as shown on Fig.4.43.

- *CLZ Deformation:*

  The CLZ displacement Δ_c increases by 165 -229 % after 50 years for $V/V_{u,0} = 0.60$-0.75 for the basic case ($a/d = 1.55$) and by 94 to 171% for the present case $a/d = 2.28$. At $0.80\,V/V_{u,0}$, Δ_c reaches 5.78 mm at failure as shown on Fig. 4.44.

4.3.4 Conclusion of the parametric analysis

1. **Shear reinforcement :**

   Without shear reinforcement, the CLZ mechanism (V_{CLZ}) becomes the dominant contributor to total shear resistance. Because V_{CLZ} is highly sensitive to creep, S0M exhibits a much larger increase in failure displacement Δ_u and a correspondingly larger reduction in ultimate shear capacity $V_{\mathrm{tot},u}$ after 50 years, compared to S1M.

   When considering time-dependency under constant loading, S1M requires a sustained load level of approximately $0.84\,V/V_{u,0}$ to fail at 50 years, whereas S0M (without shear reinforcement) fails after 50 years at a lower sustained load of only $0.815\,V/V_{u,0}$. In this case, removing the stirrups results in a larger reduction of $\approx 2.5\%$ of the shear capacity of the deep beam over 50 years under sustained loading.

   Over a 50-year period, creep also has a more pronounced effect on crack width and mid-span deflection in the absence of shear reinforcement. Even though S0M does not fail under load levels ($V/V_{u,0} = 0.60$-0.80) within 50 years, the crack width increases by 127%-255 %, and the mid-span deflection increases by 34 %-74 %. These results confirm that eliminating shear reinforcement amplifies the long-term deformations and accelerates shear-failure under sustained loads.

2. **Width of the loading plate and width of the support :**

   Increasing the width of the loading plate $l_{b1} = 450\,\text{mm}$ and the width of the support $l_{b2} = 225\,\text{mm}$ leads to a larger increase in failure displacement Δ_u compared to the baseline case ($l_{b1} = 300\,\text{mm}$, $l_{b2} = 150\,\text{mm}$), as well as a greater reduction in ultimate shear capacity $V_{\text{tot},u}$ when the beam is pushed to failure after 50 years.

   When considering time-dependency under constant loading, the present configuration ($l_{b1} = 450\,\text{mm}$, $l_{b2} = 225\,\text{mm}$) requires a sustained load of $0.78\,V/V_{u,0}$ to reach failure at 50 years, whereas the baseline beam ($l_{b1} = 300\,\text{mm}$, $l_{b2} = 150\,\text{mm}$) fails after 50 years only under a higher sustained load of $0.84\,V/V_{u,0}$. Increasing the dimensions of l_{b1} and lb_2 by a factor 1.5 leads to a larger decrease of 6% of the shear capacity of the deep beam over 50 years under sustained loading.

   Over a 50-year period, creep also has a more pronounced effect on crack width and mid-span deflection when the loading plate and support widths are increased. Although, the beam does not fail under load levels ($V/V_{u,0} = 0.60$–0.75) within 50 years, the crack width increases by 132%-296% and the mid-span deflection increases by 32.5%-79%. These results confirm that enlarging the loading plate and support dimensions amplifies long-term deformations and accelerates shear failure under sustained loads.

3. **Size of the member (a/d) :**

   Changing the size of the member by reducing or increasing the ratio a/d changes a lot the behaviour to the effect of creep.

   In fact, for small a/d ratios (such as a/d=1), the loss in ultimate shear capacity $V_{tot,u}$ when the beam is pushed to failure is very small and even more there is an increase of ultimate shear capacity under service loads such as $V/V_{u,0} = 0.6$ due to the combined effect of the aggregate interlock and CLZ mechanisms which interact with similar stiffness to provide a high shear capacity at failure.

   While, for big a/d ratios (such as a/d=2.28), the loss in ultimate shear capacity $V_{tot,u}$ when the beam is pushed to failure is high because of the very low stiffness in the CLZ.

   When considering time-dependency under constant loading, because of this very low decrease in ultimate shear capacity, it is impossible to find a time of failure even at $V/V_{u,0} = 0.9$ for the case a/d=1. Therefore, delayed shear failure under sustained loads for deep beams with very short span is excluded.
   The conclusion is different for members with longer span (a/d=2.28), where the failure occurs after 50 years for a sustained load level of $\approx V/V_{u,0} = 0.8$. It means that changing the span-to-depth ratio from 1.55 to 2.28 leads to a larger decrease of 4% of shear capacity over 50 years under sustained loading.

   However, over a 50-year period, creep has a more pronounced effect on crack width and mid-span deflection for the ratio $a/d = 1$ than for the ratio $a/d = 2.28$.
   In fact, for $a/d = 2.28$, the increase of the crack-width over 50 years goes from 45% for $V/V_{u,0} = 0.6$ to 66 % for $V/V_{u,0} = 0.7$ while for $a/d = 1$, it goes from 100% for $V/V_{u,0} = 0.6$ to 126 % for $V/V_{u,0} = 0.7$.
   Same conclusion for the total mid-span deflection where the increase goes for $a/d = 2.28$ from 10 % for $V/V_{u,0} = 0.6$ to 15% for $V/V_{u,0} = 0.7$ while for $a/d = 1$, it goes from 44% for $V/V_{u,0} = 0.6$ to 58 % for $V/V_{u,0} = 0.7$.

Chapter 5

Conclusion

The goal of this work was to study the effect of creep on the behaviour of RC deep beams. The short-term behaviour of deep beams was known with the Two-Parametric Kinematic Theory, this method computes the total shear resistance by summing the contributions of four shear-resisting mechanisms : resistance of the Concrete Loading Zone (V_{CLZ}), resistance by aggregate interlock (V_{ci}), resistance by strirrups (V_s) and resistance by dowel action (V_d).

The challenge was to implement methods to include creep in this model.

The application of creep is done in the same way in both principal mechanism which composed the 2PKT model. To discretize the CLZ or the crack for aggregate interlock allows to treat each stress of each fiber or each stress of each spring (for aggregate interlock) independently.

For the CLZ, the stress-strain curve reveals high stresses, making crucial to account for them. When the ratio σ/f_{cm} exceeds 0.75, a different type of creep, known as tertiary, begins. This phase involves micro-cracking, which leads to failure due to a rapid increase in strain.

The creep coefficient is applied independently on the stiffness of each fiber and then all the fibers are integrated to take into account all the local stiffness leading to a decrease of the compressive strength in the CLZ and by the way a decrease of shear resistance of the CLZ.

For aggregate-interlock, the crack is discretized into a set of planes at various inclinations, and micro-springs are used to model the contact between the two faces of the crack. It is a similar way to proceed because the creep coefficient is applied on the stiffness of each spring and then the integration of all the spring across the crack leads to a loss of shear resistance by aggregate-interlock.

In term of total shear capacity, the CLZ governs the behaviour of deep beams under creep because it is for this mechanism that the loss in stiffness and in resistance is the highest. It depends also on the ability of the CLZ to work with other mechanisms to contribute to the total shear resistance. In fact, the perfect example is for very short span-to-depth ratio (a/d=1) where aggregate interlock and CLZ because of their stiffness reach their own maximums closely and contribute more to the total resistance even with an important loss of resistance for the CLZ mechanism properly.

It depends also on the other mechanisms engaged such as resistance by stirrups V_s because where

there is no shear reinforcement, the contribution of CLZ mechanism to the total shear resistance is higher because the CLZ takes more resistance due to this missing mechanism. Higher contribution of the CLZ means higher stresses in the CLZ and therefore a higher effect of creep on the resistance of the CLZ itself and on the total shear resistance.

The time of reference for creep in this thesis is fixed at 50 years because going further doesn't impact the total shear resistance because the creep coefficient is stabilized as discussed when the time was extended to 100 years leading on a negligible decrease of the total shear resistance.

The shear load level versus time to failure relation give important data such as the load level that corresponds to the time of failure at 50 years. It corresponds to the the load level $V/V_{u,0}$ that the beam can sustain for 50 years but not further. In other words, it is the remaining shear capacity over 50 years.
It is computed for different configurations and different parameters and here are recalled the results in term of loss of shear capacity over 50 years under sustained load :

1. Varying the shear reinforcement (ρ_v)

	Loss of shear capacity over 50 years [%]
$\rho_v = 0,1\%$	-16%
$\rho_v = 0\%$	-19%

Table 5.1: Loss of shear capacity over 50 years

2. Varying the width of the loading plate (lb_1) and the width of the support (lb_2)

	Loss of shear capacity over 50 years [%]
$lb_1 = 300\,mm$ and $lb_2 = 150\,mm$	-16%
$lb_1 = 450\,mm$ and $lb_2 = 225\,mm$	-22%

Table 5.2: Loss of shear capacity over 50 years

3. Varying the size of the member (a/d)

	Loss of shear capacity over 50 years [%]
$a/d = 1$	$\approx 0\%$
$a/d = 1.55$	-16%
$a/d = 2.28$	-20%

Table 5.3: Loss of shear capacity over 50 years

Globally, there is a decrease of the shear capacity of $\approx 20\%$ for deep beam under sustained loads over 50 years.

In term of serviceability, three main parameters are studied :

- Crack-width w
- Total deflection at mid-span Δ
- Displacement of the CLZ Δ_c

Service loads correspond to $V/V_{u,0} = 0.6$ and $V/V_{u,0} = 0.65$ and a summary of the increase over 50 years for the three parameters are reported in Tab. 5.4 and Tab. 5.5.

	Reference case	$\rho_v = 0\%$	$lb_1 = 450\,mm$ and $lb_2 = 225\,mm$	$a/d = 1$	$a/d = 2.28$
w	+92%	+127%	+132%	+100%	+46%
Δ	+21%	+34%	+33%	+44%	+10%
Δ_c	+165%	+194%	+213%	+183%	+94%

Table 5.4: Increase in % between t_0 and t=50 years for $V/V_{u,0} = 0.6$

	Reference case	$\rho_v = 0\%$	$lb_1 = 450\,mm$ and $lb_2 = 225\,mm$	$a/d = 1$	$a/d = 2.28$
w	+108%	+141 %	+160%	+113%	+53%
Δ	+25%	+38%	+41%	+51%	+12%
Δ_c	+182 %	+211%	+257%	+204%	+110%

Table 5.5: Increase in % between t_0 and t=50 years for $V/V_{u,0} = 0.65$

These results show that creep under typical service loads has a pronounced impact on serviceability : crack openings and deflections enlarge significantly over decades.
In design and assessment of deep beams, this time-dependent deformation must be accounted to ensure long-term crack control and limit deflections below acceptable thresholds.

While numerical simulations conducted in this study provide insights into the long-term effects of creep on RC deep beams, experimental validation remains crucial to confirm or challenge the predictions.

Such tests could involve applying service-level loads to specimens and monitoring their time-dependent responses (e.g. deflection,cracking) for several months or years but also long-term creep tests to failure to confirm the predicted long-term loss in shear capacity. This would allow for a direct comparison between observations and the numerical trends.

In the absence of long-term test data, the current results should be interpreted with caution.

A relevant perspective for future research would be to investigate the effect of variable sustained loading over time. In the present study, only a single constant level is maintained throughout the simulation. However, in real structural scenarios, such as the addition of a traffic lane on an existing bridge. The applied load may remain constant for a number of years and then increase due to new usage demands before being sustained again at this higher load level.

This multi-phase loading history could influence the development of creep deformations and alter the time-to-failure response.
Therefore, incorporating variable load histories into the current framework would provide a more realistic assessment of long-term behaviour under evolving service conditions.

Bibliography

[1] Evan C. Bentz Boyan I. Mihaylov et Michael P. Collins : Two-parameter kinematic theory for shear behavior ofdeep beams. *ACI STRUCTURAL JOURNAL*, Title no. 110-S35, V. 110, No. 3, 2013.

[2] International Federation for Structural Concrete (fib) : fib model code 2010 and 2020 for concrete structures.

[3] Five Major Parts of Bridges, available on: `https://civildigital.com/the-five-major-parts-of-bridges-concrete-span-bridge/#google_vignette`.

[4] Alexandru Trandafir Boyan Mihaylov, Eissa Fathalla : Rapid crack-based assessment of deep beams based on a single crack measurement. *Engeenering Structures*, 322, 2025.

[5] [Vecchio] : [aggregate interlock and trasmitting shear across crack]. `https://www.researchgate.net/publication/305769509_Behaviour_of_RC_beams_strengthened_in_shear_with_NSM_FRP_reinforcement`.

[6] Darko TASEVSKI : Time-dependent strength of concrete in compression and shear. *These 9559*, 2019.

[7] Boyan Mihaylov : Five-spring model for complete shear behaviour of deep beams. *Structural Concrete*, 2015.

[8] J.C. Walraven : Aggregate interlock: An experimental and theoretical analysis. *PhD Thesis*, 1980.

[9] Delft University of Technology : Case study on aggregate interlock capacity for the shear assessment of cracked reinforced-concrete bridge cross sections. *Journal of Bridge Engineering*, 2016.

[10] Maekawa K. Okamura H Li, B. : Contact density model for stress transfer across cracks in concrete. *J. Faculty Eng., University of Tokyo (B)*, 40:9â52, 1989.

[11] Aurelio Muttoni Miguel FernÃ¡ndez Ruiz et Pietro G. Gambarova : Relationship between nonlinear creep and cracking of concrete under uniaxial compression. *Journal of Advanced Concrete Technology*, 10:1–15, 2023.

[12] F Bockhold, J ; Stangenberg : Modelling of the non-linear creep of concrete. *Beton- und Stahlbetonbau*, 99:209–216, 2004.

[13] Boyan Mihaylov : Behaviour of deep reinforced concrete beams under monotonic and reversed cyclic load. 2009.

[14] Janusz Holowaty : New formula for creep of concrete in fib model code 2010. *American Journal of Materials Science and Application*, 3(5):59–66, 2015.